

Electronic Thesis and Dissertation Repository

---

10-1-2012 12:00 AM

## Development of 3-D Neutronic Kinetic Model and Control for CANDU Reactors

Lingzhi Xia  
*The University of Western Ontario*

Supervisor  
Jin Jiang  
*The University of Western Ontario*

Graduate Program in Electrical and Computer Engineering  
A thesis submitted in partial fulfillment of the requirements for the degree in Doctor of Philosophy  
© Lingzhi Xia 2012

Follow this and additional works at: <https://ir.lib.uwo.ca/etd>



Part of the [Electrical and Computer Engineering Commons](#)

---

### Recommended Citation

Xia, Lingzhi, "Development of 3-D Neutronic Kinetic Model and Control for CANDU Reactors" (2012).  
*Electronic Thesis and Dissertation Repository*. 898.  
<https://ir.lib.uwo.ca/etd/898>

This Dissertation/Thesis is brought to you for free and open access by Scholarship@Western. It has been accepted for inclusion in Electronic Thesis and Dissertation Repository by an authorized administrator of Scholarship@Western. For more information, please contact [wlsadmin@uwo.ca](mailto:wlsadmin@uwo.ca).

**Development of 3-D Neutronic Kinetic  
Model and Control for CANDU  
Reactors**

(Thesis format: Monograph)

**By**

**Lingzhi Xia**

**Graduate Program in Electrical  
and Computer Engineering**

**A thesis submitted in partial fulfillment  
of the requirements for the degree of  
Doctor of Philosophy**

**School of Graduate and Postdoctoral Studies  
The University of Western Ontario  
London, Ontario**

© Lingzhi Xia, 2012

**THE UNIVERSITY OF WESTERN ONTARIO  
SCHOOL OF GRADUATE AND POSTDOCTORAL STUDIES**

**CERTIFICATE OF EXAMINATION**

Chief Advisor

Examining Board

\_\_\_\_\_  
Dr. Jin Jiang

\_\_\_\_\_  
Dr. Eleodor Nichita

Advisory Committee

\_\_\_\_\_  
Dr. Sree Ram Valluri

\_\_\_\_\_  
Dr. Ken McIsaac

\_\_\_\_\_  
Dr. Ken McIsaac

\_\_\_\_\_  
Dr. Amirnaser Yazdani

\_\_\_\_\_  
Dr. Lyndon J. Brown

The thesis by

Lingzhi Xia

Entitled

**Development of 3-D Neutronic Kinetic Model and  
Control for CANDU Reactors**

is accepted in partial fulfillment of the

requirements for the degree of

Doctor of Philosophy

Date: \_\_\_\_\_

\_\_\_\_\_  
Chair of Examining Board

## **ABSTRACT**

The development of a three dimensional (3-D) neutronic kinetic modeling process aiming at control system design for CANadian Deuterium Uranium (CANDU) reactors is carried out in this thesis using a modal synthesis method. In this method, the reactor space-time-dependent neutron flux is synthesized by a time-weighted series of precalculated neutron flux modes. These modes are eigenfunctions of the governing neutron diffusion equation at reference steady-state operating conditions. The Xenon effect has also been considered. Special attention has been paid to compare the performance of the developed 3-D model with that of a traditional coupled point kinetic model. The 3-D reactor model is implemented by MATLAB/SIMULINK software environment. A nondimensionalized SIMULINK representation of the reactor model is established.

The performance of the developed 3-D reactor neutronic kinetic model is then evaluated in a closed-loop environment with the help of a CANDU reactor regulating system (RRS) simulation platform. The dynamic behavior of the reactor model in a practical load-following mode has also been examined. The accuracy of the model has been validated against actual plant measurements under transient conditions. Through the analysis and simulation studies, it has convincingly demonstrated that the developed 3-D reactor model has significant advantages over the traditional coupled point kinetic model in terms of the improved accuracy and higher resolution in modeling the reactor internal flux behavior. Furthermore, using Graphic User Interface (GUI) techniques a user-friendly software package for the RRS simulation platform is developed.

Based on the 3-D reactor model and identified deficiencies of existing RRS' functions, an advanced 3-D reactor power distribution control is proposed and investigated. Linearization of the reactor model is performed and the performance of the linearized

reactor model is evaluated in a closed-loop RRS environment. Using the feedback control law, a newly designed control strategy tries to suppress the effects of high order neutron flux modes and to emphasize behaviors of the dominant mode – the fundamental flux distribution adopted by the nominal design. Thereby, the 3-D power distribution shape during transients is optimally maintained closer to the nominal design shape than by the traditional RRS. The benefits of 3-D power distribution include not only the improved economical operation, but also improved safety as the uncertainties and the uneven power distribution are reduced. These have been confirmed by extensive simulation studies on Regional Overpower Protection (ROP) detectors' flux transients during load following processes.

**Keywords:** CANDU, 3-D, neutronic kinetic model, RRS, reactor control

## **ACKNOWLEDGMENT**

I wish to express my sincere acknowledgement to my thesis supervisor, Dr. Jin Jiang, for his creative inspirations, guidance and encouragements throughout my academic program. His technical and philosophical advice, financial support and friendship are essential factors to the success of this study and are greatly appreciated.

I have certainly benefitted from continued technical supports from Dr. John C. Luxat at McMaster University. His generous support and friendship will always be appreciated and treasured.

I would like to express my deepest gratitude to my parents and other family members for their eternal loving and supports to me.

I appreciate the mutual encouragement and support with my best friend, Drew J. Rankin, through all these years of study together at Western University. Sincere appreciation is extended to other CIE group members, such as Dr. Xinghong Huang, Dr. Xiang Yu, Dr. Qingfeng Li, Jianping Ma, Peiwei Sun etc. Special acknowledgement is expressed to a previous group member, Dr. Hooman Javidnia.

Special appreciation goes to Prof. Jianmin Zhang at Xi'an Jiaotong University of China, Mr. Zhiliang Meng in Qinshan-III, and Dr. Wei Shen in Candu Energy Inc. I also would like to thank the Institute for Energy Technology (IFE) in Halden, Norway to share their Core Data Viewer (CDV) program for data display used in this thesis.

I would like to acknowledge both the financial and technical supports from: Atomic Energy Canada Limited (AECL), Natural Science and Engineering Research Council of Canada (NSERC), University Network of Excellence in Nuclear Engineering (UNENE), and Western University (UWO).

# TABLE OF CONTENTS

ABSTRACT .....	iii
ACKNOWLEDGMENT .....	v
TABLE OF CONTENTS.....	vi
LIST OF FIGURES.....	xi
LIST OF TABLES .....	xvi
ABBREVIATIONS AND NOMENCLATURE.....	xvii
I Introduction .....	1
1.1 Introduction to CANDU reactor .....	1
1.2 Background and motivations .....	3
1.3 Scope and methodology .....	9
1.4 Contributions .....	13
1.5 Organization of the thesis .....	14
II Reactor neutronic kinetics.....	16
2.1 Introduction .....	16
2.2 Reactor power and neutron flux.....	18
2.3 Prompt and delayed neutrons.....	19
2.4 Reactivity feedback and control.....	21
2.5 Space-time representation of the reactor neutronic kinetics .....	25

2.5.1 Neutron diffusion approximation of the reactor kinetics.....	25
2.5.2 Point kinetic equation.....	29
2.5.3 Numerical methods for solving the space-time diffusion equation.....	31
2.6 Summary.....	40
III 3-D neutronic kinetic model of CANDU reactors.....	41
3.1 Brief description of CANDU-6 assembly.....	41
3.2 The diffusion description of CANDU reactor kinetics.....	45
3.3 Modal modeling of CANDU reactors.....	48
3.3.1 3-D neutron flux harmonic modes in CANDU reactors.....	49
3.3.2 Modeling procedure for 3-D modal representations.....	55
3.4 Comparison of coupled point kinetic and modal synthesis models.....	58
3.4.1 Modeling of CANDU reactor kinetics by a coupled point kinetic method.....	58
3.4.2 Comparison of two reactor models.....	60
3.5 Vectorization and implementation within a SIMULINK environment.....	65
3.6 Initialization and steady-state solution.....	70
3.7 3-D neutron flux distribution at steady-state condition.....	72
3.8 Summary.....	79
IV Simulation of the CANDU reactor regulating system.....	80
4.1 Description of the CANDU reactor regulating system.....	80



4.1.1 Power measurement and calibration .....	85
4.1.2 Demand power .....	86
4.1.3 Reactivity control devices .....	87
4.1.4 Other routines .....	89
4.2 MATLAB/SIMULINK simulation platform of the RRS.....	90
4.2.1 Matrix and vector representation .....	91
4.2.2 Reactivity control principles.....	94
4.2.3 Efficient implementation of the RRS simulation platform.....	98
4.3 Simulations of power maneuvering operations.....	103
4.4 Evaluation of 3-D reactor model under load following operation .....	108
4.4.1 Reactor power transients .....	108
4.4.2 Water level transient in liquid zone units.....	112
4.4.3 Xenon dynamics.....	114
4.4.4 Neutron flux dynamics within regional overpower protection detectors .....	115
4.4.5 Core neutron flux distribution during transients .....	119
4.5 CANDU RRS Graphical User Interface (GUI).....	124
4.6 Summary.....	127

## V Power distribution control of CANDU reactors based on modal representation of reactor

kinetics .....	128
5.1 Brief introduction of the power distribution control problem.....	128
5.2 Control oriented kinetics models for CANDU reactors .....	131
5.2.1 Linearization of the reactor model .....	131
5.2.2 Validation of the linearized model .....	135
5.3 Control of power distribution in the reactor .....	136
5.4 Feedback control system design for the 3-D power distribution control.....	140
5.5 Performance evaluation of the power distribution control .....	142
5.5.1 Simulations of Power Regulation based on Linear and Nonlinear Reactor Models	142
5.5.2 3-D power distribution of the closed-loop reactor system.....	146
5.5.3 Power transients of ROP detectors under the new control strategies .....	149
5.6 Summary.....	152
VI Conclusions and suggestions for future works .....	154
6.1 Conclusions .....	154
6.2 Recommendation for future works.....	155
References .....	157
Appendix A.....	167
Appendix B.....	174
Appendix C-1.....	181

Appendix C-2.....	185
Appendix D.....	186
Appendix E.....	189
Appendix F.....	197
Appendix G.....	198
Appendix H.....	211
CURRICULUM VITAE .....	214

## LIST OF FIGURES

Fig. 3.1 Diagram of CANDU reactor assembly [56] .....	42
Fig. 3.2 End view of reactor showing principal calandria dimensions and fuel channels [57] .....	44
Fig. 3.3 Positions of zone control detectors in half core with respect to zone compartments [57].....	45
Fig. 3.4 The coordinate for CANDU reactor modeling, $r = (x, y, z)$ .....	48
Fig. 3.5 An illustrative diagram of core modeling using point kinetic equations .....	64
Fig. 3.6 An example of flux distribution modeled by the modal synthesis method.....	65
Fig. 3.7 Block diagram of the reactor model using modal synthesis method.....	69
Fig. 3.8 A generic block diagram for implementation of the reactor model.....	70
Fig. 3.9 Neutron flux distribution within the first layer (end face) along the axial direction .....	74
Fig. 3.10 Neutron flux distribution within the second layer along the axial direction.....	74
Fig. 3.11 Neutron flux distribution within the third layer along the axial direction .....	75
Fig. 3.12 Neutron flux distribution within the fourth layer along the axial direction.....	75
Fig. 3.13 Neutron flux distribution within the fifth layer along the axial direction.....	76
Fig. 3.14 Neutron flux distribution within the sixth layer (central plane) along the axial	

direction .....	76
Fig. 3.15 Neutron flux distribution along a fuel channel next to the central axis.....	77
Fig. 3.16 reactor power distribution by a modal synthesis model (reactor bulk power is 1.0 FPU; (a) - the sixth plane; (b) - the fourth plane; (c) - the second plane and (d) - the end plane) .....	78
Fig. 4.1 CANDU RRS block modules [55].....	83
Fig. 4.2 Block diagram of RRS in CANDU reactors.....	91
Fig. 4.3 Block diagram of a flux bulk control loop .....	95
Fig. 4.4 MATLAB/SIMULINK simulation platform for the CANDU reactor regulating system (RRS).....	99
Fig. 4.5 Bulk power responses based on coupled point kinetic and modal synthesis models (the reactor power is reduced from 1.0 FPU to 0.9 FPU at 0.1FPU/s) .....	104
Fig. 4.6 Simulation result of reactor power spatial control (1.0 FPU – 0.9 FPU, at a rate of 1%FP/second).....	105
Fig. 4.7 LZU water level transient simulation result (Xenon effect excluded) .....	106
Fig. 4.8 LZU water level transient simulation result (Xenon effect included) .....	106
Fig. 4.9 Simulation result of Xenon dynamic reactivity .....	107
Fig. 4.10 Comparison of 4 power transients' simulations at different power changing rates .....	108

Fig. 4.11 Changes in reactor bulk power in a load-following process.....	109
Fig. 4.12 Changes in zonal normalized powers during load-following process using modal synthesis method .....	110
Fig. 4.13 Comparison of LZU average water levels for load-following process .....	112
Fig. 4.14 Simulation results of 14 LZU water level variations for load following transient .....	114
Fig. 4.15 Comparison of Xenon dynamic reactivity for load following operation.....	115
Fig. 4.16 ROP detector location for SDS1 within the center cross section of the core.....	117
Fig. 4.17 Simulation results of the neutron flux varying within selected ROP detectors for load following process .....	118
Fig. 4.18 Simulation results of Xenon amplitudes for flux modes 2 and 3.....	119
Fig. 4.19 Schematic representation of flux modes 2 and 3 for the CANDU reactor .....	119
Fig. 4.20 The relative position of the fourth layer within the CANDU reactor core .....	120
Fig. 4.21 Neutron flux distribution at the fourth layer along the z-direction (reactor power is 1.0 FPU) .....	120
Fig. 4.22 Neutron flux distribution at the fourth layer along the z-direction (reactor power is 0.95 FPU) .....	121
Fig. 4.23 Neutron flux distribution at the fourth layer along the z-direction (reactor power is 0.9 FPU) .....	122

Fig. 4.24(a) Neutron flux distribution along the z-axis at different power levels.....	123
Fig. 4.24(b) Neutron flux distribution along the x-axis within the central plane at different power levels .....	123
Fig. 4.24(c) Neutron flux distribution along the y-axis within the central plane at different power levels .....	124
Fig. 4.25(a) MATLAB GUI for CANDU RRS simulation platform .....	126
Fig. 4.25(b) 3-D flux distribution module of the CANDU RRS GUI.....	126
Fig. 5.1 Simulation results of reactor dynamics with two reactor models using RRS' simulation.....	136
Fig. 5.2 A block diagram of the state-feedback design for CANDU reactor power distribution control.....	141
Fig. 5.3 The closed-loop dynamic system responses of the designed control strategy under two reactor models.....	144
Fig. 5.4 Variations of 14 zonal powers under linearized and nonlinear reactor models....	145
Fig. 5.5 Simulation results of 14 zone water levels using the newly designed control strategy.....	146
Fig. 5.6 Normalized power distributions of the fourth layer of the core at 4,620 s under two different control schemes (a) RRS control, and (b) new control scheme.....	147
Fig. 5.7 Simulation results of the power dynamics within selected ROP detectors implemented by 3-D control strategy .....	150

Fig. 5.8 Simulation results of Xenon amplitudes for flux modes 2 and 3 implemented by 3-D control strategy .....	150
Fig. 5.9 Simulation results of 7E ROP detector power transients implemented by RRS and the new control strategy .....	152
Fig. C-2 SIMULINK module of reactor kinetic modal modeling .....	185
Fig. D-1 Files of CANDU RRS GUI software package .....	186
Fig. F-1 SIMULINK module for CANDU reactor's 3-D power distribution control.....	197



## LIST OF TABLES

Table 2.1 The parameters of delayed neutron precursors from $U^{235}$ thermal-fissions <sup>[33]</sup> ....	20
Table 3.1 Gross features of the CANDU-6 reactor core [57].....	43
Table 3.2 Neutron flux harmonic modes $\psi_i(r)$ (CANDU-6 type), $i = 1$ to 13 and their respective characteristics.....	51
Table 3.3 Reactivity devices with their total reactivity worth.....	53
Table 4.1 Reactivity worth and maneuvering rates of reactivity control devices .....	89
Table 4.2 Normalized power distributions at eight time instances (in FPU).....	111
Table 4.3 Relative changes in actual power distributions at eight time instances (in MW) .....	111
Table 4.4 Response errors of the average levels for both reactor models .....	113
Table 5.1 Selected mesh power changes under different control methods.....	148

# ABBREVIATIONS AND NOMENCLATURE

## Abbreviations

3-D	Three-Dimensional
AECL	Atomic Energy Canada Ltd.
CANDU	CANadian Deuterium Uranium
CATHENA	Canadian Algorithm for THERmalhydraulic Network Analysis
CDV	Core Data Viewer
DCC	Digital Control Computer
ELOCA	Element Loss-Of-Coolant Accident
FPU	Full Power Unit
FLU	Full Level Unit
GUI	Graphic User Interface
LOCA	Loss of Coolant Accident
LZU	Liquid Zone Unit
LQR	Linear Quadratic Regulator
NPP	Nuclear Power Plant
ODE	Ordinary Differential Equation
PDE	Partial Differential Equation
PLD	Programmable Logic Device
PWR	Pressurized Water Reactor

PHWR	Pressurized Heavy Water Reactor
RFSP	Reactor Fuelling Simulation Program
RRS	Reactor Regulating System
ROP	Reactor Overpower Protection
SDS1	Shutdown System No. 1
SDS2	Shutdown System No. 2

## Nomenclature

$A$	the coupling volume integration matrix of all the modes
$A_p$	a matrix containing first nine columns of $A$
$B^2$	the reactor curvature
$B_{9 \times 14}$	a constant matrix of controller signal
<i>blkdiag</i>	block diagonal matrix
$C_j$	the concentration of the delayed neutron precursor
$C_{ij}(t)$	the amplitude of the delayed neutron group $j$ for mode $i$
$D$	the diffusion length
<i>diag</i>	diagonal matrix
$E_R$	energy release per fission
$E$	neutron energy spectrum

$F(r,t)$	neutron production operator
$I$	the Iodine $I^{135}$ concentration
$I_i(t)$	the amplitude of Iodine for mode $i$
$\mathbf{I}$	vector of Iodine amplitudes
$J$	the optimum performance index – quadratic cost function
$k_{eff}$	effective multiplication factor
$k_{ex}$	excess multiplication factor
$k_i$	eigenvalue associated to the $i^{th}$ flux mode
$K, K_i$	the designed control system gains
$l_k^*$	the prompt neutron generation time for $k^{th}$ mode
$n_i(t)$	the amplitude of the thermal neutron flux for mode $i$
$N$	average nucleus number of fission materials in core
$\mathbf{N}$	vector of neutron flux amplitudes
$P$	reactor power
$\mathbf{P}$	vector of delayed neutron precursor amplitudes
$P_{3D}$	3-D normalized core pin power
$P_r$	the designed power maneuvering set-point as the function of time
$Q_x, Q_y$	non-negative definite matrices
$r$	the spatial vector in core
$\mathfrak{R}_{sck}$	matrix representing the subcritical reactivity of all the modes

$\mathfrak{R}_L$  matrix of the modal coupled reactivity induced by the movement of the reactivity devices

$\mathfrak{R}_X$  matrix of the dynamic reactivity feedback of the Xenon concentration

$R(r,t)$  neutron loss operator

$R$  positive definite matrix

$S$  the external neutron sources

$T$  the time variable

$U$  14 water levels in liquid zone controllers

$v$  the neutron velocity

$V$  the reactor volume

$x$  state variable of the reactor model

$X$  the Xenon concentration

$X^s$  the referenced Xenon concentration

$X_i(t)$  the amplitude of Xenon for mode  $i$

$X_i^s$  the referenced amplitude of Xenon for mode  $i$

$X$  vector of Xenon amplitudes

$y$  output of the control system

### **Greek letters**

$\phi$  the prompt neutron flux

$\rho$  the reactivity

$\alpha_{condition}$	the reactivity coefficient under different conditions
$\chi_p$	the fission neutron spectrum
$\nu_p$	the fission yield
$\psi_i(r)$	the normalized neutron flux mode $i$
$\lambda_j$	the decay constant of the delayed neutron group $j$
$\beta_j$	the fission fraction of the delayed neutron group $j$
$\beta$	the total fission fraction of the delayed neutron groups
$\gamma_I$	the direct fission yield of $I^{135}$
$\gamma_X$	the direct fission yield of $Xe^{135}$
$\nu$	the fission yield
$\lambda_I$	the Iodine decay constant
$\lambda_X$	the Xenon decay constant
$\sigma_X$	the Xenon microscopic absorption cross-section
$\sigma_f$	microscopic fission cross-section
$\delta(r)$	spatial reactivity perturbation area
$\rho_{sck}$	the subcritical reactivity of the flux mode $k$
$\rho_{ki}$	the modal cross coupling reactivity between $k^{th}$ and $m^{th}$ modes
$\rho_{ki}^X$	the modal reactivity reflecting Xenon effect build-up
$\phi_f$	the flux-squared weighted fundamental mode
$\Lambda$	the prompt neutron generation time

$\Sigma_a$	the macroscopic absorption cross-section
$\Sigma_s$	the macroscopic scattering cross-section
$\Sigma_f$	the macroscopic fission cross-section
$\bar{\nabla}$	the Laplace operator
$\Theta_{55,n}$	the modal reactivity regarding the water level in the $n^{th}$ zone at 0.55 FLU
$\Theta_{25,n}$	the modal reactivity regarding the water level in the $n^{th}$ zone at 0.25 FLU

## Subscripts

$i$	neutron flux mode number
$j$	group number of delayed neutron precursors
$M$	the number of the selected modes
$k, m$	count of symbols

# **I Introduction**

## **1.1 Introduction to CANDU reactor**

The CANadian Deuterium Uranium (CANDU) reactor is a reactor of unique design that utilizes natural uranium as fuel and heavy water as moderator and coolant [1]. This reactor achieves substantial financial savings due to the absence of fuel enrichment costs. However, a chemical plant is required to produce the quantities of heavy water.

The original CANDU designer is AECL (Atomic Energy of Canada Limited), a federal crown corporation created in 1952. Over 150 private companies in Canada supply components for the CANDU system. As of October 1, 2011, responsibility for all commercial CANDU design, maintenance services and marketing was transferred to the Mississauga, Ontario-based Candu Energy Inc., a wholly owned subsidiary of Montreal-based engineering firm SNC Lavalin.

CANDU-6 is a 700 MW nuclear power reactor. The first CANDU-6 plant went into service in the early 1980s, and the design continues to evolve to maintain superior technology and performance. In Canada, CANDU reactors are used to supply power in Ontario, Quebec and New Brunswick. The Pickering facility east of Toronto on Lake Ontario and the Bruce facility northwest of Toronto have 8 reactors per site. AECL has also provided CANDU reactors to utilities in Argentina, India, South Korea, Pakistan, Romania and China.



The thermal efficiency of a CANDU reactor plant is approximately 29%, but the CANDU reactor uses a larger fraction of U-235 in uranium ore than other reactors and also makes better use of the U-238 to Pu-239 conversion process to extend fuel burnup [2]. Moreover, statistics show that, among large reactors, CANDU reactors have outstanding reliability records, with annual capacity factors (the ratio of annual electrical energy output to maximum possible annual output) as high as 96% and cumulative capacity factors as high as 88% [3].

Compared to other types of nuclear power plants, CANDU plants have some design features and unique characteristics:

- a reactor core containing several hundred fuel channels rather than one pressure vessel
- natural uranium or other low fissile material for fuel
- on-line refueling
- heavy water for moderator and coolant; separated low pressure moderator and high pressure fuel coolant
- three types of reactivity devices located within the cool, low pressure moderator
- two fully capable, independent shutdown systems, and the reactor regulating system

## 1.2 Background and motivations

Computer programs are used in every aspect of nuclear power plants from design to operation. For design and safety analysis of CANDU reactors, the commonly used codes for thermalhydraulic, reactor physics, and LOCA analysis are: Canadian Algorithm for THERmal-hydraulic Network Analysis (CATHENA) [4] (Hanna, 1998), Reactor Fuelling Simulation Program (RFSP) [5], and Element Loss-Of-Coolant Accident (ELOCA) [6], respectively. During plant operations, real-time computer algorithms have also been developed for online monitoring and real-time regulation of the key system variables, such as neutron flux or reactor power. A good example is the reactor regulating system (RRS), which regulates the reactor power by adjusting the reactivity devices. Despite the above design, analysis and operational tools, one area that seems to be either left out, or ignored, is software design tools for CANDU reactor control system design and analysis.

Control of nuclear reactors is also an important issue in the operation of nuclear power plants. Improved control of the nuclear reactor can ameliorate plant productivity and safety by, for example, increasing plant availability, economic utilization of nuclear fuel, and operational flexibility. Nuclear reactor control is complicated as many processes are involved, including local and global power regulation and damping of Xenon oscillation. Reactor control problems often contain two major aspects: the first is the reactor kinetic modeling, which provides a principal description of space-time dynamics of reactor variables; the second is the development of control strategies to meet safety and

performance requirements. Modeling of reactor kinetics is an essential component of this process. To achieve high performance reactor control system, it is highly desirable to have an accurate reactor kinetic model. Even for development of nuclear power plant simulators, the sophisticated reactor dynamic model will bring a good effect on operations. For these reasons, advanced mathematic methods should be used for nuclear reactor dynamic modeling and advanced control of CANDU reactors should be identified and investigated.

Many people have performed reactor kinetics modeling and control research on nuclear reactors, including CANDU systems. From postwar to the end of the 1970s, the nuclear industry has experienced a golden period of development. B. Frogner published a paper that describes the detailed applications, problems, trends, and perspectives of control of nuclear power plants [7]. Frogner also proposed areas in which researchers developing control methods can contribute to improved control design. In the 1970s, D. Cherchas and his students, R. Lake, C. Mewdell, S. Ng, G. Yorke and M. Berka, investigated CANDU power stations, employing control methods for optimum control, multivariable control and discrete control [8]-[12]. Cherchas' research includes use of the nuclear reactor point kinetic model and modal expansion model. Some useful conclusions are obtained for load following and reactor operating cost during load cycling intervals. However, their research is limited to theoretical derivations and simulations.

A.Tiwari's research focused on kinetic modeling of a large Pressurized Heavy Water

Reactor (PHWR) in India and investigated new control strategies [13]. This PHWR is similar to the CANDU-6 reactor. The reactor model is developed based on the point kinetic method and simplified nodal techniques and is applied to a 500 MW PHWR. Control problems are proposed based on this model. However, this reactor model cannot provide the core internal information in detail. In industrial applications, more detailed, accurate reactor model can be found, for example, in the application of RFSP codes. These codes provide reasonably accurate neutronic modeling for reactor physics, as well as the steady-state and transient behaviors of the reactor. However, the modeling process that employs the partial differential equations (PDE) are difficult to be directly used in conventional control system studies, which are often based on ordinary differential equations (ODE).

Generally speaking, there are two main approaches for reactor kinetic modeling, which can be directly associated with conventional control system design: one is based on point kinetic models, and the other on modal synthesis models. A coupled point reactor kinetic modeling for CANDU neutronic kinetics has been developed in the Nuclear Instrumentation and Control Group at the University of Western Ontario, London, ON [14]. This reactor kinetic model is based on the CANDU-6 reactor type and is similar to the PHWR model developed by Tiwari. The modeling method also employs the coupled point kinetic method, which can be considered as a simplified nodal method. In this model, the entire reactor is divided into 14 zones. For each zone, a point kinetic model is

used. The interactions between neighboring zones are accounted for by coupling reactivity coefficients. In addition to neutron kinetics, reactivity feedback from Xenon buildup is also considered. This reactor model is sequentially combined with a CANDU reactor regulating system (RRS) in a MATLAB/SIMULINK simulation environment. Throughout the analysis, although it can satisfy the basic requirements of a CANDU RRS operation, it could not provide accurate information on the reactor as a three-dimensional model can, due to the assumption of point kinetics. Particularly, it cannot simulate the time-varying spatial neutronic behavior within each reactor zone, which is important in the analysis of local reactivity disturbance.

In order to improve the quality of the reactor models beyond point kinetic, another option to consider is the modal method. The modal method is able to characterize the behavior of the reactors in a three-dimensional representation [15]. Using this method, one can synthesize the kinetic variables such as neutron flux, delayed precursor concentration, and Xenon concentration from a time-weighted sum of the independent spatial flux modes. These modes can be obtained through steady-state calculations using the reactor physics code. Since all the flux modes are represented in a 3-D spatial mesh structure manner, the reactor model can also provide the internal 3-D dynamic information. As a result, the new model provides more accurate neutronic kinetics than the previous point kinetic model. Based on this new model, the MATLAB/SIMULINK simulation platform for the CANDU RRS can be enhanced. Furthermore, such a reactor model can potentially

be tailored to control system designs because it is in the form of ordinary differential equations. It is important to note that while the reactor considered in this research is a CANDU-6 reactor, the technique described herein can be extended to other reactors.

In nuclear power plants, reactor power control is crucial since it concerns the safe operation and the economic benefits of the plant. Nuclear power plants often improve operating efficiency such that maximum electric power can be produced. However, nuclear power plants should operate safely and reliably, and should possess desired levels of safety margins, suitable peak overshoots and transients.

For CANDU nuclear power plants, a reactor regulating system (RRS) is employed to perform the power regulating functions so as to meet requirements on safety and power output [16]. The RRS manipulates the reactivity devices to perform the bulk and spatial power control by minimizing the error between the reactor bulk power (14 liquid zonal powers) and the bulk power setpoint. In this way, the bulk and 14 zonal powers are regulated according to the power setpoint transient. However, the local power dynamics within each zone cannot be individually controlled by the RRS. Thus, it is impossible for the RRS to regulate the genuine 3-D mesh power distribution within the reactor core. One of RRS' main functions is to be maintaining the shape of reactor power distribution similar as the nominal designed shape, in order to provide the maximum output without overriding the power limits of the fuel bundle and the channel. The way for the RRS to perform this function is to continually adjust and balance 14 zonal powers such that the

3-D power distribution shape can be maintained similar to the nominal designed shape. The power distribution shape obtained in this way is not accurately consistent with the designed shape. Thus, how to accurately adjust the 3-D mesh-power dynamics of the core is the subject of this research. New control strategies are investigated for the proposed objective.

The design of a 3-D power distribution control strategy is based on the developed 3-D reactor modal model. This reactor model begins with a modal synthesis method and expands the reactor dynamic variables such as neutron flux, delayed neutron precursors' concentration, Iodine and Xenon concentrations to a weighted sum of pre-designated neutron flux modes, such that the space-time dependant reactor dynamic system model is transformed to an only time-dependant one, which can be used for conventional control problems. A closed-loop performance evaluation regarding this 3-D reactor model is manipulated with the help of the RRS simulation platform. By validating the simulation results with real plant data and comparing them to those from 14-coupled point kinetic model, the 3-D reactor model is to be demonstrated to be accurate and reliable. Although this reactor model is still using a mesh-structure to represent the 3-D power distribution and the fidelity depends on the size of meshes, this model can still be applied to the 3-D power distribution control system design. Subsequently, the newly developed control strategy can be applied to achieve more effective control. The simulation results will be compared with those of original RRS' control and the performance of the new control law

is evaluated.

### **1.3 Scope and methodology**

The first important problem, which is encountered in this research, is modeling of the reactor kinetic system. Many mathematical methods have been developed for system modeling and numeric calculation. For nuclear reactor time-spatial kinetics, some classical methods such as point kinetic method, finite difference method, nodal method and modal expansion approximation are set up for modeling processes [17]. All these methodologies are developed to analyze spatial-time dependent kinetics. These methods can be used for static and dynamic analysis of nuclear reactors. A number of new or advanced numerical methods have been developed in nuclear reactor physics analysis, such as advanced nonlinear iteration nodal method, finite element analysis method and Monte Carlo method [18]. These methods can be used to develop spatial kinetic models of nuclear reactors in good manner, which can provide the more detailed information on reactor characteristics. More specifically, 3-D kinetic models can be established. However, the applications are not amenable when used in control problems. As it is known, control problems often need models described in the form of ordinary differential equations. Not only most of the advanced numerical methods mentioned above, but also the finite difference and nodal methods, are represented in a PDE manner. These features limit the application of these methods to control problems. A cell nerve net method can be taken into account to solve partial differential equations of nuclear diffusion theory, but it's very



complicated and not the mainstream application [19].

Point kinetic model is very useful in small and medium size reactors, where the entire dynamic characteristics of the reactor can be approximated as a single point and the internal behavior of the core can be ignored. However, in cases where the internal behaviors within large reactors are required to be considered, this method cannot be used. Specifically for local dynamic analysis in large reactors, point kinetic method is definitely unsuitable to do the analysis. In A. Tiwari and H. Javidnia's research [14], simplified nodal method is operated on modeling of CANDU nuclear reactors. Each of 14 liquid control zones of CANDU reactor is treated as a large point and all internal physics properties are assumed to be homogenous. This model can reflect the zone dynamic responses as each zone works as a unit. But it cannot represent the detailed information within the zones, such that it cannot reflect the accurate 3-D dynamics. This kind of reactor model might be improved by adding more nodes to the original model. For example, each zone (a node) of 14 liquid control zones can be divided into subzones where fine point kinetic nodes can be used. Nevertheless, the problem becomes more complex since more reactivity coefficients need to be calculated, and even if this is successfully resolved, the order of the kinetic equations will be increased, which makes the control problems more difficult.

Modal expansion approximation method can be suggested [20]-[22]. The suggested approach is to synthesize the spatial flux distributions, delayed neutron precursor

concentrations, Xenon and Iodine concentrations by a time-weighted sum of spatial flux modes [22]. These flux modes are eigenfunctions of the steady-state diffusion equation and satisfy the bi-orthogonality conditions. The flux modes can be prepared by using the multidimensional diffusion codes. Modal method with only a few flux modes can achieve as accurate results as the finite differential or nodal method does, when dealing with the basic transient analysis. In case of complex transient analysis with large reactivity perturbations, a high-order modal model is required. However, the increased order also brings to the simulations computational burdens which cannot be anticipated. Thus, the balance of the model order and the computational burden has to be considered and evaluated.

Classical control methods such as PID controller are often used in the design of conventional feedback control for nuclear power plants [7]. However, modern multivariable control theories have been widely used in other technological systems [23]. There is no evidence showing that comparison has been performed between classical and modern control methods with applications to a commercial reactor. Advanced multivariable control methods, such as optimum control and adaptive control, have been used in different research areas of nuclear reactor control, including control of spatial-time flux distribution, load following and Xenon transient [24-31]. In this research, since the 3-D reactor neutronic kinetic model belongs to a MIMO dynamic system with multiple internal variables, it is difficult to use traditional methods such as PID to design

the feedback control system. However, modern control method can take into account such a complex coupled dynamic system. As for the proposed 3-D power level control problem, the objective is to achieve optimal performance criterion and meanwhile maintain the stability of the closed-loop system with the least amount of the control-signal energy. To achieve the above objectives, a linear quadratic regulator (LQR) feedback control scheme is employed to solve the 3-D control problem.

The steps of this research can be represented as follows.

- systematically study CANDU reactor kinetics and control
- establish the reactor neutronic kinetic model by using modal synthesis method
- compare the reactor modal model with the coupled point kinetic model
- decompose the simulation platform of CANDU reactor regulating system by using MATLAB/SIMULINK
- develop new simulation platform for the CANDU RRS, integrating the modal synthesis reactor model
- evaluate the performance of new RRS simulation platform by validating the simulation results with the power plant data and comparing the results against those of couple point kinetic model

- design an optimum control algorithm for CANDU reactor 3-D power level control and analyze the simulation results

## **1.4 Contributions**

The contributions of this thesis can be summarized as follows:

1. The modal synthesis model illustrating 3-D space-time neutronic kinetic behaviors of the CANDU reactor has been developed.
2. The 3-D modal reactor model has been compared to the coupled point kinetic reactor model by theoretical analysis and the numerical simulations.
3. The 3-D modal reactor model is nondimensionalized by using MATLAB/SIMULINK functions and is integrated to the RRS simulation platform, such that an improved RRS simulation platform is developed.
4. The performance of the newly-developed RRS simulation platform has been evaluated by comparing the simulation results with power plant data and those of the coupled point kinetic model.
5. A user-friendly MATLAB graphical user interface (GUI) software package for the RRS simulation platform is created, which brings reliable convenience to industrial applications and manipulations for research, educational purposes.

6. The 3-D power level control strategy is developed, which not only satisfies the requirements of reactor bulk and more accurate spatial control for the load following manipulations, but also brings more safety margins to the current power plant operation.

## **1.5 Organization of the thesis**

This thesis is organized as follows: Chapter 1 is the introduction. The research background and motivations, methodology and contributions are summarized. Chapter 2 represents the functional principles of reactor neutronic kinetics. Numerical simulation methods for solving the space-time dependent neutron diffusion process are discussed and compared.

Chapter 3 brings out the detailed process of CANDU reactor 3-D neutronic kinetic model by using modal synthesis method. The methodology is illustrated in detail. The 3-D flux distribution modes are also described. The reactor model is then simulated under steady-state conditions. The simulation results are represented, which highlights the dynamic characteristic of the 3-D modal model.

Chapter 4 is to evaluate the performance of the developed CANDU RRS simulation platform containing the 3-D reactor kinetic model in closed-loop form using simulations. The dynamic behavior of the reactor model in a practical load-following mode has also been examined. The accuracy of the model has been validated against actual plant

measurements under both transient and steady-state conditions. Through the analysis and the simulation studies, it has convincingly demonstrated that the developed 3-D model has significant advantages over traditional coupled point kinetic models in terms of the improved accuracy and the higher resolution in modeling the reactor internal dynamics. Furthermore, a user-friendly MATLAB/GUI software package for CANDU RRS simulations is described.

Chapter 5 focuses on research and design of a feedback control strategy for CANDU reactor 3-D power regulation for load following operation. Linearization of the reactor model is performed and control objectives are proposed. Feedback control law based on the power distribution control is designed. The newly designed control strategy is then simulated to both the reactor linearized and original nonlinearized models for a typical load following transient. Simulation results are analyzed, which validates the effectiveness of the control law. Furthermore, ROP detectors are selected to examine the local in-core power transients. By comparing the simulation results with those of RRS' simulation, it is demonstrated that the designed control strategy based on a 3-D model achieves improved performance on the 3-D power regulating over the RRS' representation.

Chapter 6 represents the conclusion and the potential research suggestions.

## **II Reactor neutronic kinetics**

This chapter describes the main principles of reactor neutronic kinetics. Basic concepts of reactor neutronic kinetics such as short- or long- term transients and their corresponding characteristics, prompt and delayed neutrons, internal reactivity feedback and Xenon effect are represented. Particular attention has been paid to explaining the neutron diffusion process, space-time dependent diffusion equations, and how to solve them. The point kinetic reactor model is introduced since it is widely used. Furthermore, different numerical simulation methods to solve the diffusion equations are illustrated, and the basic principles are discussed. At the end of this chapter, the features of all the methods are compared for investigation of reactor control problems and the conclusions are drawn.

### **2.1 Introduction**

Reactor neutronic kinetics studies how neutron behaviors change with time within the reactor core. Usually, it is associated with long or short term changes induced by natural perturbations or imposed transients. Control systems have to be designed to maintain the desired neutron power in the presence of both types of changes. Dynamic neutron behaviors induced by the production and disappearance of neutrons will be affected by the reactivity change in the reactor core. Some elements concerned by the reactivity influence are: movement of the reactivity control devices; temperature variations; fission isotopes; fuel burn-up and probable accidents; etc.

In a short term, “reactor neutronic kinetics” represents the fast variation of neutron flux caused by anticipated or accidental change in the reactor system. This short-term reactor change can be a result of change in reactivity devices, internal temperature feedback and the generation of neutron absorbers in certain period of time. The flux transient is crucial to the reactor operation, performance and safety analysis.

In a long term, there are reactivity changes due to the build-up of some fission products, such as  $\text{Xe}^{135}$  and  $\text{Sm}^{147}$ , and fuel burn-up in the reactor core. Particular attention has to be paid to  $\text{Xe}^{135}$  and  $\text{Sm}^{147}$  since they have big thermal neutron capture cross-sections, which may cause the phenomena of “Poisoning” or “Iodine pit”. However, in this long term process, only neutron flux kinetics affected by reactor temperature change is contained by the category of “reactor neutronic kinetics” [32]. Fission isotope accumulation is considered in very long term transients. But in the fast neutron energy region, the neutron absorption cross-sections of all fission productions are too small to essentially affect the neutron flux of the reactor core. Furthermore, the long term phenomena contain the swelling of reactor structure materials, fuel pellets’ change due to the burn-up, and so on. All these have little impact on the reactor neutron flux variation.

In fact, the long term phenomenon has led to different approaches for their studies than the short-term problem [32]. In this thesis, only short term effects are considered, which means that the reactor neutronic behaviors affected by the reactivity controllers and the internal feedbacks of the reactivity are the main causes of the transients.



## 2.2 Reactor power and neutron flux

The relationship of the reactor power and the neutron flux can be illustrated by the following Eqn. (2-1).

$$P = E_R N \sigma_f \phi V \quad (2-1)$$

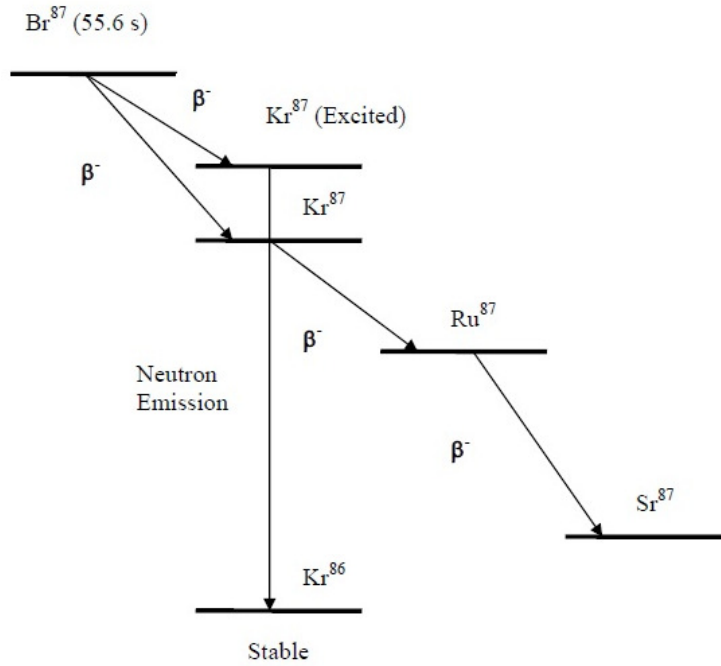
where,  $P$  is reactor power, in W;  $E_R$  is energy release per fission, 200MeV ( $3.2 \times 10^{-11}$ W);  $N$  is the average fissile number density in the core,  $10^{24}/\text{cm}^3$ ;  $\sigma_f$  is the average microscopic fission cross-section,  $\text{m}^2$ ;  $\phi$  is average neutron flux in the core,  $1/\text{cm}^2 \cdot \text{s}$ ;  $V$  is the reactor volume,  $\text{cm}^3$ .

For a given reactor configuration it is evident that the reactor power is proportional to the neutron flux, since the other factors in the equation are constant in the short term. Any variation in neutron flux will therefore be reflected in the variation of the reactor power. Although the reactor kinetics equations are related to variations in neutron flux, they are often related directly to the variations of the reactor power. In practice, a normalized concept is often used, illustrated as normalized power (normalized neutron flux), which represents the percentage of the ratio of the real power (real neutron flux) over the reference power (reference neutron flux). This normalization prevents complex unit conversions in derivation process. In the most parts of this thesis, normalized power or flux concept is used.

### 2.3 Prompt and delayed neutrons

About 99.9% of fission neutrons are designated as "prompt neutrons" since they are emitted within a short time interval of  $10^{-17}$  sec of the fission process. The remaining neutrons are emitted after certain delay as a part of the radioactive decay of the fission products to several minutes beyond the fission process itself, and are designated as "delayed neutrons".

An example represented in Fig. 2.1 shows the delayed neutron emission from the fission product isotope  $\text{Br}^{87}$ , which has a half-life of 55.6 seconds [33]. The beta decay of  $\text{Br}^{87}$  starts in its ground state. Subsequently it decays into the stable isotope  $\text{Sr}^{87}$  through two continuous beta emissions. In addition, it is possible for the delayed neutron precursor,  $\text{Br}^{87}$  nucleus, to beta-decay into an excited state of the  $\text{Kr}^{87}$  nucleus at the energy of 5.5MeV, which is larger than the binding energy of a neutron within the  $\text{Kr}^{87}$  nucleus. Then, a neutron is emitted in the process of beta emission, which leads to the stable  $\text{Kr}^{86}$  isotope.



**Fig. 2.1 The process of the neutron emitted from  $\text{Br}^{87}$  [33]**

It is known that there are more than ten varieties of neutron delayed precursors produced by the thermal-fission of  $\text{U}^{235}$ . They are arranged into 6 groups according to different half-life times in Table 2.1.

**Table 2.1 The parameters of delayed neutron precursors from  $\text{U}^{235}$  thermal-fissions [33]**

Group NO.	Half-life T1/2 (s)	Decay constant $\lambda_i$ ( $\text{s}^{-1}$ )	Lifetime $t_i$ (s)	Energy (KeV)	Yield $y_i$	Fraction $\beta_i$
1	55.72	0.0124	80.65	250	0.00052	0.000215
2	22.72	0.0305	32.79	560	0.00346	0.001424
3	6.22	0.111	9.09	405	0.00310	0.001274
4	2.30	0.301	3.32	450	0.00624	0.002568
5	0.610	1.14	0.88	-	0.00182	0.000748
6	0.23	3.01	0.33	-	0.00066	0.000273

In Table 2.1, yield  $y_i$  represents the number of delayed neutron precursors of group  $i$  emitted by each fission; fraction  $\beta_i$  represents the fraction of fission neutrons that are born as delayed neutrons out of all the fission neutrons including the prompt neutrons for group  $i$ . If the number of all emitted neutrons per fission is  $\nu$ ,

$$y_i = \nu\beta_i \quad (2-2)$$

In the reactor kinetics, another important variable, total fraction of delayed neutron precursors, is frequently used, and can be represented by

$$\beta = \sum_{i=1}^6 \beta_i \quad (2-3)$$

The total fraction of delayed neutron precursors from  $U^{235}$  is 0.0065.

The occurrence of delayed neutrons is important for the reactor control. The weighted average of mean lifetime of the delayed neutrons is much larger than that of the prompt neutrons. Although the fraction of delayed neutrons is small, it provides a large time constant that slows down the response of a nuclear reactor to make it controllable through the withdrawal and insertion of control rods containing neutron absorbing materials.

## **2.4 Reactivity feedback and control**

In order to maintain a stable chain reaction, a nuclear reactor is designed to achieve a balance between fission reaction, neutron capture and leakage. A neutron is generated in a

fission process and it will scatter in the reactor core until either it is absorbed by a nucleus, or it leaks out of the core. At one time, certain numbers of neutrons will be absorbed by the fissile or fissionable materials and induce further fissions, such that more neutrons are generated. If a number is used to measure these two successive processes, the ratio of the neutron numbers in these two generations can be defined. In a finite volume reactor, this number can be represented by the effective multiplication factor  $k_{eff}$ , which is

$$k_{eff} = \frac{N_2}{N_1} \quad (2-4)$$

where,  $N_1$  represents the number of neutrons produced in the current generation;  $N_2$  indicates the number of neutrons produced in the next generation.

A reactor at critical condition has an effective multiplication factor of  $k_{eff}$  equal to unity. When this nuclear reactor deviates from the criticality, its effective multiplication factor can be greater or less than unity. In this case an “excess multiplication factor” can be defined:

$$k_{ex} = k_{eff} - 1 \quad (2-5)$$

which can be either positive or negative.

The ratio of the excess multiplication factor to the effective multiplication factor is defined as “reactivity”:

$$\rho = \frac{k_{ex}}{k_{eff}} = \frac{k_{eff} - 1}{k_{eff}} \quad (2-6)$$

Thus reactivity describes the deviation of a reactor's status from the critical condition with the time varying. For a reactor at steady state (criticality), the reactivity is zero.

During the reactor transients, changes in the operating parameters of the reactor, such as temperature or fuel burn-up, can result in reactivity feedback. The principal factors include fuel temperature, coolant temperature, coolant void, moderator temperature, reactor power, moderator poisons, and fission products. The influence is described by different reactivity coefficients. The reactivity coefficient can be described as the variation of the reactivity  $\Delta\rho$  over the variation of the parameter  $\Delta\xi$ .

$$\alpha_{condition} = \frac{\Delta\rho}{\Delta\xi} \quad (2-7)$$

where,  $\alpha_{condition}$  is the reactivity coefficient for different conditions. If the reactivity coefficient is negative, the reactor power will decrease; and if it is positive, the power will increase.

The effects of the reactivity feedback factors can vary significantly. Some long term reactivity changes are slow and span a long-range due to the fuel burn-up or production in a breeder reactor. Fuel depletion causes decrease in the power level, whereas breeding causes an increase. Sometimes, the effects of the reactivity temperature coefficient can be

felt immediately. Furthermore, the accumulation of the fission products absorbs neutrons and decreases the reactor power level.

All fission products can be called “poisons” since they absorb neutrons. They contribute to long term reactivity decrease as fuel burns up. Within them, the Xenon isotope  $^{135}\text{Xe}$  plays an important role in the power reactors. It has a very large absorption cross-section for thermal neutrons and therefore represents a considerable influence on the chain reaction. The  $^{135}\text{Xe}$  concentration has an impact on, and in turn is affected by the reactor power distribution variation, by the power level change and by the movements of reactivity devices.  $^{135}\text{Xe}$  is produced somewhat directly in fission, but mostly as the result of the beta decay of its precursor  $^{135}\text{I}$ .  $^{135}\text{Xe}$  disappears in two ways: one is through its own radioactive decay, and the other is by neutron absorption to convert it into  $^{136}\text{Xe}$ .

The principal factors which can affect reactivity in a CANDU reactor can be listed below, as well as a briefly explanation of how each factor affects the reactivity and how this can be controlled by reactivity devices or operational strategies.

#### **a) Reactor Power Variations**

If the power is increased from a shutdown state to a full power, reactivity decreases due to the increase in the fuel and coolant temperatures. In such cases, the effect can be compensated by rapidly removing light water from the liquid zone controllers.

### **b) Coolant & Moderator Temperature Variations**

If the coolant and fuel temperatures increase, reactivity decreases. The same control actions are needed as in (a).

### **c) Fuel Burnup, Xenon Transient**

The reactivity decreases slowly and regularly depending on both the burn-up history and the refueling strategy. The effect can be compensated by poison relief in the moderator or withdrawal of the adjuster rods from the reactor core. The Xenon transient can be overcome by the excess reactivity margin of the adjuster rods.

### **d) Flux Variation within Zones**

The power may vary locally in a CANDU reactor core due to channel refueling and Xenon oscillations. The effect can be dealt with by light water level adjustments in the liquid zone controllers.

## **2.5 Space-time representation of the reactor neutronic kinetics**

### **2.5.1 Neutron diffusion approximation of the reactor kinetics**

The accurate description of neutron flux distribution within the lattice cells requires the solution of the general Boltzmann transport equation based on the neutron transport theory [18]. The solutions of the transport equations homogenize the characteristic



properties such as cross-sections, diffusion coefficients, and so on, for some given lattice cells representative of the reactor core. The steady-state solution is suitable for a refined description of the related processes and can be achieved by using a fine energy discretization. Accurate dynamic solutions depend on the detailed distribution of the angular flux density. However, in many situations, details of the angular flux dependence are not required. What is needed is the angle integrated neutron flux. If the neutron transportation equation can be integrated over all angles and some approximations are employed, the neutron diffusion approximation can be derived from the neutron transport equation, which greatly simplifies the computational task of the numerical solution processes.

The formulation based on a diffusion equation constitutes an approximation to the transport equation. This approximation is more functional for a full reactor core description and contains a realistic representation of the internal components. It is assumed that the directional neutron flux density is angularly independent and can be described by the scalar flux density and the net current density.

The general form of the diffusion equation is:

$$\begin{aligned} \frac{1}{v} \frac{\partial}{\partial t} \phi(r, E, t) = & -\Sigma(r, E, t)\phi(r, E, t) - \bar{\nabla} \cdot D(r, E)\bar{\nabla} \phi(r, E, t) \\ & + \int_0^{\infty} \Sigma_s(r, E' \rightarrow E, t)\phi(r, E', t)dE' + \chi_p(E) \int_0^{\infty} \nu_p(E')\Sigma_f(r, E', t)\phi(r, E', t)dE' \\ & + S(r, E, t) \end{aligned} \quad (2-8)$$

where,  $v$  is the neutron velocity;  $t$  is the time;  $\phi$  is the neutron flux;  $r$  is the spatial coordinate;  $E$  represents the neutron energy spectrum;  $\Sigma$  is the total macroscopic cross-section;  $\bar{\nabla}$  is the Laplace operator;  $D$  is the diffusion length;  $\Sigma_s$  is the macroscopic scattering cross-section;  $\chi_p$  represents the fission neutron spectrum;  $\nu_p$  is the fission yield;  $\Sigma_f$  is the macroscopic fission cross-section;  $S$  represents the external neutron sources.

The fission production operator,  $F\phi(r, E, t)$  and the neutron loss operator,  $M\phi(r, E, t)$  can be defined as

$$F\phi(r, E, t) = \chi_p(E) \int_0^\infty \nu_p(E') \Sigma_f(r, E', t) \phi(r, E', t) dE' \quad (2-9)$$

$$M\phi(r, E, t) = \Sigma(r, E, t) \phi(r, E, t) - \bar{\nabla} \cdot D(r, E) \bar{\nabla} \phi(r, E, t) - \int_0^\infty \Sigma_s(r, E' \rightarrow E, t) \phi(r, E', t) dE' \quad (2-10)$$

The diffusion equation becomes

$$\frac{1}{v} \frac{\partial}{\partial t} \phi(r, E, t) = (F - M)\phi(r, E, t) + S(r, E, t) \quad (2-11)$$

The steady-state diffusion equation without the external neutron source can be derived

under  $\frac{\partial}{\partial t} \phi = 0$ , such that

$$M\phi = \frac{1}{k_{eff}} F\phi \quad (2-12)$$

Here the multiplicative parameter  $k_{eff}$  is to be adjusted such that a balance is achieved between neutron production and loss.

In order to obtain the general diffusion equation, the derivation begins with the continuity equation, which is described regarding the two independent variables: the net current density, and the scalar flux density. Using the diffusion coefficient, these variables are then linked together; the resulting approximation is the general diffusion equation. As long as the neutron sources and sinks are homogenized within the representative lattice cells and correctly distributed in the core, the diffusion approach can be used in either static or dynamic neutron flux calculations.

Reactor theory owes a great debt to the diffusion model of the neutron transport, because its high level of detail enables scientific insights, and its simplicity allows for the examination of crucial aspects of design. Another manner of reducing the problem's intricacy is to characterize the neutrons by a single energy or speed, instead of multiple group energy of speed.

Considering 6 groups of delayed neutron precursors, the single energy group diffusion equation can be written as

$$\frac{1}{v} \frac{\partial}{\partial t} \phi(r,t) = \nabla \cdot D \nabla \phi(r,t) + (1 - \beta) k_{\infty} \Sigma_a \phi(r,t) + \sum_j^6 \lambda_j C_j(r,t) - \Sigma_a \phi(r,t) \quad (2-13)$$

$$\frac{\partial}{\partial t} C_j(r,t) = -\lambda_j C_j(r,t) + \beta_j k_{\infty} \Sigma_a \phi(r,t) \quad (2-14)$$

where  $\beta$  and  $\beta_j$  are respectively total and delayed neutron fission fractions;  $k_\infty$  is the infinite multiplication factor;  $\Sigma_a$  is the absorption cross-section;  $j$  is the group number of delayed neutron precursors;  $\lambda_j$  is the decay constant of the  $j^{\text{th}}$  group delayed neutron precursor; and  $C_j$  is the concentration of the  $j^{\text{th}}$  group delayed neutron precursor.

### 2.5.2 Point kinetic equation

The point kinetic reactor model is widely used in reactor kinetic analysis due to its simplicity. The main difficulty of this method exists in obtaining the necessary parameters of the reactor core. However, many characteristics of the dynamic behavior of a reactor can be deduced from it. Furthermore, this point kinetic method can be used as a benchmark to evaluate the more sophisticated methods adopted in full space-time simulations. If a given method cannot pass the test of a reactor core considered as a point kinetic model, this method may not be suitable for simulation studies.

The start of the point kinetic method is also the space-time neutronic diffusion equation. The main idea is to separate the neutron flux in the diffusion equation by multiplying a space-only-dependent flux distribution shape and a time-only-dependent time variable. The neutron flux is

$$\phi(r,t) = n(t)\varphi(r) \quad (2-15)$$

where  $\varphi(r)$  represents the space-only-dependent flux shape;  $n(t)$  represents the

time-only-dependent time variable.

Similarly, the concentration of the delayed neutron precursors can be expressed in this way:

$$C_j(r,t) = C_j(t)\varphi(r) \quad (2-16)$$

where  $C_j(r,t)$  represents the concentration of the  $j^{th}$  group delayed neutron precursors;  $C_j(t)$  represents the corresponding time variable.

Assuming that the flux shape function satisfies the wave equation,

$$\nabla^2 \varphi(r) + B^2 \varphi(r) = 0 \quad (2-17)$$

where  $B^2$  is the reactor curvature, and apply this equation and Eqns. (2-15) and (2-16) to the diffusion equation, the point kinetic equation can be derived as follows,

$$\frac{d}{dt} n(t) = \frac{\rho(t) - \beta}{\Lambda} n(t) + \sum_j^6 \lambda_j C_j(t) \quad (2-18)$$

$$\frac{d}{dt} C_j(t) = \frac{\beta_j}{\Lambda} n(t) - \lambda_j C_j(t) \quad (2-19)$$

where  $\rho(t)$  represents the reactivity within the reactor core as a function of time;  $\Lambda$  is the neutron generation time.

Depending on the value of  $\rho$ , the reactivity associated with a given reactor transient,

and on  $\beta$ , the fraction of delayed neutrons, the different reactor states and the related characteristics can be classified as follows:

- a) if  $\rho < \beta$ , the divergence of the prompt kinetics can be avoided. When  $K_{eff} > 1$  the reactor is super-critical but the reactivity insertion can be less than a fraction of delayed neutron production. The power variation is then dominated by delayed neutrons. The neutronic power increases during the transient and converges to the prompt jump value.
- b) if  $\rho = \beta$ , the chain reaction becomes less dependent on the delayed neutrons, hence power changes more rapidly. The reactor state is then called prompt-critical. The nuclear reactor may become unstable since any small positive fluctuation in the reactivity can be amplified and may result in a divergent power offset.
- c) if  $\rho > \beta$ , the reactor state is called super-prompt-critical. The neutronic power increases without having to “wait” for the delayed neutrons according to the prompt kinetics behavior since the prompt neutrons dominate the neutron imbalance.

### **2.5.3 Numerical methods for solving the space-time diffusion equation**

The importance of the space-time dependent treatment of transient analysis problems is highlighted by the fact that the point reactor results are not only inaccurate, but also non-conservative. Since the prerequisite for the point kinetic reactor model is that the

neutron flux distribution has an invariable shape, the point kinetic model is not suitable for investigating the internal behaviors within the reactor core.

Therefore, the true dynamic behaviors within the reactor core should be revealed. This is usually represented by a space-time dependent neutron diffusion equation with certain spatial dimensions. There is no doubt that the space and time dependent problem has two main issues: one is illustrated by the space dependent neutron diffusion process; the other by the time-varying characteristic. Essentially, the whole problem is performed in two steps. One is the spatial discretization of the neutron diffusion process in one time spot; the other is the time-integration of the dynamic values in each time spot. From review of [34], many time-integration techniques, such as  $\theta$  method, ADI method, stiffness confinement method, SSOR iterative method, Runge-Kutta method and linear matrix system solution method, etc., have been discussed. However, along with the rapid development of modern computing techniques, many systematic integration software packages are developed to solve the time-differential equations. For example, the MATLAB/SIMULINK software package represents a flexible environment to perform the time-differential or integral problems [35][36]. A variety of different numerical time-integration algorithms have been included into SIMULINK such that it is unnecessary to develop one's own routines for time-integration to obtain the transient results. Instead, it becomes logical to convert the space-time coupled problem into the space-only-dependent one and let MATLAB/SIMULINK solve the time-only-dependent

problem.

Thus, the space-time dependent neutron kinetic problem has turned into how to discretize the space and time factors in the diffusion equation. Usually, the spatial treatment methods can be categorized as follows: direct method, flux factorization method, and modal synthesis method [18][34][37]. The direct methods are characterized by the solution of time-evolution equations for a space-time discretization of the group flux. Flux factorization method involves a factorization of the space- and time- dependent flux into two parts: one part includes most of the time-dependent information, while the other part includes all of the space-dependent terms, but only slightly dependent on time. Furthermore, the modal synthesis method uses a similar methodology as in the flux factorization approach. However, the modal synthesis method approximates the time-dependent flux using a linear combination of predesigned time-independent spatial flux modes.

The direct methods can be divided into three main groups: finite difference method, coarse-mesh method, and nodal method. The finite difference method is the most straightforward one within the space-energy dependent dynamics approaches. It basically consists of representing the spatial and time differential operators by forms of the corresponding finite difference quotients. The space coordinate is discretized by superimposing a computational mesh, within which the material properties are treated as uniform. Coupled matrix equations for the values at discrete points on the mesh are



obtained by integrating the corresponding diffusion equations over volume elements surrounding each point. The spatial variation of the flux within each integration volume is approximated by a truncated Taylor series. The advantage of the finite difference method is that, for sufficiently small time steps it obtains the correct solution of the time-dependent diffusion equations. However, the disadvantage is that the computational time can be too long for practical applications, since usually the mesh structure can have hundreds of thousands of space-energy-time points to adequately describe the reactor dynamic model. Thus, computer codes based on this method are normally only applied as the benchmark for other approximate methods. The finite difference method has been used and validated in some codes, such as WIGGLE [38], TWIGLE [39], 3DKIN [40], DIF3D [41] and RFSP [42].

Under certain conditions, the reactor may be properly described by a model consisting of homogeneous regions that are relatively large, i.e. with dimensions significantly larger than the diffusion length. However, application of the finite difference method to these regions still requires a relatively fine mesh structure to maintain accuracy. To deal with this situation, coarse-mesh methods have been developed to solve problems with a mesh size larger than what the finite difference method uses. This method achieves reduction in discretization error by using higher-order approximations to the spatial variation of the variables within a mesh box. Thus, although this method cannot achieve the comparable simulation accuracy of the finite difference method, it often results in significantly

reduction in computational time and storage requirements. It is this advantage which makes this method very useful in many practical simulations. A coarse mesh reactor model is used to simulate the transient behavior of local and global pressurized water reactor (PWR) properties [43]. A demonstration has been performed in [44] to illustrate that the utilization of a coarse-mesh method represents a better performance than a fine-mesh method on CANDU reactor diffusion calculations.

Like the coarse-mesh method, the nodal method also uses a relatively large mesh structure to represent the multi-dimensional reactor kinetic equations. It also uses significantly less computer resources than the fine-mesh finite difference method. The basic idea of this method is to approximate the time-dependent flux distribution by non-overlapping flux branches in a set of spatial nodes. If only one node is employed and the initial flux distribution is adopted, the nodal method is efficiently reduced to the point kinetic reactor model. It is assumed that the macroscopic cross-sections are uniform within the volume of a node. This uniformity may be true, or may result from homogenizing a heterogeneous model. Neutron leakage between neighboring nodes leads to a coupling of the flux distribution within both nodes. This relationship is represented by a time-independent coupling coefficient. After this the neutronic kinetic problem implies the computation of the coupling coefficient. For example, in the Gross Coupling Method [45][46], the coupling coefficient for a node is defined as the ratio of the interface-integrated out-going partial current to the node-averaged flux. These parameters

are calculated based on the analysis of a fine-mesh reference condition. Therefore, if the analyzed condition closely resembles the reference condition, these coupling parameters may work properly. However, when the difference between both conditions is large, particularly in transient analysis, the coupling coefficients are often inappropriate. Thus, the coupling coefficients have to be selected to match different transients as much as possible. However, these processes add more complexity and computational burdens. Consequently, the nodal method is not applied in many reactor kinetic and safety investigations in practice. Despite these difficulties, the node method is still frequently used, particularly in simulations where the speed of execution is not of importance. A typical nodal coupling method is utilized in [47] to perform a 3-D neutronic simulation function. It delivered a significant performance, as compared to the computational burden of the conventional finite difference method. Similar approach is applied to a reactor training simulator, as reported in [48]. A 240-node core model, using a semi-implicit solution technique, has been developed to meet the need. The SI model has been tested with a range of transients and is found to provide excellent simulation efficiency. The conventional nodal methods have been extensively used in 3-D simulations in [49]. The execution reactor model is faster as compared to more elaborate nodal schemes and finite difference models, and is suitable for real-time simulators.

The space-time factorization method has been developed as a potential alternative to the complex fine-mesh direct method. This method is to factorize the time-dependent flux

distribution into the product of the time-only-dependent amplitude function and the space-only-dependent flux shape function. The motivation is that, in many conditions, the flux distribution-shape function changes very little with time. As a result, it may be unnecessary to recalculate the flux shape at each time step. In this way, this method can employ different time intervals for recalculations of time-amplitudes and flux shape functions. Computation time can be reduced by choosing larger time intervals between flux shape function recalculations instead of between time amplitudes recalculations. The accuracy of this method partially depends on the frequency of the flux shape recalculations. The time required to calculate the flux shape is relative long, and so this method is used predominantly in cases where the neutron flux distribution is slightly time-dependent. This approach is close to the point kinetic method. However, they differ in that the shape function within the point kinetic model never changes, while in the factorization model, the shape function is recalculated every period of intervals. For example, \*CERBERUS, the spatial kinetics module in RFSP, which is based on the improved factorization method, uses macro-intervals of 50ms to 100ms for the first few seconds to iterate the flux shape during the analysis of loss of a coolant accident (LOCA) of CANDU reactors [50].

The modal synthesis method is used to construct or to synthesize the space-, energy-, and time- dependent neutron flux, delayed neutron precursors and other dynamic variables by the time-weighted superposition of some flux modes. These flux modes are pre-calculated

and often taken from the eigenfunctions of a steady-state diffusion equation, or solutions of the diffusion equation in case of some specified set of core conditions. Then, the space-time dependent neutron diffusion problem becomes how to solve the time-dependent amplitudes. This significantly reduces online computational time. Although this method achieves the objective of reducing computational time and simplifies the numerical simulations, it often requires considerable experience to choose the number of flux modes, such that the desired accuracy can be ensured. Furthermore, the precision of the pre-calculated flux modes can also affect the simulation result to a certain extent.

Another benefit of the modal method is that, a simplified dynamic reactor model in the form of a system of ordinary differential equations, which is closely associated with the conventional control system design, can be derived from the diffusion reactor model. As it is known, a point kinetic reactor model can be directly employed to investigate reactor control problems due to its simple form and ordinary differential equation characteristic. However, this model cannot reflect the internal behavior of the reactor core, since it essentially assumes a time-invariant neutron flux distribution shape. Therefore, this model can be seen as a non-dimensional system that is often used to approximate the reactor gross dynamics, but only when the reactor internal dynamic variables are not important. In order to investigate the reactor internal variables and propose reactor control problems such as power control, the point kinetic model becomes inappropriate.

Thus, the description of neutron diffusion process within the core is required. From the above discussion on different numerical simulation methods, it can be seen that most of the direct methods, such as the finite difference method, coarse-mesh method, and nodal method, are still in the form of partial differential equations. Although some advanced modern control strategies, such as neural network intelligent control [51], are potentially able to deal with the partial differential equations, it is still far from being used in practical nuclear industry applications. Furthermore, even for the space-time factorization method, the recalculation of flux shape after each time interval also employs the finite difference method. Essentially, this method cannot be directly used for conventional control problems either. Thus, the modal method becomes a good choice, as it can represent a simplified reactor dynamic model in the form of ODEs. Furthermore, if the flux modes are prepared in a 3-D grid structure, this reactor model can also represent 3-D dynamic information within the reactor core. Another important point is that a simplified nodal reactor model can also be used for control problem design and analysis, if the reactor core is divided into several volumes and only the relationship among these volumes is studied. This type of reactor model has been employed in [13][14] to respectively establish the PHWR and CANDU reactor kinetic models. However, both works use a 14-coupled point kinetic reactor model to represent the reactor, which certainly cannot characterize the details within the reactor in a 3-D perspective. Another reactor kinetic model regarding Indian-based advanced heavy water reactor has been reported in [52], which is for control system design. After many calculations and

comparison of schemes, a 17-node reactor model is decided. However, this is still not comparable to a 3-D model.

For CANDU reactors, using the modal method, a hybrid approach is employed to simulate an early CANDU type reactor kinetics [53]. A flux mapping scheme based on a modal synthesis method has been used to reconstruct the 3-D power distribution in order to calibrate the spatial flux measurements [54].

## **2.6 Summary**

Some concepts of the reactor neutronic kinetics are summarized and fundamental principles are described. Particular attention has been paid to the diffusion approximation of 3-D space-time neutron behaviors. Several numerical methods used to solve 3-D space-time neutron diffusion equations are introduced and compared. The advantages and disadvantages for applying these methods in reactor modeling are highlighted. Based on the current research objective, modal synthesis method has been chosen for this study.

### **III 3-D neutronic kinetic model of CANDU reactors**

In this chapter, the structure and characteristic parameters of the CANDU reactor are described first. Then, a mathematical model based on the modal synthesis method is developed to represent the space-time dependent neutronic kinetics of CANDU reactors. The modal method expands the reactor dynamic variables including neutron flux, the concentration of delayed neutron precursors, and Iodine and Xenon concentrations to a time-weighted superposition of a series of neutron flux modes. The modes are chosen as eigenfunctions of the governing neutron diffusion equation at a steady-state condition. The typical characteristics, as well as the chosen mode number are discussed.

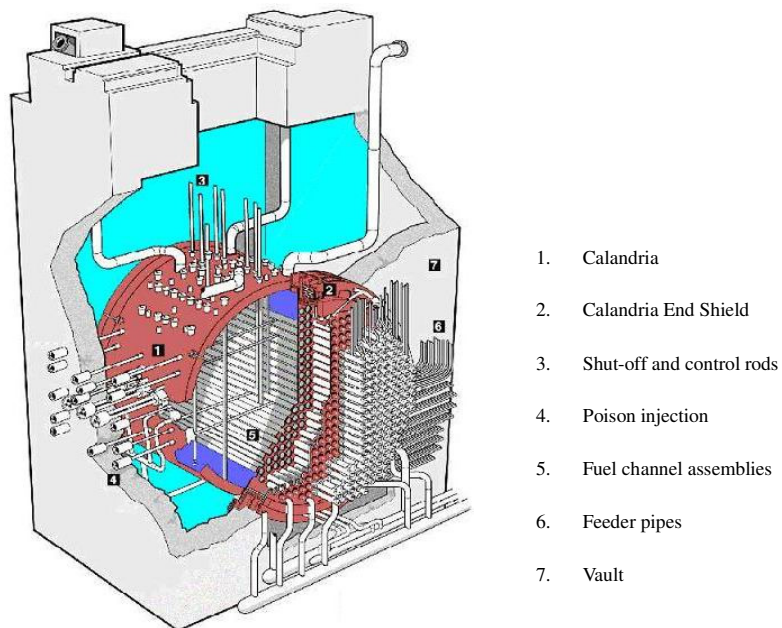
After this, the modeling procedure is presented in detail. Specific attention has been paid to compare the developed modal model and the 14-coupled point kinetic model in different perspectives. Furthermore, the vectorization technique is applied to explain the mathematic principles of the reactor modal model, which is implemented by the MATLAB/SIMULINK software environment. Subsequently, the initialization, as well as the steady-state operation, is illustrated. At the end of this chapter, a 3-D flux distribution of the reactor core under the steady-state condition is represented, which shows the 3-D characteristics of the reactor model.

#### **3.1 Brief description of CANDU-6 assembly**

A CANDU reactor consists of a horizontal cylindrical calandria vessel, which is filled



with heavy water ( $D_2O$ ) moderator, reflector and fuel channels [55]. For a 600 MW CANDU-6, there are 380 fuel channels in total. Each channel houses 12 fuel bundles, and heavy water is used as the coolant. Reactivity control mechanisms include adjuster rods, mechanical absorbers, liquid zone control absorbers and shut-off rods. A cut-away diagram of the CANDU reactor assembly is illustrated in Fig. 3.1. The detailed parameters of CANDU-6 are listed in Table 3.1. Because of a relatively large core size, the neutron flux at different location in the core can be significantly different. Consequently, a space-dependent 3-D representation of neutron flux distribution would be particularly significant for monitoring and control system design of the reactor.



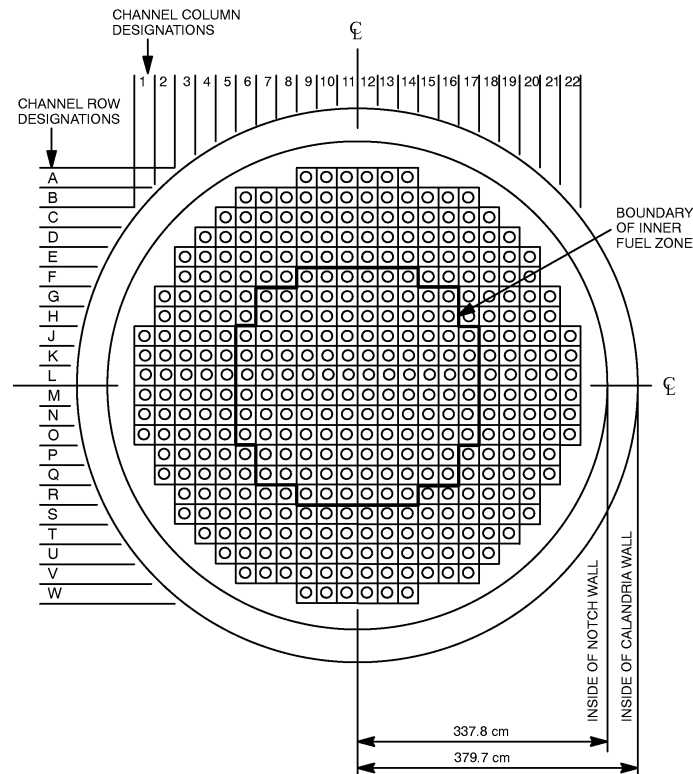
**Fig. 3.1 Diagram of CANDU reactor assembly [56]**

**Table 3.1 Gross features of the CANDU-6 reactor core [57]**

Fission Power	MW	2158.5
Reactor Radius	cm	379.7
Number of Fuel Channels		380
Channel Length	m	5.944
Square Lattice Pitch	cm	28.575
Fuel Bundle Design		37-element
Design Heat Rating	KW/m	4.2
Average Coolant Temperature	°C	288
Average Moderator Temperature	°C	69
Overall Form Factor		0.555
Xenon Override System		21 adjusters
Design Adjuster Worth	mk	15 (nominal)
Liquid Zone Control Rods		14 light water units
First Shutdown System		28 Shut off rods
Second Shutdown System		poison injection
Number of Flux Mapping Detectors		102
Basic Fuelling Scheme		8-bundle shift

Since the fraction of all produced neutrons absorbed in the fuel is high, CANDU is characterized by good neutron economy, with the utilization of natural uranium as fuel and heavy water as moderator and coolant, combined with ability to refuel the reactor online. In the reactor design, the fuel channels are arranged on a square lattice with a 28.575 mm pitch in Fig. 3.2. This is a near optimum geometry from a reactivity standpoint. A consequence of the particular lattice geometry used in the CANDU reactor is that the neutron energy spectrum is very well thermalized. The associated long migration length for neutrons and the long neutron lifetime have an important impact on

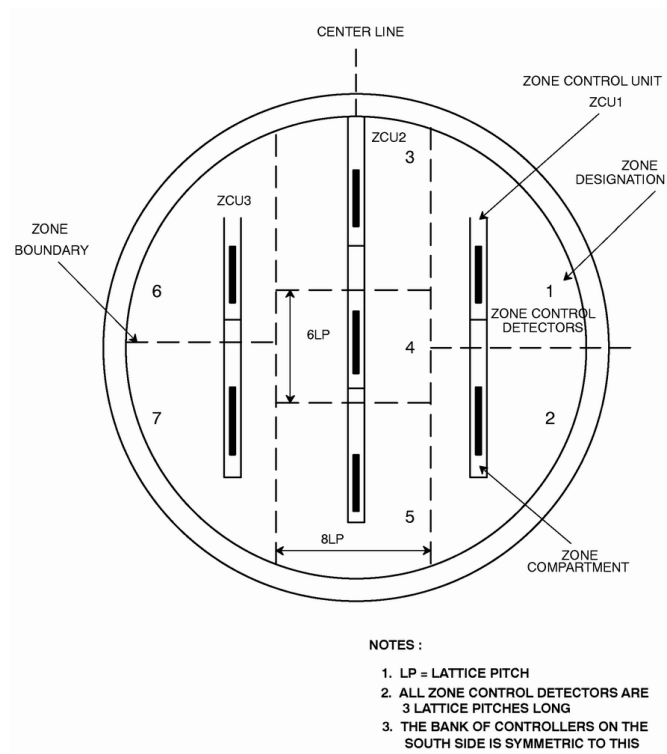
methods used in the reactor physics analysis and on the requirements for the shutdown systems.



**Fig. 3.2 End view of reactor showing principal calandria dimensions and fuel channels [57]**

The primary method for long-term reactivity control in CANDU is on-power refueling. For short-term reactivity global and spatial control, reactivity control devices are employed. They are liquid zone controllers, adjuster rods and mechanical control absorbers. For reactor safety controls, the shutoff rods are prepared. 14 liquid zone controllers separate the reactor core into 14 zones, as illustrated by Fig. 3.3, and operate to maintain a specified amount of reactivity in the reactor zones at a controllable rate. If the zone

control system is unable to do this, other reactivity control devices are called on. 21 adjuster rods are removed from the core for positive reactivity compensation. Negative reactivity is made up by 4 mechanical control absorbers. In addition, two special shutdown systems, SDS1 (28 shutoff rods) and SDS2 (6 poison-injection nozzles) can effectively independently shut down the reactor under postulated accident conditions.



**Fig. 3.3 Positions of zone control detectors in half core with respect to zone compartments [57]**

### 3.2 The diffusion description of CANDU reactor kinetics

An accurate description of the nuclear spatial kinetics of a reactor is given by the

Boltzman equation [18]. Neutron Transport Theory, which gives a rigorous description of the nuclear reactor kinetics, based on neutron movement, scattering, absorption and leakage, is generally inconvenient for simulation purposes. With some assumptions, it is possible to derive a simplified diffusion equation for the neutron flux. Some of these assumptions are, all neutrons have the same energy and all neutron scatters occur without change in neutron speed. The absorption and scattering properties of the core medium are assumed to be independent of the direction of incident neutrons. The macroscopic absorption cross section is assumed to contain a large time and space varying term determined by the concentration of  $Xe^{135}$  and a constant term which represents the absorption of the calandria material and the fuel. In this way, Diffusion Theory, which removes the directional dependency, is very useful to provide a set of diffusion equations to describe the neutron diffusion processes.

In a CANDU reactor, because the core is relatively large, it is assumed that there are no gross discontinuities. Therefore, the neutron scattering dominates the absorption cross-section. In the neutronic energy spectrum, CANDU reactor is well thermalized, since 95% of the neutrons in the moderator are thermal neutrons [58]. Thus, the neutron diffusion equation with a single energy group is sufficient to describe neutron behaviors in this case. A detailed set of thermal diffusion equations to describe CANDU reactor kinetics is shown in Eqns. (3-1) to (3-4).

$$\frac{1}{v} \frac{\partial}{\partial t} \phi(r,t) = D \nabla^2 \phi(r,t) + (1 - \beta) v \Sigma_f \phi(r,t) + \sum_j^J \lambda_j C_j(r,t) - \Sigma_a \phi(r,t) - \sigma_{aX} (X(r,t) - X^s(r)) \phi(r,t) \quad (3-1)$$

$$\frac{\partial}{\partial t} C_j(r,t) = -\lambda_j C_j(r,t) + \beta_j v \Sigma_f \phi(r,t) \quad (3-2)$$

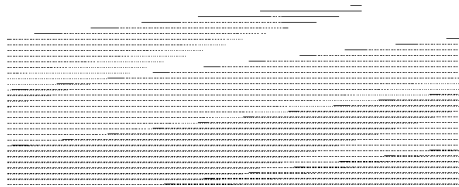
$$\frac{\partial}{\partial t} I(r,t) = -\lambda_I I(r,t) + \gamma_I \Sigma_f \phi(r,t) \quad (3-3)$$

$$\frac{\partial}{\partial t} X(r,t) = -\lambda_X X(r,t) + \gamma_X \Sigma_f \phi(r,t) + \lambda_I I(r,t) - \sigma_{aX} X(r,t) \phi(r,t) \quad (3-4)$$

where  $v$  is neutron velocity;  $\phi$  is prompt neutron flux;  $r$  is spatial vector in the core;  $t$  is time variable;  $D$  is diffusion coefficient;  $\nabla$  is gradient operator;  $\beta$  and  $\beta_j$  are respectively total and delay group fission fractions;  $v$  is fission yield (neutrons/fission);  $\Sigma_f$  and  $\Sigma_a$  are respectively macroscopic fission and absorption cross-section;  $J$  is number of delayed groups;  $\lambda_j$ ,  $\lambda_I$  and  $\lambda_X$  are respectively delayed neutron group, Iodine and Xenon decay constants;  $C_j$  is delayed neutron precursor concentration;  $\sigma_{aX}$  is Xenon microscopic absorption cross-section;  $X$  is  $\text{Xe}^{135}$  concentration;  $X^s$  is some reference steady-state concentration of  $\text{Xe}^{135}$  (It should be noted that the absorption term  $\Sigma_a$  includes the absorption due to  $X^s$ );  $\gamma_I$  and  $\gamma_X$  are respectively direct fission yields of  $\text{I}^{135}$  and  $\text{Xe}^{135}$ .

Among all the variables in the above equations, an important one is the spatial vector  $r$ . Fig. 3.4 shows the coordinate used in this thesis. The orientation of the coordinate system is such that the  $x$ - $y$  plane coincides with the reactor face and the  $z$ -axis is the central axis, which is parallel to fuel channels. The origin of the coordinate is located in the center of

the face plane. Then, the spatial coordinate  $r$  is represented by  $(x, y, z)$ . By using this coordinate, the reactor model is discretized into a 3-D array of meshes.



**Fig. 3.4 The coordinate for CANDU reactor modeling,  $r = (x, y, z)$**

### **3.3 Modal modeling of CANDU reactors**

The modal synthesis method is to synthesize the reactor kinetic variables, including neutron flux, concentrations of delayed neutron precursors, Xenon and Iodine, in terms of sum of the time-weighted steady-state neutron flux modes. The neutron flux modes are 3-D flux distributions within the reactor core. By including time as a weighting parameter, this method provides time-dependent 3-D representation of variables in the reactor core.

The modeling process of CANDU reactor kinetics refers to the neutronic kinetic model in SMOKIN [59]. The SMOKIN family is a collection of codes developed for simulating the space-time kinetics behavior of CANDU-PHW reactors and for the reactor safety analysis. The time-scale can range from milliseconds (for accident analysis) to hours or

days (for analysis of refueling transients).

Under the modal expansion approximation, the space-time dependent variables are expanded in terms of separate space- and time-dependent functions, which are called mode shapes and modal amplitude functions respectively.

$$\phi(r,t) = \sum_{i=1}^M \psi_i(r) n_i(t) \quad (3-5)$$

$$C_j(r,t) = \frac{1}{\nu} \sum_{i=1}^M \psi_i(r) C_{ij}(t) \quad (3-6)$$

$$I(r,t) = \frac{1}{\nu} \sum_{i=1}^M \psi_i(r) I_i(t) \quad (3-7)$$

$$X(r,t) = \frac{1}{\nu} \sum_{i=1}^M \psi_i(r) X_i(t) \quad (3-8)$$

where  $\psi_i(r)$  is the normalized spatial flux mode  $i$ ;  $M$  is the number of the modes selected;  $n_i(t)$  is the amplitude of the thermal neutron flux for mode  $i$ ;  $C_{ij}(t)$  is the mode  $i$  amplitude of delayed neutron group  $j$ ;  $I_i(t)$  is the amplitude of Iodine for mode  $i$ ;  $X_i(t)$  is the amplitude of Xenon for mode  $i$ .

### 3.3.1 3-D neutron flux harmonic modes in CANDU reactors

The spatial mode functions  $\psi_i(r)$  are generated under the steady-state conditions (typically, a time-averaged equilibrium core with all adjusters inserted, all zone controllers at average fill, and all control absorbers and shut-off rods withdrawn). These modes can be



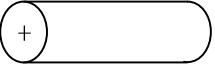
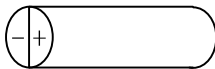
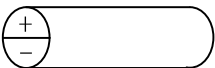
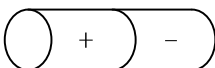

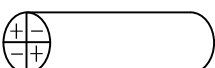
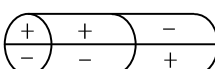
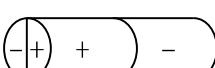
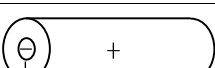
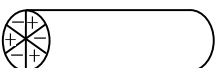
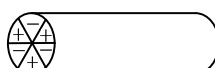
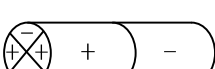
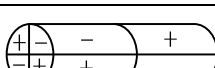
referred to the eigenfunctions of the following static diffusion equation, i.e.

$$(-D\nabla^2 + \Sigma_a)\psi_i(r) = \frac{1}{k_i}(\nu\Sigma_f)\psi_i(r) \quad (3-9)$$

In Eqn. (3-9), each spatial eigenfunction  $\psi_i(r)$  has an associated eigenvalue  $k_i$ .

The flux modes are referred to  $\lambda$  harmonics [60]. Using 3-D finite-difference methods, the reactor core can be discretized into meshes and the neutron diffusion equation can be solved over the reactor core. Reactor physics analysis code MONIC is used to calculate the modes [61]. MONIC employs an iterative procedure to generate the harmonic modes. Starting from a fundamental flux distribution that corresponds to a nominal reference core configuration, each harmonic mode of the diffusion equation can be generated by removing all components of previously calculated flux modes from the flux distribution. The detailed information of 13 primary flux mode shapes and their corresponding characteristics is represented in Table 3.2. Two practical simulated time-amplitudes under load following conditions when the reactor power is 0.92 FPU (full power unit) or 0.98 FPU, are selected for each mode, which is also arrayed in the last two columns of the table. Their corresponding 3-D flux distributions are respectively illustrated in Appendix A.

**Table 3.2 Neutron flux harmonic modes  $\psi_i(r)$  (CANDU-6 type),  $i = 1$  to 13 and their respective characteristics**

Mode No.	Designation	Shape	Eigenvalue ( $k_i$ )	Subcriticality (mk)	Amplitudes (0.92FPU)	Amplitudes (0.98FPU)
1	Fundamental		1.000000	0	0.92	0.98
2	1st Azimuthal(1)		0.987450	-12.7095	$2.37 \times 10^{-3}$	$-2.68 \times 10^{-5}$
3	1st Azimuthal(2)		0.987128	-13.0398	$5.01 \times 10^{-3}$	$1.44 \times 10^{-5}$
4	1st Axial		0.975457	-25.1605	$1.0 \times 10^{-3}$	$2.03 \times 10^{-5}$
5	2nd Azimuthal(1)		0.966940	-34.1903	$3.65 \times 10^{-5}$	$1.04 \times 10^{-6}$
6	2nd Azimuthal(2)		0.965614	-35.6105	0	0
7	1st Axial/1st Azimuthal(1)		0.960025	-41.6395	$-3.9 \times 10^{-4}$	$-1.4 \times 10^{-5}$
8	1st Axial/1st Azimuthal(2)		0.960015	-41.6504	$5.8 \times 10^{-4}$	$1.66 \times 10^{-5}$
9	1st Radial		0.950995	-51.5302	$5.3 \times 10^{-4}$	$8.78 \times 10^{-6}$
10	3rd Azimuthal (1)		0.939464	-64.4367	$< O(10^{-4})$	$< O(10^{-6})$
11	3rd Azimuthal (2)		0.939431	-64.4741	$< O(10^{-4})$	$< O(10^{-6})$
12	1st Axial / 2nd Azimuthal (1)		0.939061	-64.8935	$< O(10^{-4})$	$< O(10^{-6})$
13	1st Axial / 2nd Azimuthal (2)		0.93883	-65.1556	$< O(10^{-4})$	$< O(10^{-6})$

It is important to point out that these harmonic modes are time-independent. There are many pre-calculated neutron flux modes available. The number of modes chosen in a given application depends on the application itself. A simple rule of thumb is that the number of modes should be high enough such that the static reactivity worth of the dominant reactivity control devices are adequately represented by the selected mode shapes. Of course, more mode shapes will improve the modeling accuracy. However, they will also increase the computational load. As it can be seen from Table 3.2, the subcriticality increases from low order mode to high order mode and particularly from mode 10 on, the spatial effect of the flux mode has been significantly highlighted by the distribution shapes in the third columns. Regarding this, there are two main issues concerned by the research.

a) Table 3.3 represents different reactivity devices with their functions and total reactivity worth. For the purpose of power regulating in load following cases of the current research, adjuster rods are fully inserted; mechanical absorbers are fully withdrawn; and only liquid zone controllers (LZCs) are manipulated in order to regulate the reactor bulk and zonal powers. It can be seen that the total reactivity worth of LZCs is 7 mk, which indicates that it is hard to trigger the high-order modes having big subcriticality if they are used.

**Table 3.3 Reactivity devices with their total reactivity worth**

Function	Reactivity Devices	Total Reactivity Worth (mk)
Control	14 Zone Controllers	7
Control	21 Adjusters	15
Control	4 Mechanical Control Absorbers	-10
Control	Moderator Poison	-15
Safety	28 Shutoff Units	-80
Safety	6 Poison-Injection Nozzles	-300

b) Since the spatial effect of the flux modes after mode 9 has been highlighted, the higher order modes are mainly used to dispose the simulations with large local reactivity perturbations. Although 14 liquid zone controllers are used to regulate the reactor bulk and spatial power, the dynamic process of power regulating is relatively slow and smooth, and particularly, the spatial effect of each zone controller results in reactivity perturbations in large volumes of the core. As far as this issue is concerned, the high order modes may not contribute too much.

The objective is to ensure the most accurate representation of the core kinetics, while keeping number of modes being minimal for computational efficiency. To examine closely the contributions of each mode to the overall subcriticalities, the amplitudes of

each mode under two power conditions (0.92FPU and 0.98FPU) are shown in two right columns of Table 3.2. As can be seen, the associated amplitude decreases as it moves to higher order modes. To be more specific, the amplitude associated with modes higher than 9<sup>th</sup> is so small that they would not contribute significantly to the accuracy of the model, but to add additional complexity in the modeling process.

Therefore, the first 9 modes are chosen to represent a balance between the required modeling accuracy and the computational complexity. It should be mentioned that the methodology presented in this research does not preclude use of additional modes, if deemed necessary.

A very important property for the thermal-group flux harmonic modes is bi-orthogonality, i.e.

$$\begin{aligned} \int_V \psi_k(r) C \psi_m(r) dr &= 0, k \neq m \\ \int_V \psi_k(r) C \psi_m(r) dr &\neq 0, k = m \end{aligned} \quad (3-10)$$

where  $C$  represents the physical property which is uniformly distributed across the reference reactor core.  $V$  is the volume of the reactor core. Eqn. (3-10) can also be written in a short notation as

$$\begin{aligned} \langle \psi_k | C | \psi_m \rangle &= 0, k \neq m \\ \langle \psi_k | C | \psi_m \rangle &\neq 0, k = m \end{aligned} \quad (3-11)$$

This bi-orthogonality allows us to separate the time-independent and space-dependent mode shapes from the time-varying and space-independent amplitude functions. Since the physical property constant is relatively uniform across the entire reactor core, the orthogonality property can be extended to the entire reactor (including core and reflector), given by

$$\langle \psi_k | \psi_m \rangle_{reactor} \ll \langle \psi_m | \psi_m \rangle_{reactor}, k \neq m \quad (3-12)$$

### 3.3.2 Modeling procedure for 3-D modal representations

Using the modal expansion equations (3-5) to (3-8) and the unique properties of flux modes, the diffusion Eqns. (3-1) to (3-4) in the form of PDE are converted to the modal kinetic equations in the form of ODE. This will bring convenience to investigation of conventional control problems.

Applying the bi-orthogonality properties of the modes as represented in Eqns. (3-11) and (3-12), substituting the above mode expansion Eqns. (3-5) to (3-8) into the reactor diffusion Eqns. (3-1) to (3-4), multiplying them throughout by the spatial mode function  $\psi_k(r) (k \in [1, M])$  and integrating over the reactor volume, the following dynamic equations illustrating CANDU reactor kinetics can be obtained.

$$\frac{dn_k(t)}{dt} = \frac{\rho_{sck} - \beta}{l_k^*} n_k(t) + \frac{1}{l_k^*} \sum_{i=1}^M (\rho_{ki} + \rho_{ki}^X) n_i(t) + \sum_j^J \lambda_j C_{kj}(t) \quad (3-13)$$

$$\frac{dC_{kj}(t)}{dt} = \frac{\beta_j}{l_k^*} n_k(t) - \lambda_j C_{kj}(t) \quad (3-14)$$

$$\frac{dI_k(t)}{dt} = \frac{\gamma_I}{\nu l_k^*} n_k(t) - \lambda_I I_k(t) \quad (3-15)$$

$$\frac{dX_k(t)}{dt} = \frac{\gamma_X}{\nu l_k^*} n_k(t) + \lambda_I I_k(t) - \lambda_X X_k(t) - \sigma_X \phi_f \sum_{i=1}^M \sum_{m=1}^M A_{kim} X_m(t) n_i(t) \quad (3-16)$$

where  $\rho_{sck}$  is the subcritical reactivity of mode  $k$ , defined as

$$\rho_{sck} = 1 - \frac{1}{k_k} \quad (3-17)$$

The detailed derivation of the reactor dynamic Eqns. (3-13) to (3-16) is presented in Appendix B.

$l_k^*$  is the prompt neutron generation time for  $k^{\text{th}}$  mode, defined as

$$l_k^* = \frac{\left\langle \psi_k \left| \frac{1}{\nu} \right| \psi_k \right\rangle}{\left\langle \psi_k \left| \nu \Sigma_f \right| \psi_k \right\rangle} \approx \Lambda \quad (3-18)$$

$\Lambda$  is the prompt neutron generation time.

With the following definition of the neutron loss operator and the neutron production operator,

$$R(r,t) = \nabla D \nabla - \Sigma_a(r,t) \quad (3-19)$$

$$F(r,t) = \nu \Sigma_f(r,t) \quad (3-20)$$

the modal cross coupling reactivity between  $k^{\text{th}}$  and  $m^{\text{th}}$  modes due to the perturbation  $[\Delta R(r) + \Delta F(r)]\delta(r)$  within a certain area  $\delta(r)$  can be obtained as

$$\rho_{ki} = \frac{\langle \psi_k | [\Delta R(r) + \Delta F(r)] \delta(r) | \psi_i \rangle}{\langle \psi_k | F_0 | \psi_k \rangle} \quad (3-21)$$

where  $F_0$  is the steady-state reference neutron production operator.

$\phi_f$  is the flux-squared weighted fundamental mode for the fuel flux, defined as

$$\phi_f = \frac{\langle \psi_1 | \psi_1 | \psi_1 \rangle_f}{\langle \psi_1 | \psi_1 \rangle_f} \quad (3-22)$$

$A_{kim}$  is the coupling volume integration of all the modes, defined as

$$A_{kim} = \frac{\langle \psi_k | \psi_i | \psi_m \rangle_f}{\langle \psi_k | F_0 | \psi_k \rangle_f \phi_f} \quad (3-23)$$

$\rho_{ki}^X$  is the modal reactivity reflecting Xenon effect build-up, defined as

$$\rho_{ki}^X = -\sigma_X \phi_f l_k^* \sum_{m=1}^M A_{kim} (X_m(t) - X_m^s) \quad (3-24)$$

Analog to Eqn. (3-8),  $X_m^s$  in Eqn. (3-24) can be defined by



$$X^s(r) = \frac{1}{v} \sum_{i=1}^M \psi_i(r) X_i^s \quad (3-25)$$

In order to accelerate the numerical simulation and reduce computational costs, some parameters such as  $l_k^*$ ,  $\rho_{ki}$ ,  $\phi_f$  and  $A_{kim}$  are prepared off-line. The reactivity of each reactivity device, such as liquid zone controllers or adjuster rods, is modeled as a function of its related position. Reactivity data corresponding to designated positions are prepared. Then, the reactivity for an unknown position is linearly interpolated by the reactivity data series.

### **3.4 Comparison of coupled point kinetic and modal synthesis models**

#### **3.4.1 Modeling of CANDU reactor kinetics by a coupled point kinetic method**

The coupled point kinetic model of CANDU reactor kinetics described in [14] is similar to the model considered in [13]. The modeling process starts with a two energy-group diffusion equation. As far as the geometric structure is concerned, a simplified nodal method is used. Each of the 14 zones is treated as one big node of the model. Since 14 discretized nodes are utilized to represent the spatial information, the continuous spatial coordinate  $r$  is removed from Eqns. (3-1) to (3-4). Thus, point kinetic model can then be used to describe each zone's dynamic behavior. The neutron diffusion between adjacent zones is characterized by the reactivity coupling coefficients. This simplified nodal reactor model has only 14 nodes. Essentially, it is not the widely recognized nodal model. To be distinguished, this is named as "14-coupled point kinetic model".

With the simplified two-group diffusion theory, the neutronic kinetics in zone  $i$  can be represented by the following equations [14].

$$l \frac{d\hat{P}_i}{dt} = (\rho_i - \beta) \hat{P}_i - \sum_{j=1}^Z \alpha_{ij} \hat{P}_j + \sum_{j=1}^Z \eta_{ji} \hat{P}_j + \sum_{h=1}^{m_d} \beta_h \hat{C}_{hi} \quad (3-26)$$

$$\frac{d\hat{C}_{hi}}{dt} = \lambda_h (\hat{P}_i - \hat{C}_{hi}) \quad (3-27)$$

where,  $l$  is the prompt neutron life time;  $i$  and  $j$  are indices of the cells;  $\hat{P}_i$  is a nondimensionalized variable to represent the power in zone  $i$ ;  $\rho_i$  is the net reactivity of zone  $i$ ;  $\beta$  and  $\beta_h$  are respectively the total and the delay group fission fractions;  $Z$  is the number of the zones making up the entire reactor (in this case, 14);  $\alpha_{ij}$  is the coupling coefficient between zone  $i$  and zone  $j$ ;  $\eta_{ji}$  is the element of a modified coupling coefficient defined as  $\eta_{ji} = \alpha_{ji} \frac{P_{j,r}}{P_{i,r}}$ , where  $P_{i,r}$  and  $P_{j,r}$  respectively represent the referenced power in zone  $i$  and  $j$ ;  $\hat{C}_{hi}$  is a nondimensionalized variable of the delayed neutron precursor concentration;  $m_d$  is the number of groups of the delayed neutron precursors;  $\lambda_h$  is the delay neutron group decay constant.

Similarly, the kinetics for Iodine and Xenon build-up can be described by Eqns. (3-28) to (3-30).

$$\frac{d\hat{I}_i}{dt} = \lambda_I (\hat{P}_i - \hat{I}_i) \quad (3-28)$$

$$\frac{d\hat{X}_i}{dt} = \frac{\lambda_x + c_x}{\gamma_I + \gamma_X} (\gamma_X \hat{P}_i + \gamma_I \hat{I}_i) - (\lambda_x + c_x \hat{P}_i) \hat{X}_i \quad (3-29)$$

$$\rho_{X,i} = -\frac{\Sigma_{fi}}{\Sigma_{ai}} \cdot \frac{(\gamma_I + \gamma_X) \bar{\sigma}_{Xi} P_{i,r}}{\lambda_x + \bar{\sigma}_{Xi} P_{i,r}} \hat{X}_i \quad (3-30)$$

where,  $\hat{X}_i$  and  $\hat{I}_i$  are nondimensionalized Xenon and Iodine concentrations in zone  $i$ ;  $\lambda_x$  and  $\lambda_I$  are the Xenon and Iodine decay constants;  $\gamma_I$  and  $\gamma_X$  are the direct fission yields of the Iodine and Xenon;  $c_X$  is a new parameter defined as  $c_X = \frac{\epsilon \sigma_{aX}}{E_f \Sigma_f}$ ;  $\epsilon$  is the averaged reactor power density;  $\sigma_{aX}$  is the microscopic absorption cross-section of Xenon;  $E_f$  is the energy released per fission;  $\Sigma_f$  is the macroscopic fission cross-section;  $\rho_{X,i}$  is the Xenon load reactivity;  $\Sigma_{fi}$  and  $\Sigma_{ai}$  respectively are the macroscopic fission and absorption cross-sections in zone  $i$ ;  $\bar{\sigma}_{Xi}$  is the scaled Xenon absorption cross-section for zone  $i$ , defined as  $\bar{\sigma}_{Xi} = \frac{\sigma_{aX}}{E_f \Sigma_{fi} V_i}$ ;  $V_i$  is the volume of zone  $i$ .

### 3.4.2 Comparison of two reactor models

In order to further illustrate the difference between the 14-coupled point kinetic and the modal synthesis modeling approaches, both models are compared in the framework of CANDU reactor kinetic representations. Several aspects have been considered: assumptions, advantages, limitations, and complexity. At the end of this section, graphic illustrations of the core models are used to highlight the difference between these two approaches. Additional comparisons have been made in a closed-loop environment under

different reactor operating modes in Chapter IV by using the RRS simulation platform.

- o The coupled point kinetic model developed in [14] is based on a simplified nodal method. The point kinetic approach is motivated by the assumption that the neutron flux distribution shape within a vicinity of a chosen region does not change with time. The dynamic characteristics in the entire region can then be approximated by that of a point. In [14], the core of a CANDU-6 reactor has been divided into 14 homogeneous zones. One point kinetic model is used for each zone. All physics properties within a single zone are assumed to be identical. Hence, the spatial information is lost within the zone. In the modal synthesis approach, the entire reactor is considered as a single unit. The flux distribution at any point in the core can be represented as a time-spatial function. The essence of the modal synthesis method is to decouple the time and spatial variables by defining a number of time-independent, but space-dependent, flux mode shapes, and then to develop a time-dependent, but space-independent, weighting functions for those modes. Theoretically, the number of mode shapes can be infinite. However, in a practical reactor, one can select a number of dominant modes and truncate minor ones without causing significant error in the model. As shown in Section 3.3.1, these modes can be calculated as the eigenfunctions of the steady-state diffusion equation. These modes are

space-dependent to provide basic functions in 3-D representation of the flux distribution throughout the core. Once the flux modes are determined, the issues in reactor modeling become determination of suitable time-dependent weighting functions. In summary, these two modeling techniques approach the same problem from different perspectives based on distinctive assumptions.

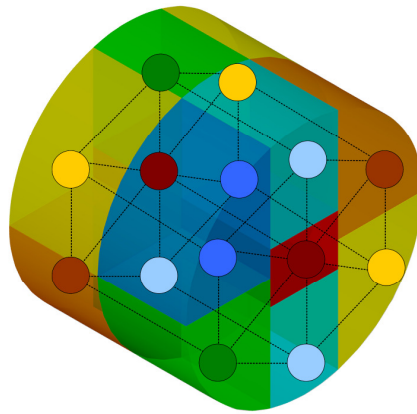
- o The concept of a point kinetic model is easy to understand. By dropping the spatial parameter, the analysis is simplified significantly. This technique has proved to be very useful in situations where the modeling of the detailed flux distribution within the core is not the main consideration. On the other hand, a modal synthesis model is capable of providing detailed 3-D spatial-mesh description of the reactor kinetics throughout the entire core. Meanwhile, by calculating the mode shapes off-line, the computational complexity of this modeling approach is comparable to that of a point kinetic model. The advantage of modal synthesis method becomes even more attractive, if multiple point kinetic models are employed as in [14].
  
- o A vital limitation of the 14-coupled point kinetic model is its inability to represent spatial dynamic flux distribution. One way to deal with such a limitation is to increase the number of nodes, which increases the

computational complexity. Nevertheless, one can only have a finite number of nodes. In the modal synthesis approach, this problem does not exist. In fact, this issue has been transferred to the way of calculating the mode shape functions off-line.

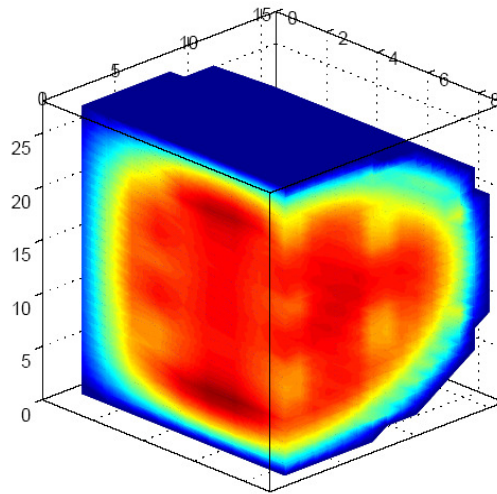
- o Considering 6-group delayed neutron precursors, 9 equations will be used to describe the reactor neutronic kinetics including neutron flux, 6-group delayed neutron precursors, Xenon and Iodine. If a point kinetic method is used to model each of 14 zones, the total number of the equations is  $14 \times 9 = 126$ . In the mean time, if the modal synthesis method is used with 9 flux modes for each kinetic equation, the total number of equations amounts to  $9 \times 9 = 81$ . The high dimensionality certainly increases the computational burden of the method. However, the number of equations employed in the modal synthesis method is less than that of the multiple point kinetic method (assuming 14 zones). Generally speaking, the simulation of the modal synthesis model is still more complicated than that of the point kinetic model due to mode calculations. For the problem considered in this research, the computational loads of the two techniques are comparable.

The concept based on the coupled point kinetic model can be illustrated in Fig. 3.5, where it shows that a CANDU reactor core is divided into 14 zones. For illustration purpose,

each zone is designated with a specific color and a point kinetic equation is used to model its neutron flux dynamics. As shown, each zone of the core is considered as a big node. Then the spatial information within the zone is lost. For comparison purposes, a cut-away diagram of the flux distribution in the core simulated using the 3-D modal synthesis is shown in Fig. 3.6. In contrast, the modal synthesis approach results in a much more detailed description of the flux distribution.



**Fig. 3.5 An illustrative diagram of core modeling using point kinetic equations**



**Fig. 3.6 An example of flux distribution modeled by the modal synthesis method**

### **3.5 Vectorization and implementation within a SIMULINK environment**

Technically speaking, evaluation of the accuracy of the 3-D models can be carried out by using any programming language. Because the MATLAB/SIMULINK environment has widely been used for dynamic system simulation and control system designs, this simulation tool is chosen in the current study. Added advantages of using MATLAB/SIMULINK environment are rich data manipulation tools, and various control system design and analysis toolboxes. The program also allows vectorization of multi-dimensional variables for dynamic manipulation, such as integrations, which simplifies the implementation of 3-D reactor core model considerably.

To implement the simulation platform for the modal synthesis reactor model, if the individual equation is solved one by one, there will be 81 coupled equations. For each





$$\begin{aligned}
\frac{d}{dt} \begin{bmatrix} C_{11} \\ \vdots \\ C_{16} \\ \vdots \\ C_{91} \\ \vdots \\ C_{96} \end{bmatrix}_{54 \times 1} &= - \begin{bmatrix} \lambda_1 & & & \\ & \ddots & & \\ & & \lambda_6 & \\ & & & \ddots \\ & & & & \ddots \\ & & & & & \lambda_6 \end{bmatrix}_{54 \times 54} \begin{bmatrix} C_{11} \\ \vdots \\ C_{16} \\ \vdots \\ C_{91} \\ \vdots \\ C_{96} \end{bmatrix}_{54 \times 1} \\
+ \frac{1}{\Lambda} & \begin{bmatrix} \beta_1 \\ \vdots \\ \beta_6 \\ \vdots \\ \beta_1 \\ \vdots \\ \beta_6 \end{bmatrix}_{54 \times 9} \begin{bmatrix} n_1 \\ \vdots \\ n_9 \end{bmatrix}
\end{aligned} \tag{3-32}$$

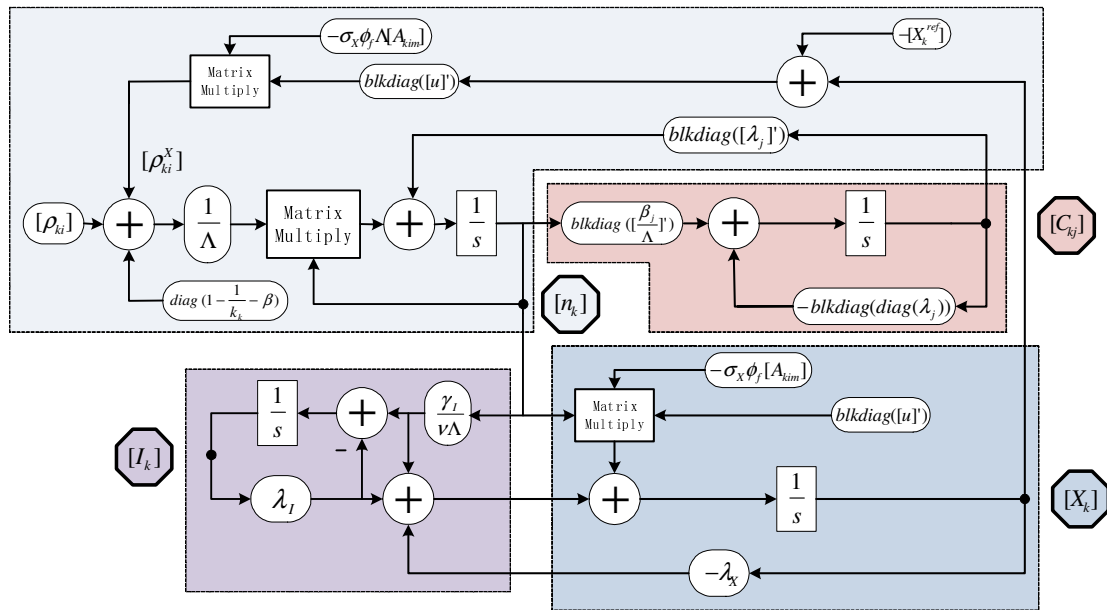
$$\frac{d}{dt} \begin{bmatrix} I_1 \\ \vdots \\ I_9 \end{bmatrix} = -\lambda_I \begin{bmatrix} I_1 \\ \vdots \\ I_9 \end{bmatrix} + \frac{\gamma_I}{v\Lambda} \begin{bmatrix} n_1 \\ \vdots \\ n_9 \end{bmatrix} \tag{3-33}$$

$$\begin{aligned}
\frac{d}{dt} \begin{bmatrix} X_1 \\ \vdots \\ X_9 \end{bmatrix} &= -\lambda_X \begin{bmatrix} X_1 \\ \vdots \\ X_9 \end{bmatrix} + \lambda_I \begin{bmatrix} I_1 \\ \vdots \\ I_9 \end{bmatrix} + \frac{\gamma_X}{v\Lambda} \begin{bmatrix} n_1 \\ \vdots \\ n_9 \end{bmatrix} \\
-\sigma_X \varphi_f & \begin{bmatrix} [A_{111} \cdots A_{119}] & \cdots & [A_{191} \cdots A_{199}] \\ \vdots & \ddots & \vdots \\ [A_{911} \cdots A_{919}] & \cdots & [A_{991} \cdots A_{999}] \end{bmatrix}_{9 \times 81} \begin{bmatrix} X_1 \\ \vdots \\ X_9 \end{bmatrix}_{81 \times 9} \begin{bmatrix} n_1 \\ \vdots \\ n_9 \end{bmatrix}
\end{aligned} \tag{3-34}$$

From the perspective of control engineering, the above set of equations can be represented in the form of state-space equations. The modal method has transformed the partial differential equations into ordinary differential equations. However, as it can be

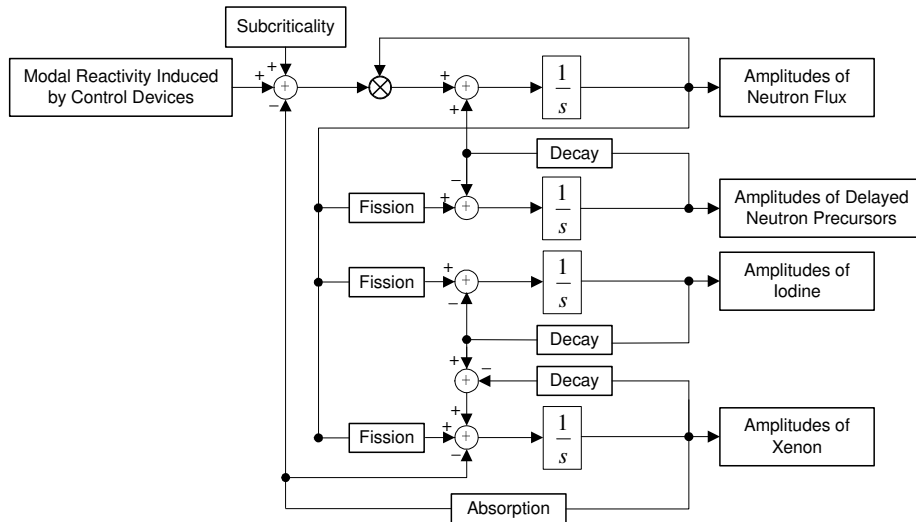
seen from Eqns. (3-31) to (3-34), they are still nonlinear dynamic equations. How to use this nonlinear reactor kinetic model to develop advanced control systems will be discussed in Chapter V. This reactor kinetic model can be simulated in SIMULINK environment. Modal reactivity matrices in response to the positions of reactivity devices, as well as data used to calculate Xenon modal reactivity, are pre-calculated and stored in the initialization file.

With the definition of vectors and matrix gains completed, the reactor model can be implemented. A block diagram representing models in Eqns. (3-31) to (3-34) is shown in Fig. 3.7. This diagram can be divided to four sub-sections as the shaded areas. For easy reference, the order of the shaded areas from top-down and left-right corresponds to Eqns. (3-31) to (3-34) respectively. Within each shaded area, it can be seen that the variables are collected to form vectors for matrix calculations. As shown, only four integrators are needed to implement this reactor model. The corresponding SIMULINK module of the reactor model implementation is represented in Appendix C-2.



**Fig. 3.7 Block diagram of the reactor model using modal synthesis method**

A generic block diagram for implementation of the reactor model based on Eqns. (3-31) to (3-34) is illustrated in Fig. 3.8. This block diagram is applicable to both the 14-coupled point kinetic and the 3-D modal synthesis models. The difference is that, in the former model, the reactivity change in each of the 14 zones directly contribute to the reactor dynamic variables, while in the modal synthesis model, the modal coupled reactivity change causes dynamic change in amplitudes of the fundamental modes. Recalling the reactor diffusion Eqns. (3-1) to (3-4), the dynamics of the neutron flux, delayed neutron precursor concentration, Iodine, Xenon are coupled through the internal feedbacks. The reactivity change initiated by the control devices affects the reactor power.



**Fig. 3.8 A generic block diagram for implementation of the reactor model**

### 3.6 Initialization and steady-state solution

Before performing transient simulations, the initial variables in the model must satisfy the steady state conditions. The initial condition for the transient analysis is a critical steady-state core configuration corresponding to a given components of the reactivity devices and initial Xenon distribution. The reference condition in this thesis is designated to be 1.0 FPU steady-state operation, which is called the fundamental condition. The flux distribution of the starting point adopts the fundamental mode.

Applying the fundamental condition to Eqn. (3-5), since the first harmonics  $\psi_1(r)$  is the fundamental flux mode, the initial amplitudes of flux modes  $[n_1, n_2, \dots, n_9]^T$  can be designated to be  $[1, 0, \dots, 0]^T$ , i.e.

$$\begin{bmatrix} n_1 \\ n_2 \\ \vdots \\ n_9 \end{bmatrix} = \begin{bmatrix} 1 \\ 0 \\ \vdots \\ 0 \end{bmatrix} \quad (3-35)$$

If the steady state power level is not at 1.0 FPU, the initial amplitudes of the neutron flux can be scaled to a certain percentage of the amplitudes used in the 1.0 FPU fundamental manipulations. The appropriate scaling factor refers to the performed steady-state power levels.

Substituting Eqn. (3-35) into Eqns. (3-32) and (3-33) under the steady-state condition, it yields the initial time-amplitudes of the delayed precursors' concentration and the Iodine concentration, i.e.

$$\begin{bmatrix} [C_{11}] \\ \vdots \\ [C_{16}] \\ [C_{21}] \\ \vdots \\ [C_{26}] \\ \vdots \\ [C_{91}] \\ \vdots \\ [C_{96}] \end{bmatrix}_{54 \times 1} = \begin{bmatrix} \left[ \begin{array}{c} \frac{\beta_1}{\Lambda \lambda_1} \\ \vdots \\ \frac{\beta_6}{\Lambda \lambda_6} \end{array} \right] \\ [0] \\ \vdots \\ [0] \\ \vdots \\ [0] \\ \vdots \\ [0] \end{bmatrix}_{54 \times 1} \quad (3-36)$$

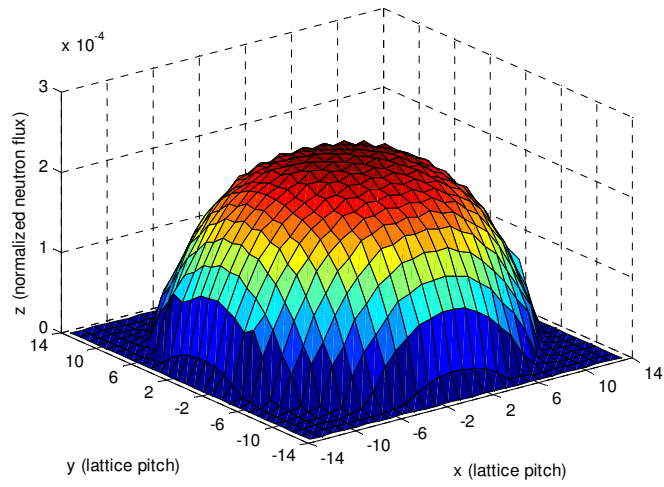
$$\begin{bmatrix} I_1 \\ I_2 \\ \vdots \\ I_9 \end{bmatrix} = \begin{bmatrix} \frac{\gamma_I}{v \Lambda \lambda_I} \\ 0 \\ \vdots \\ 0 \end{bmatrix} \quad (3-37)$$



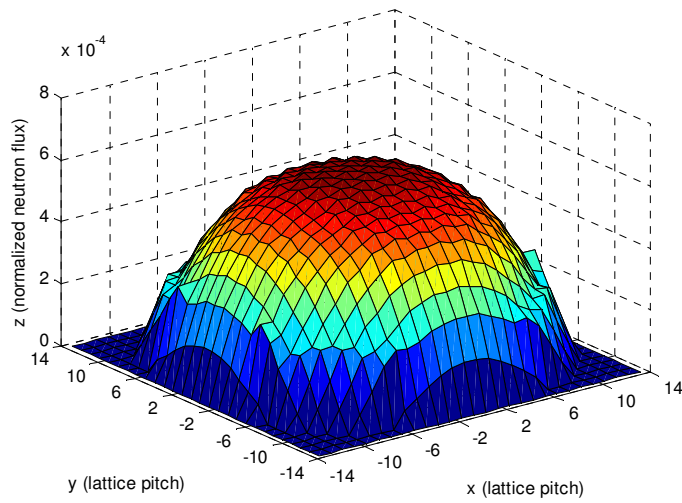
generalized such that the x-y plane coincides with the reactor face plane, while the z-axis is located to the central axis of the reactor calandria. The basic mesh-structure has 26 meshes in both the x- and y-directions and 12 meshes in the z-direction. Thus, the core's geometric structure has a dimension of 26×26×12. In order to include reflector areas, 2 lattice pitches are added in both x- and y- directions. The neutron flux in the area outside the reactor is assumed to be zero. The core can be separated into 12 layers along z-axis. Due to the symmetrical characteristic of the reactor core in z-direction, reactor neutron flux distributions within 6 layers in half core are used for illustrations.

The simulation illustrates the real-time 3-D spatial flux distribution during the transient process, which cannot be obtained by point kinetic models. Fig. 3.9 to Fig. 3.14 respectively illustrates the radial flux distributions within six layers from the end face to the central plane along z-direction. Fig. 3.15 shows the flux distribution along one fuel channel in the central area of the reactor core. In Fig. 3.12, it can be seen that due to the absorption of light water in seven liquid zone controllers, there are seven notches distributed in the corresponding zones, indicating relatively lower neutron flux levels. While in Fig. 3.13 and 3.14, a similar observation illustrates the presence of adjuster rods whereby neutron flux in the central area of the reactor has been flattened to an equilibrium level.

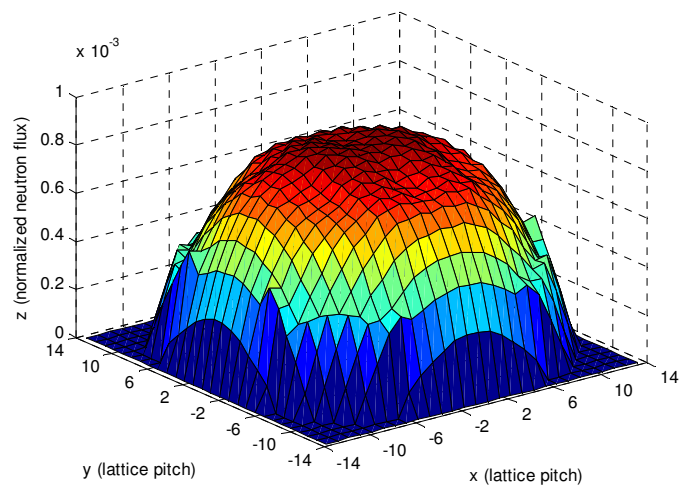




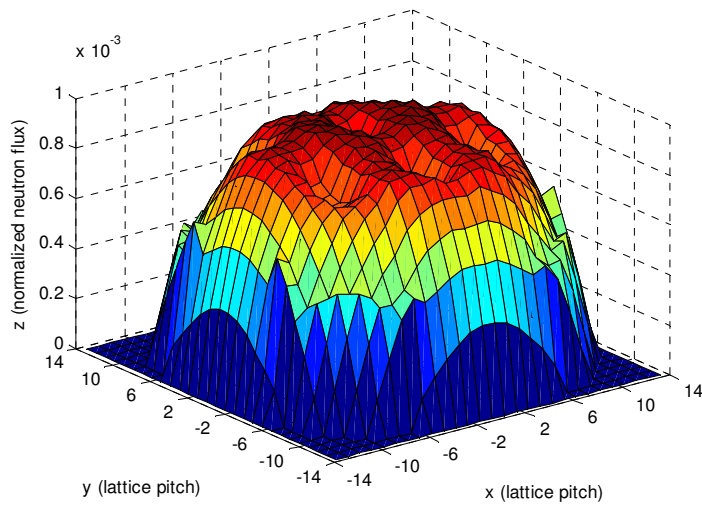
**Fig. 3.9 Neutron flux distribution within the first layer (end face) along the axial direction**



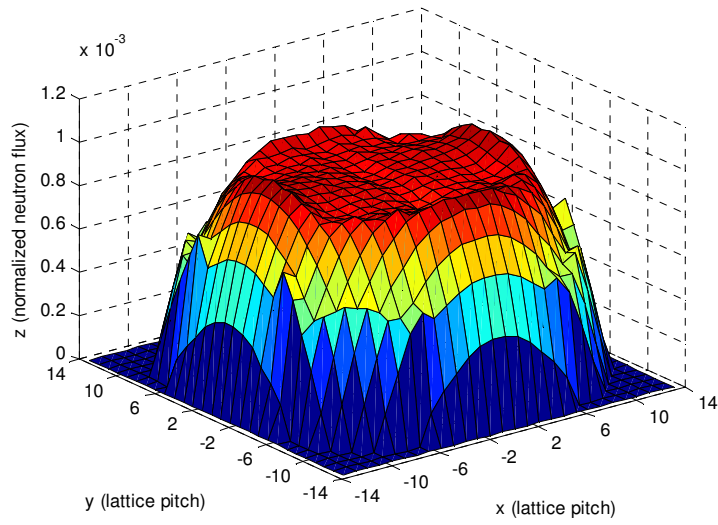
**Fig. 3.10 Neutron flux distribution within the second layer along the axial direction**



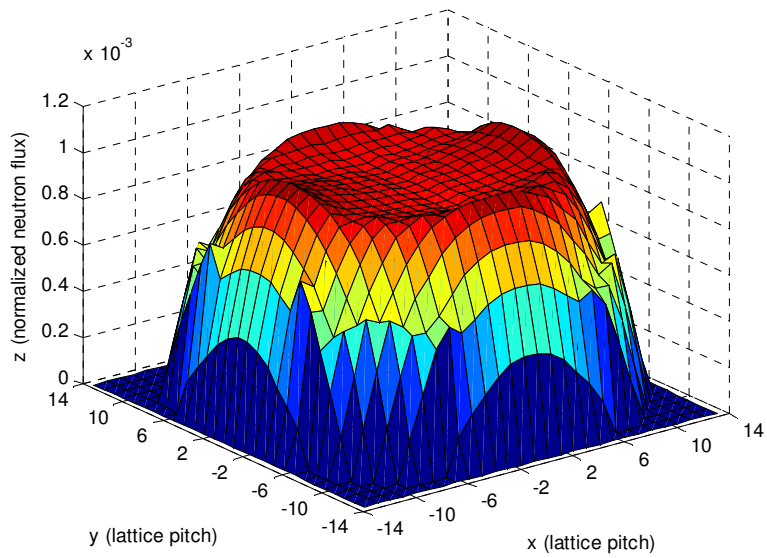
**Fig. 3.11 Neutron flux distribution within the third layer along the axial direction**



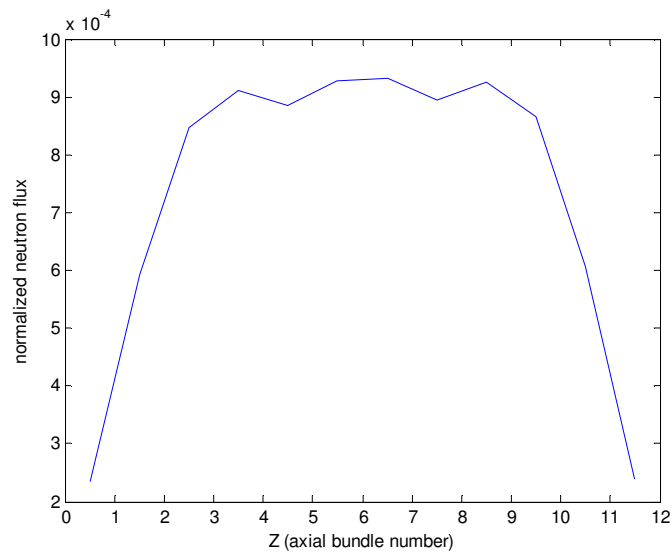
**Fig. 3.12 Neutron flux distribution within the fourth layer along the axial direction**



**Fig. 3.13 Neutron flux distribution within the fifth layer along the axial direction**



**Fig. 3.14 Neutron flux distribution within the sixth layer (central plane) along the axial direction**

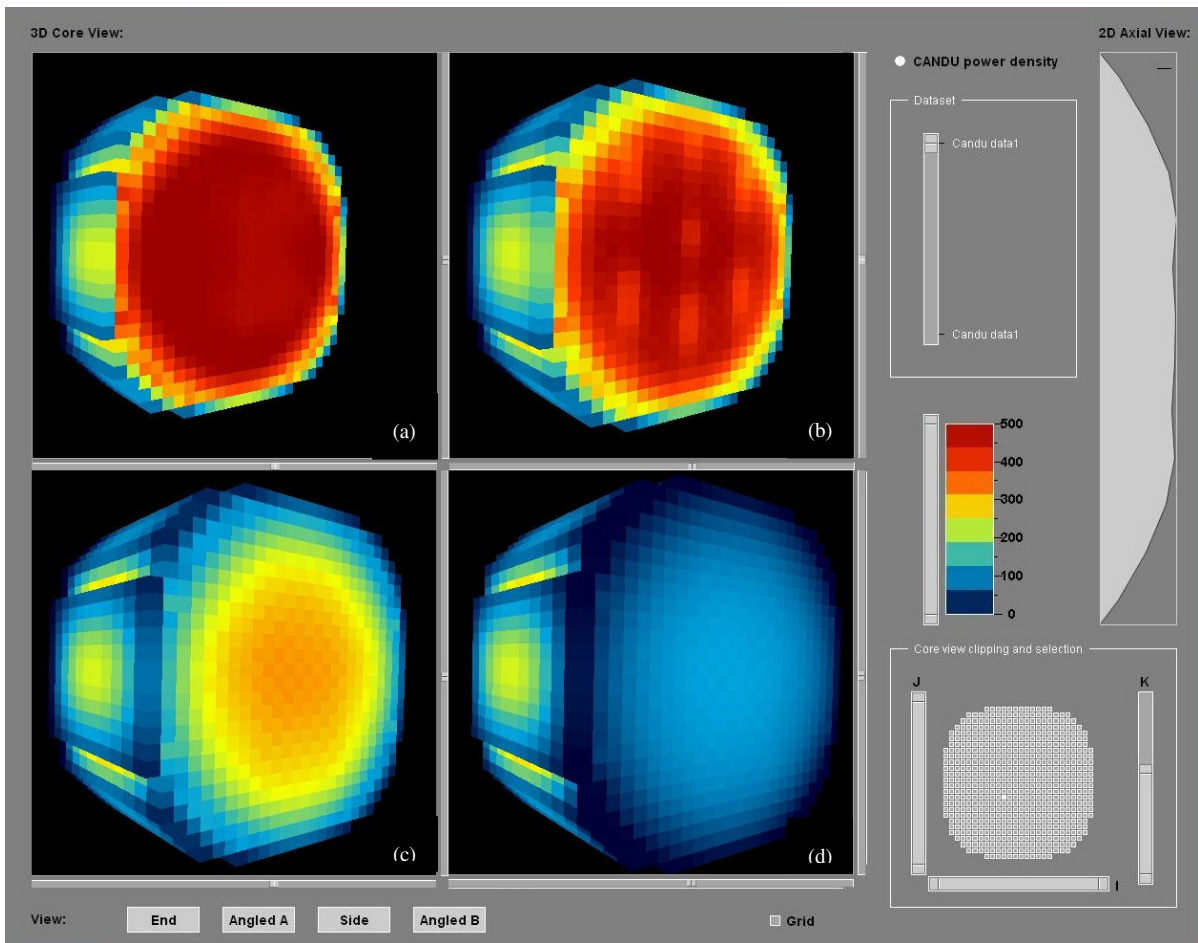


**Fig. 3.15 Neutron flux distribution along a fuel channel next to the central axis**

Furthermore, a user-friendly 3-D visualization software package, which is called “Core Data Viewer” (CDV) [62][63], is employed to create 3-D illustrations of the reactor power distribution in a different view.

Fig. 3.16 illustrates the 3-D power distribution within the reactor core at the same condition of steady-state, when the reactor power is 1.0 FPU. Detailed information about power distributions within the sixth (central plane), fourth, second and end planes along the axial direction is arranged in an order from Fig. 3.16(a) to Fig. 3.16(d). The unit of the color bar is Kilowatt. Since 7 of 21 adjuster rods are located within the sixth plane to flatten the power in the central area, the color – continuous, uniform dark red within the sixth plane - Fig. 3.16(a) representing the power distribution spreads from the center to the surrounding regions. Seven liquid zone controllers are distributed within the fourth layer - Fig. 3.16(b). Then, it can be distinctively observed that seven areas with brighter

red color represent that the reactor power in these areas are lower than that in other areas. This is due to the thermal neutron-absorption of light water in seven liquid zone controllers. Compared to the above two illustrations, Fig. 3.16(c) and Fig. 3.16(d) illustrate the reactor power gradually decays along the axis from the center to the tip. This is also demonstrated by the 2-D axial power distribution on the right side of Fig. 3.16.



**Fig. 3.16 reactor power distribution by a modal synthesis model (reactor bulk power is 1.0 FPU; (a) - the sixth plane; (b) - the fourth plane; (c) - the second plane and (d) - the end plane)**

### **3.8 Summary**

The modal synthesis model for 3-D space-time neutronic behaviors of a CANDU reactor has been developed. Subsequently, a nondimensional representation of the reactor kinetic model based on MATLAB/SIMULINK software environment is proposed. Special attention has been paid to compare the performance of the developed 3-D model with that of a traditional coupled point kinetic model. The 3-D reactor model is then implemented in SIMULINK. A steady-state calculation method is described to determine the initial conditions for the simulation. The methodology of the modal synthesis developed for analyzing 3-D space-time neutronic kinetics is proved to be very effective. It has been shown that the modal method is able to produce a detailed 3-D neutron flux distribution in the reactor core.

## **IV Simulation of the CANDU reactor regulating system**

This chapter describes the CANDU RRS and its implementation in MATLAB/SIMULINK software environment. Functional modules of the RRS are represented. The principles of reactivity control devices are illustrated. Consequently, power manoeuvre tests have been performed to detect the fundamental characteristics of the modal model. Furthermore, a typical load following experiment from a power plant is simulated by the RRS simulation platform based on both the modal and coupled point kinetic models. Simulation results are compared with each other and validated by the power plant data. The advanced dynamic features of the modal synthesis model based on implementation of the RRS simulation platform have been clarified throughout the analysis.

At the end of this chapter, a user-friendly MATLAB/GUI software package will be described for the CANDU RRS simulation. The specific properties of this software package are embodied in the individual and flexible installation and applications, which may be a good complement to academic and industrial users.

### **4.1 Description of the CANDU reactor regulating system**

The reactor regulating system, as a part of the overall plant control system, directly controls the reactor power, and sets it either to an operator-allocated power setpoint (Alternate Mode) or to the power level required to maintain certain steam pressure in the

steam generator (Normal Mode) [16]. Specifically, it includes input sensors, a collection of Digital Control Computer (DCC) programs, reactivity control devices and the related control logics.

The main functions of the RRS are to:

- a) Automatically control the reactor bulk power to the power setpoint between  $10^{-6}$  FPU and 1.0 FPU at a controlled rate. This is called bulk (global) control.
- b) Maintain the neutron flux distribution close to its nominal design shape, so that the reactor can be operated at the full power without violating channel and bundle power limits. This indicates the spatial (differential) control.
- c) Insert or withdraw reactivity devices at a controlled rate to maintain reactivity balance in the core. These reactivity devices compensate for the reactivity change due to variations in Xenon concentration, fuel burn-up, moderator poison concentration, and refueling effects, etc.
- d) Monitor some important plant parameters and reduce power quickly when any parameter exceeds the limit. Parameter limits may be specified for economic or safety-related issues.
- e) Withdraw shutoff rods automatically when the trip channels have been reset following a reactor trip on SDS1.



Furthermore, as a safety-related system, the RRS also meets the requirements for preventing loss of regulation (LOR). The frequency of LOR must be as low as possible. The RRS also is required to prevent LOR on any seismic event of intensity up to design basis earthquake (DBE) intensity. The reliability of the RRS is also very important. However, the RRS is not required to be functional under conditions associated with a Loss-of-Coolant Accident (LOCA), such as high temperature, humidity or radiation.

Fig. 4.1 represents specified information of the RRS.

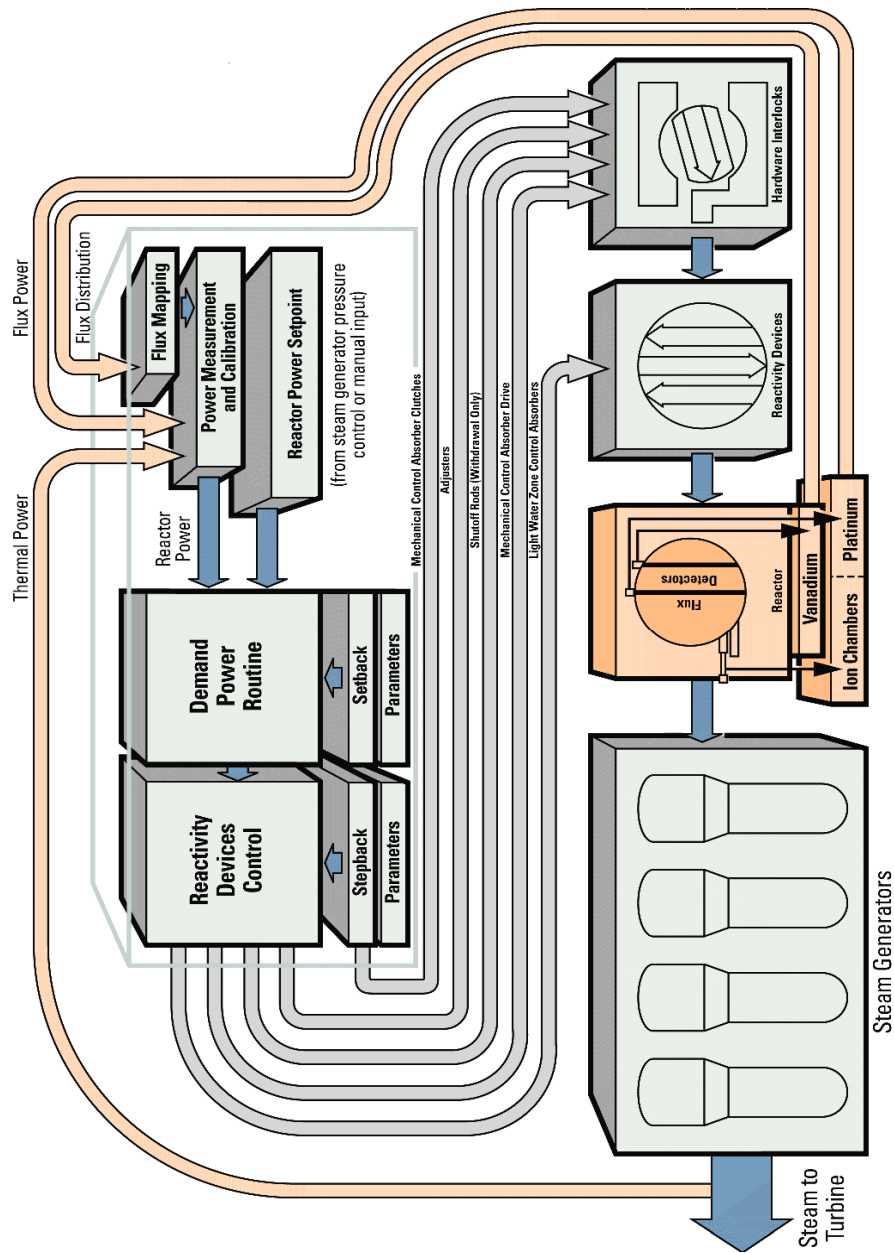


Fig. 4.1 CANDU RRS block modules [55]

The basic function of the RRS is to maintain both the reactor power and the rate of power change at specified setpoints. This function is performed using feedback control based on neutron flux (power). Reactor power is estimated from flux measurements from the ion

chambers in a low power range or the platinum flux detectors in a high power range. The demand power routine determines the power trajectory for following the reactor target power. The calibrated values of those flux measurements are compared to the demanded power, which generates an error signal. This error signal is used to fill or drain the liquid zone controllers either in unison or differentially to perform the bulk or spatial power control.

Although the liquid zone controllers represent the primary means of reactivity control in the reactor, in some situations reactivity variations exceed the limited capability of the zone controllers. In these cases, adjuster rods or mechanical control absorbers are employed to keep the reactivity balance maintained.

The setback routine monitors a number of plant parameters and reduces reactor power in a ramp manner, if any operating variables exceeds specified operating limits. When certain plant variables are beyond their ranges to potentially damage the core, the stepback routine releases the mechanical control absorbers to result in a rapid decrease in reactor power.

Furthermore, the flux mapping routine helps to calibrate the zone power detectors to properly reflect the spatial flux distribution and provides information for optimizing power output and fuel management. SDS1 is the primary method for quickly shutting down the reactor when some parameters enter an unacceptable range. This shutdown

system employs a logic system, which is independent of the RRS. However, withdrawal of the shutoff rods is controlled by the RRS.

#### **4.1.1 Power measurement and calibration**

In order for the RRS to perform its functions, both power measurement as well as calibration in the reactor core is required to estimate the reactor bulk and zone powers. Reactor bulk power is determined by 3 ion chamber signals (<5%FP) and 28 self-powered in-core platinum flux detector signals (>15%FP), or a combination of both signals (5%-15%FP). Additionally, in-core platinum flux detectors produce measurements of zone powers with minimum delay.

Power measurements are preferably quick and able to provide the spatial average either over the entire core, or a certain number of zones. However, although the signal from the platinum detectors is fast, it is easily affected by local disturbance, and because each detector measures only one single point, it is unable to reliably indicate the average power. Other drawbacks include: platinum detector characteristics change with irradiation; vanadium detectors, while accurate, are too slow to respond for direct use in flux control; and finally, ion chamber measurements are intensely vulnerable to moderator poison.

Therefore, the reactor power signals from either platinum detectors, ion chambers or a combination of both are filtered and calibrated by comparison with estimations of the reactor power based on thermal measurements. Twelve pairs of Resistance Temperature

Detectors (RTD) are located at the reactor inlet and outlet headers, and each of these pairs measures the temperature rise across the reactor. The average temperature rise generates an accurate estimation of the reactor power, which is then used to calibrate the platinum flux signals below 0.5 FPU. Steam generator steam flow, feed-water flow and feed-water temperatures are measured and the reactor power is estimated from enthalpy and flow calculations, anytime the reactor power is over 0.7 FPU. A linear combination of both types of measurements is used as the calibrating signal, within the intermediate power range (0.5-0.7FPU). In addition to this, processing the measurements from the vanadium flux detectors, through the flux mapping routine, produces accurate estimations of average zone powers; these estimates then gradually calibrate the zone powers to represent accurate long-term spatial control.

#### **4.1.2 Demand power**

The demand power routine serves three functions: a) selecting the mode for the plant operation; b) calculating the reactor power setpoint (demand power) and power rate setpoint; and c) calculating the effective power error that is used as the control signal to the reactivity control devices. The power error is a measure of the difference between the measured power and the demand power, and is a critical part of the RRS, which controls the movement of reactivity devices. If required, the demand power routine is also capable of adding poison to the moderator.

The program decides which of the three power demands should be used and ramps the flux setpoint up or down at a controlled rate to meet the demand. The source of the requested power depends on which of the three operating modes is selected: normal mode, alternative mode, or setback. The reactor follows the turbine in the normal mode, and the request comes from the steam generator pressure control program. Reactor maneuvering rate limits are built into the demand power routine. This mode is ideal for the performance of turbine power maneuvers. In the alternative mode, where the turbine follows the reactor, the requested power is set by the operator who also selects the maneuvering rate. During plant upsets or at low power, when the steam generator pressure is insensitive to the reactor power, the alternative mode is preferred, although it can also be used in steady-state plant operations. In the setback mode, the demand power routine receives a negative maneuvering rate from the setback routine. If the reactor is already reducing power at a greater rate, the setback is ignored; otherwise, the setpoint is ramped down at the setback rate. The effective power error is calculated as both the difference between the set and measured rates, as well as a weighted sum of the difference between the set and measured flux powers.

#### **4.1.3 Reactivity control devices**

The function of reactivity control is performed by the light water liquid zone controllers, the adjuster rods and the mechanical control absorbers. Of all the reactivity control devices, 14 liquid zone controllers are the most dominant method of adjusting the reactor

power in a permitted area and rate. Within each liquid zone unit, it will alter the water levels by the same amount to realize the bulk power control, and also acts differentially on each individual water level to realize the differential control. However, limiting the error between the water levels must be treated as another important factor of differential control, because excessive adjustment of individual water levels can potentially affect system stability.

Other reactivity devices are required, when extra positive or negative reactivity, beyond the adjustment range of liquid zone controllers, needs to be compensated. Normally, 21 adjuster rods are inserted in a CANDU reactor core specifically to flatten the power distribution, although they can be withdrawn vertically when extra positive reactivity is required. Primarily, this aims to override the negative reactivity that occurs either as a result of Xenon buildup following large power reduction, or, if the online refueling system is unavailable when the reactor starts up. Usually parked above the core, 4 mechanical control absorber rods are either driven in pairs, at a certain rate, to supply the negative reactivity exceeding the ability of the liquid zone controllers, or dropped in by gravity to effect an immediate reduction in reactor power. Table 4.1 illustrates the approximate reactivity worth of these devices, as well as the corresponding highest average rates at which the reactivity can be added or removed.

**Table 4.1 Reactivity worth and maneuvering rates of reactivity control devices**

Devices	Worth (mk)	Highest Average Rate (mk/s)
Liquid Zone Control System	7	$\pm 0.14$
Mechanical Control Absorbers	10	$\pm 0.075$
Adjusters	15	$\pm 0.1$
Automatic Gadolinium Poison Addition		-0.0125

Despite not being part of the reactor regulating system, two more reactivity control devices should be mentioned: the shutoff rods associated with SDS1, and the liquid injection nozzles associated with SDS2 that largely control reactivity in only one direction. Although they are not for the purpose of reactivity control, the shutoff rods are mentioned here because they are withdrawn by the RRS following a reactor trip. There are 28 shutoff rods in two banks which are normally withdrawn simultaneously. Using cadmium absorber elements, the shutoff rods are able to quickly shut down the reactor under both normal and emergency conditions. The SDS2 consists of 6 horizontal nozzles through which liquid poison (neutron absorber in the form of dissolved gadolinium salts) is injected at high speed into the moderator.

#### **4.1.4 Other routines**

The setback routine is another key routine involved in the RRS which monitors a variety of plant variables, and if any variable exceeds acceptable operating limits, it reduces reactor power in a ramp manner. After monitoring the values of some variables, the

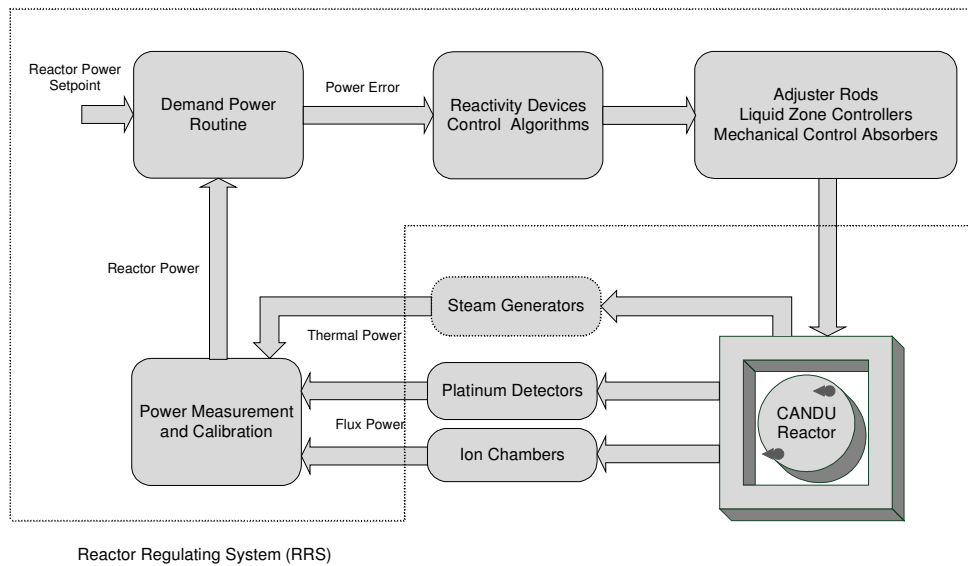


stepback routine will open the clutch contacts of all 4 mechanical control absorbers, should the power stepback be necessary. The absorbers fall into the core, resulting in a rapid power decrease. The addition of such soluble poisons as boron or gadolinium to the moderator enables the maintenance of reactivity balance, and an ion exchange system removes the poisons when needed. Due to its slower burnout rate, boron can be used to compensate excessive levels of fresh fuel, whereas when the Xenon load is markedly lower than equilibrium, gadolinium is added. In order to limit the consequences of a gross loss of regulation, reactivity mechanisms are subject to a number of interlocks external to the control computers.

Because the primary goal is to evaluate the simulation performance of the reactor kinetic model applied within the RRS simulation platform, these routine are rarely linked to the simulation cases. Indeed, they are left out in the RRS simulation platform, due to the absence of any perceivable affect that this omission has on the simulation results.

## **4.2 MATLAB/SIMULINK simulation platform of the RRS**

MATLAB/SIMULINK software environment has facilitated the simulation of the CANDU RRS. Since our research mainly focuses on the reactor power short-time regulating, a simplified block diagram of the CANDU RRS, which contains the most functional routines and control algorithms, is represented in Fig. 4.2.



**Fig. 4.2 Block diagram of RRS in CANDU reactors**

#### 4.2.1 Matrix and vector representation

MATLAB/SIMULINK software provides a convenient environment to perform the matrix operations, such that the entire RRS system can be simulated in a matrix form. The idea is to decompose every module/routine of the RRS, express all the principles by mathematic equations, and write the equations to the criteria matrix form. Then the software chooses the appropriate synthetic internal functions from the SIMULINK library to develop each block, which represents the mathematic model of the RRS' module, and finally connects all the blocks, compiles them and performs simulations. A necessary procedure before the simulation is that the initialization of all the parameters involved in the simulation is required. For dynamic simulations, steady-state authorization also needs to be assessed.

The detailed vectorization process about the reactor modal model has been provided in Chapter III. Here, only a simplified form of the dynamic equations is briefly represented to show the process.

The reactor kinetic state-space Eqns. from (3-31) to (3-34) in Section 3.5 are written to an easy form as follows,

$$\frac{d}{dt} \mathbf{N} = (\mathfrak{R}_{SCK} + \frac{\mathfrak{R}_L + \mathfrak{R}_X}{\Lambda}) \mathbf{N} + \text{blkdiag}([\lambda_1 \dots \lambda_6]) \cdot \mathbf{P} \quad (4-1)$$

$$\frac{d}{dt} \mathbf{P} = \frac{1}{\Lambda} \text{blkdiag}([\beta_1 \dots \beta_6]^T) \cdot \mathbf{N} - \text{blkdiag}(\text{diag}(\lambda_i)) \cdot \mathbf{P} \quad (4-2)$$

$$\frac{d}{dt} \mathbf{I} = \frac{\gamma_I}{v\Lambda} \mathbf{N} - \lambda_I \mathbf{I} \quad (4-3)$$

$$\frac{d}{dt} \mathbf{X} = \frac{\gamma_X}{v\Lambda} \mathbf{N} + \lambda_I \mathbf{I} - \lambda_X \mathbf{X} - \sigma_X \phi_f \mathbf{A} \cdot \text{blkdiag}(\mathbf{X}) \cdot \mathbf{N} \quad (4-4)$$

where

$$\mathbf{N} = [n_1 \dots n_9]^T; \quad \mathbf{P} = [[C_{11} \dots C_{16}] \dots [C_{91} \dots C_{96}]]^T; \quad \mathbf{I} = [I_1 \dots I_9]^T; \quad \text{and} \quad \mathbf{X} = [X_1 \dots X_9]^T. \quad (4-5)$$

Some coefficients of Eqns. (4-1) to (4-4) are illustrated as follows:

$$\mathfrak{R}_{SCK} = \begin{bmatrix} \frac{\rho_{sc1} - \beta}{\Lambda} & & & \\ & \ddots & & \\ & & \ddots & \\ & & & \frac{\rho_{sc9} - \beta}{\Lambda} \end{bmatrix} \quad (4-6)$$

$$\mathfrak{R}_L = \begin{bmatrix} \rho_{11} & \cdots & \rho_{19} \\ \vdots & \ddots & \vdots \\ \rho_{91} & \cdots & \rho_{99} \end{bmatrix} \quad (4-7)$$

$$\mathfrak{R}_X = \begin{bmatrix} \rho_{11}^X & \cdots & \rho_{19}^X \\ \vdots & \ddots & \vdots \\ \rho_{91}^X & \cdots & \rho_{99}^X \end{bmatrix} \quad (4-8)$$

$$\mathbf{A} = \begin{bmatrix} [A_{111} \cdots A_{119}] & \cdots & [A_{191} \cdots A_{199}] \\ \vdots & \ddots & \vdots \\ [A_{911} \cdots A_{919}] & \cdots & [A_{991} \cdots A_{999}] \end{bmatrix}_{9 \times 81} \quad (4-9)$$

It should be pointed out that MATLAB functions - *blkdiag* and *diag* are defined as follows [64]:

$$diag(\lambda_i) = \begin{bmatrix} \lambda_1 & & \\ & \ddots & \\ & & \lambda_6 \end{bmatrix} \quad (4-10)$$

and for a matrix  $\mathbf{M}$ ,

$$blkdiag(\mathbf{M}) = \begin{bmatrix} \mathbf{M} & & \\ & \ddots & \\ & & \mathbf{M} \end{bmatrix}_{9 \times 9} \quad (4-11)$$

From a perspective of control engineering, the above set of Eqns. (4-1) to (4-4) is represented in a form of state-space structure. Unlike the normal linear differential equation, this belongs to nonlinear control problems. However, the modal method has transformed the partial differential equations into ordinary differential equations, which

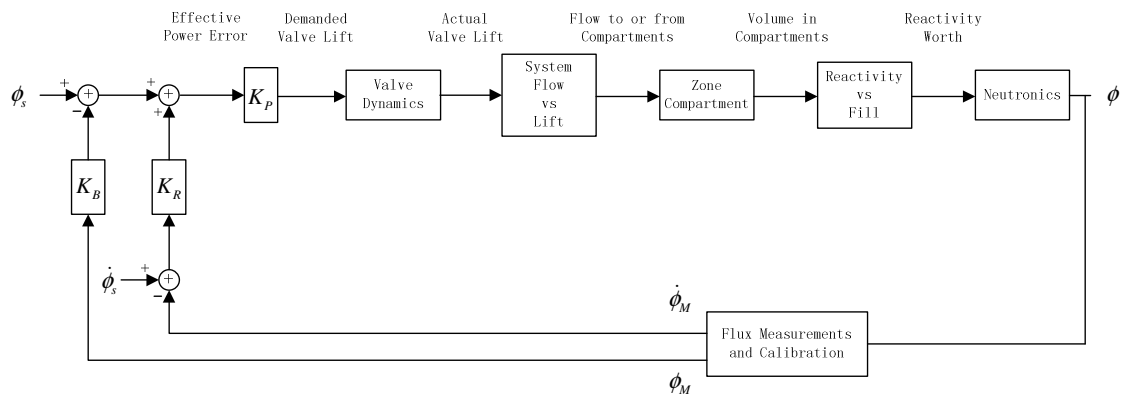
can be directly associated with conventional control problems.

#### **4.2.2 Reactivity control principles**

Principally, the reactor control is realized by controlling the number of neutrons available for fission from one generation to the next, thus affecting the behavior of the reactor core. The main method of controlling the number of neutrons is to change the amount of neutron absorbers in the core. Other methods are occasionally employed according to the circumstances such as adding neutron sources, more fissile material, changing leakage rate and resonance capture. For CANDU reactors, maintaining the long-term stability of the reactor operation power relies on the online refueling. Short-term changes in the reactor bulk power and reactor internal changes require reactivity control devices such as liquid zone controllers, adjuster rods and control absorbers to achieve. Among these three reactivity devices, 14 liquid zone controllers are designated to constitute the most dominating function in adjusting the reactor power in a permitted area and rate. Adjuster rods and control absorbers are increasingly manipulated when rapid power changing related to safety functions is required.

It has been established that the basic functions of the RRS are to maintain reactor power and rate of change in power at specified setpoints (bulk control), and to maintain the reactor power distribution shape close to its nominal design shape (spatial control); the use of stable feedback controls based on neutron flux accomplishes these functions. Fig. 4.3 shows a block diagram of the flux control loop for bulk power control. An effective

power error is computed as the weighted sum of the error between flux and its setpoint, and the error between the flux change rate and the flux setpoint change rate. Making zone controller valve lift proportional to power error achieves and maintains control, which, combined with the high reliability of the distributed control system, leads to the very high availability of the reactor control system. The demand power routine is able to generate a bulk power error signal that is used to drive the reactivity device by computing the desired reactor power setpoint and comparing it with the measured bulk power.



**Fig. 4.3 Block diagram of a flux bulk control loop**

For the purpose of regulating reactor power, the reactivity adjustment is performed by minimizing certain error signals. For the reactor bulk power control, the error signal between the bulk power and the power setpoint is minimized, such that the bulk power is regulated to the setpoint. For the reactor spatial control, 14 errors between the 14 zones' normalized powers and their averaged value are minimized such that the power distribution in the core is maintained. For any position within the reactor core, the

normalized power is defined as the ratio of the real power to the referenced target power when the reactor is operated with the full power steady-state. The unit is FPU.

In fact, for CANDU-6, when operated with the full power steady-state condition, each of the 14 zones has a target power that has been optimized by the designer. This is to prevent negative effects on the fuel, such as having high-powered zones neighboring zones at low power, while the bulk power remains constant. When power tilts occur, corrective measures are immediately taken to prevent them from developing further. The efficient way is to minimize the 14 errors between the 14 normalized zone powers and their average, so as to maintain the normalized zone powers close to each other and essentially to 1.0 FPU.

For a transient process during a load following, this phenomenon is represented when all the normalized zone powers are regulated to the value of the bulk power in each time instant. Although each zone has a similar normalized power, and the real power distribution has a similar shape as the initial steady-state, it is still significant to note that the RRS' function is only to maintain the power distribution shape in a basic manner by minimizing the deviations among 14 zone power levels. As such, this method cannot accurately track the power distribution shape. However, this is determined by the controller design of the current RRS. How to improve the current control system will be investigated in Chapter V.

Therefore, the primary method of short term reactivity control is performed by varying

the water levels in 14 liquid zone controllers. The reactivity represented by the zone controllers are varied either in unison for bulk power control or differentially for spatial control. Normally, adjuster rods are fully inserted in the core, mechanical control absorbers are fully withdrawn, and the average zone level is between 30% and 50% full level. The light water zone control program converts the calculated power errors from the demand power routine into lift signals for the light water zone control valves. The total lift signals to a given light water zone control valve consists of a signal proportional to the effective power error, a differential component proportional to the zone level error, and a constant value (bias), which corresponds to the valve lift required to maintain a constant level in a zone controller compartment. The detailed logics are represented as follows [16].

Power error is defined as

$$ER_{PU} = K_B * (P_{LGCA} - CP_{LOG}) + K_R * (T_{LOGI} - CT_{MAN}) \quad (4-12)$$

where, the first term is about the power term component, which is the difference between the measured power and the demanded power; the second term is about the power rate term component, which represents the difference between the logarithmic rate of the ion chambers defined in the measurement and calibration routine,  $T_{LOGI}$  and the power rate setpoint,  $CT_{MAN}$ . Then the steady-state error is mainly decided by the first term-the power term component.  $K_B$  and  $K_R$  are the defined gains.



For global control,

$$B_{LIF} = K_P * ER_{PU} \quad (4-13)$$

where,  $K_P$  is a gain.

For differential control,

$$D_{LIFTS_i} = \alpha_{Ti} * K_T * D_{PZ_i} + (1 - \alpha_{Ti}) * K_H * E_{NIV_i} + K_L * E_{NIV_i} \quad (4-14)$$

in which the first term is about power alignment, and the second and third terms are about zonal level alignment.  $D_{PZ_i}$  is 14 zonal power deviations, which is the difference between 14 calibrated zonal powers,  $P_{ZC_i}$  and the average calibrated zonal power,  $P_{ZCM}$ .  $\alpha_{Ti}$  is the 14 spatial command activation factors.  $K_T$  is a gain.  $E_{NIV_i}$  represents each of the 14 zone level deviations, which is the difference between the average zone level,  $N_{MBL}$  and each individual zone level,  $N_{IV_i}$ .  $K_H$  and  $K_L$  are gains.

Then the 14 opening signals of the LZCs can be represented by

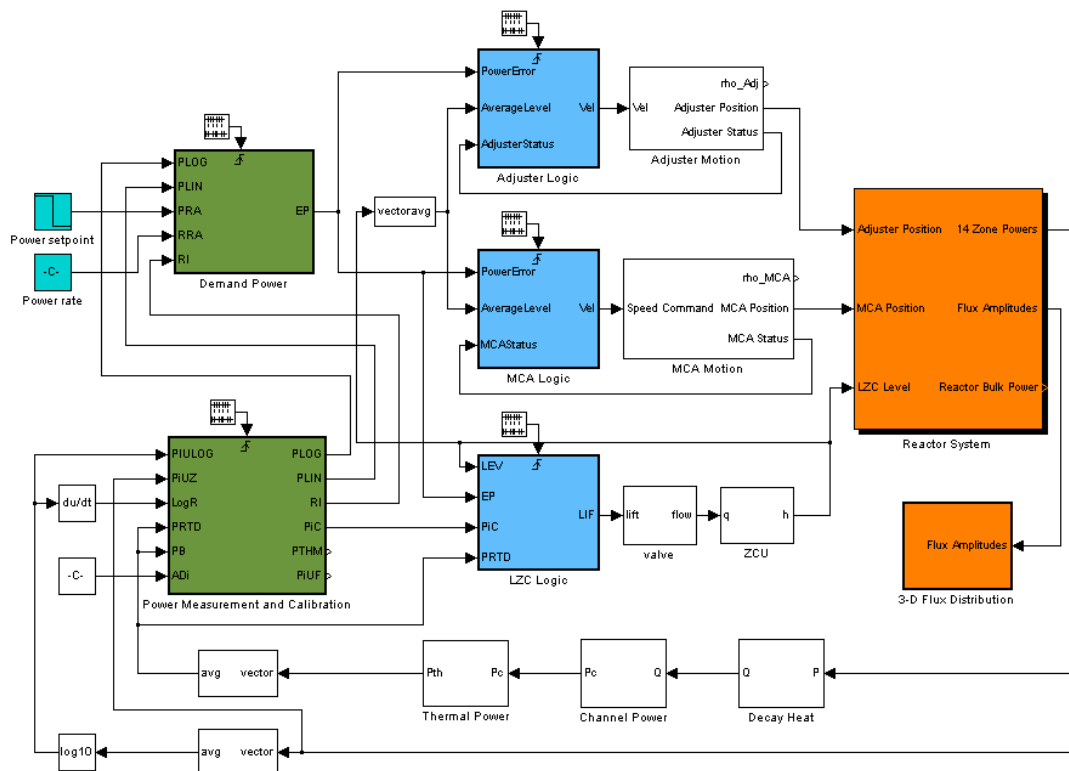
$$R_{LIF_i} = B_{LIF} + D_{LIFTS_i} \quad (4-15)$$

This will be limited by the minimum and maximum  $R_{LIF_i}$  values in order to prevent the compartments from flooding or running dry.

#### 4.2.3 Efficient implementation of the RRS simulation platform

A CANDU RRS simulation platform established by MATLAB/SIMULINK is illustrated

in Fig. 4.4. As shown, main control routines and devices are simulated, including reactor neutron and thermal power measurement and calibration, demand power and power error calculation, control algorithms and mechanical characteristics of liquid zone controllers, adjuster rods and mechanical control absorbers, and the reactor dynamic system.



**Fig. 4.4 MATLAB/SIMULINK simulation platform for the CANDU reactor regulating system (RRS)**

Neutron powers of 14 zones measured by the platinum-clad detectors in the linear scale and the averaged power in the logarithm scale are introduced into the power measurement and calibration routine, and then calibrated by the thermal power measurement. The

thermal power measurement contains two techniques: RTDs are used to measure the thermal power before the onset of boiling in the channels; and the measurements from the steam generators are used to calculate the thermal power once the boiling has started. However, due to the lack of the relative information, the measurements from the steam generators are approximately replaced by the RTDs' measurements in the research. After the calibration of measurements from different sources is completed, one bulk power signal (in logarithmic scale), one rate signal, and 14 zonal flux signals (linear scale) will be available for the RRS to use in the demand power routine. It is important to note that the measured or calculated physical quantities are designed to work with the normalized unit. For example, the reactor power is presented in FPU, and the water levels in the liquid zone controllers are measured in full level unit (FLU).

Although the plant is designed such that the reactor is normally operated in the alternative mode in which the turbine follows the reactor power, in this case, the reactor power setpoint and the desired rate are provided by the operator. By comparing the calibrated power and the power rate with the power setpoint (including the rate), an output signal in logarithm scale called "power error" is calculated step-by-step after computations. This is one of the most important signals in the RRS.

The power error signal is used to control three main reactivity devices: liquid zone controllers, adjuster rods and mechanical control absorbers. Each of the devices has its own specific control logic and mechanical linkage to decide its status. Liquid zone

controllers play a major role either in reactor bulk control or in spatial control. Adjuster rods and mechanical absorbers are committed to compensate excessively positive and negative reactivity or its rate beyond the operating range of liquid zone controllers. The task of the LZC program is to calculate the lift signals for the 14 control valves of the zone compartments. The input signals are the power error, reactor bulk power, 14 zone powers and the measurement of water levels. The outflow from the zone compartment is kept at a constant value, so any changes in the inflow will alter the amount of water in the compartment, and hence its level.

The positions of adjuster rods are determined by the power error and the average zone level. Depending on whether the power is increasing or decreasing, the adjuster rods are moved when the absolute power error is less than 4% FP and the average water level is between 15% and less than 75%. In addition, the drive is initiated by the RRS automatically. The adjuster rods are driven in seven banks. The banks that are withdrawn first during a transient have lower reactivity worth, and the banks are moved in a “first out, last in” scheme by the RRS.

The logic for withdrawal and insertion of the mechanical absorbers is fundamentally similar to the logic of adjuster rods. The positions of the mechanical absorbers are also related to the power error and the average zone level. They are arranged in two symmetric banks and are operated in the order of priority according to the region classified by the power error and the average zone level. Absorber drive is stopped if the average zone

level is between 75% and 80% and the power error is between -4% FP and 3% FP.

Since MATLAB provides many convenient ways for creating vectors and matrices, as well as an environment for matrix calculation, both the modal synthesis and coupled point kinetic reactor models can be implemented in an easy way. Reactivity change induced by the action of control devices, as a control signal, affects the transient response. The difference is that, in the point kinetic model the reactivity change within each zone out of 14 zone units directly results in the response of the reactor dynamic variables such as neutron flux on a zonal basis; while in the modal synthesis model the modal coupled reactivity change causes the response of the dynamic amplitudes, and thus synthesizes the 3-D dynamic response of the neutron flux, Xenon dynamic reactivity, etc. through the modal expansion Eqns. (3-5) to (3-8). The reactor system in Fig. 4.4 is represented by a 3-D modal reactor model. An adjunct subsystem is particularly designed to highlight the 3-D neutron flux dynamic distribution.

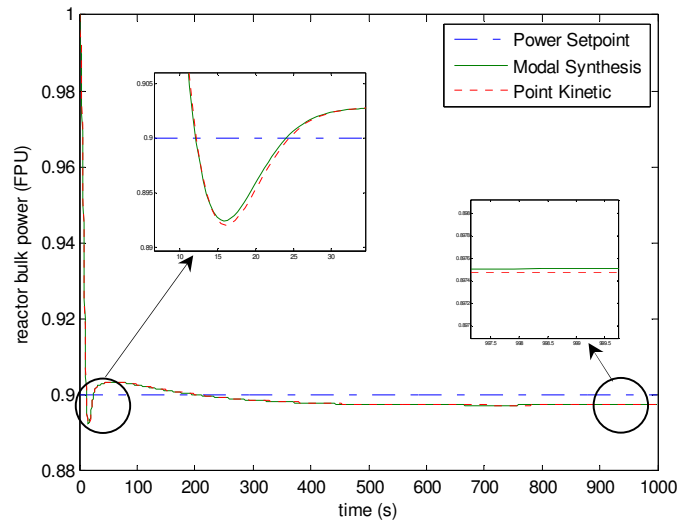
Before performing transient simulations, it is necessary to perform the parameters' initialization and the steady-state analysis. All initial parameters related to the reactor properties and the RRS' process variables are arrayed within an initialization file, which should be executed before rest of the simulations. The starting point for a transient usually makes use of a critical steady-state core configuration corresponding to given components of reactivity devices and initial Xenon distribution. The reference condition in this research is designated to be 1.0 FPU steady-state operation. The average water

level of the liquid zone controllers is 0.547 FLU with all adjuster rods fully inserted and all mechanical absorbers completely withdrawn. The detailed derivation of the initial conditions for the reactor dynamic variables has been provided in Section 3.6.

This novel RRS simulation platform can be easily manipulated. The transient simulation is performed after the data initialization and manual designation of the power setpoint and its rate. The dynamics of reactor bulk power, 14 zone powers and the 3-D flux distribution can be observed through the subsystem of the reactor system and its adjunct module. Other important information, such as water levels of the liquid zone controllers, can also be observed from the corresponding routines.

### **4.3 Simulations of power maneuvering operations**

In this study, power maneuvering test scenarios have been simulated. The reactor power setpoint is reduced gradually from 1.0 FPU to 0.9 FPU at a rate of 0.1 FPU/s. The reactor bulk power control under this command is illustrated in Fig. 4.5. For comparison purposes, the response from the coupled point kinetic model is also included. As far as the bulk power is concerned, the simulation results show clearly that both models can achieve the load following requirements successfully. The local enlargements of Fig. 4.5 illustrate that both the overshoot and the steady-state error of the modal synthesis model are close to those of the coupled point kinetic model. However, both the overshoot and steady-state error of the modal synthesis model are relatively smaller than those of the coupled point kinetic model.

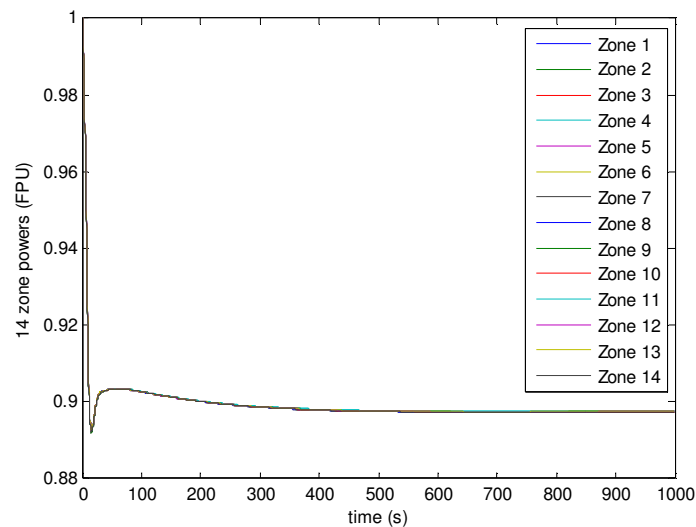


**Fig. 4.5 Bulk power responses based on coupled point kinetic and modal synthesis models (the reactor power is reduced from 1.0 FPU to 0.9 FPU at 0.1FPU/s)**

As mentioned before, one of the main tasks of the CANDU RRS is to maintain the reactor bulk power at the desired level commanded by the operator or to maneuver the reactor bulk power to a different level at a controlled rate, which is called “bulk power control”, as well as “global control”. Another important function is “spatial power control”, also called “differential control”, where the objective is to reduce the discrepancies between the zone powers and water levels and to assure that the neutron flux spatial distribution remains close to the nominal design shape. Thus, the reactor can operate at full power without violating the bundle or channel power limits.

Fig. 4.6 illustrates the simulation of reactor zonal power responses under the same power maneuvering condition. The 14 curves represent normalized power dynamics within 14 zones. Therefore, it is observed that powers in 14 zones are almost regulated to the level

of bulk power. Basically, the requirement of the spatial control is met, while the power distribution shape is somewhat maintained. From Fig. 4.5 and Fig. 4.6, it can be concluded that reactor modal modeling implemented within the RRS simulation platform can meet the requirement of power transient simulation and analysis.

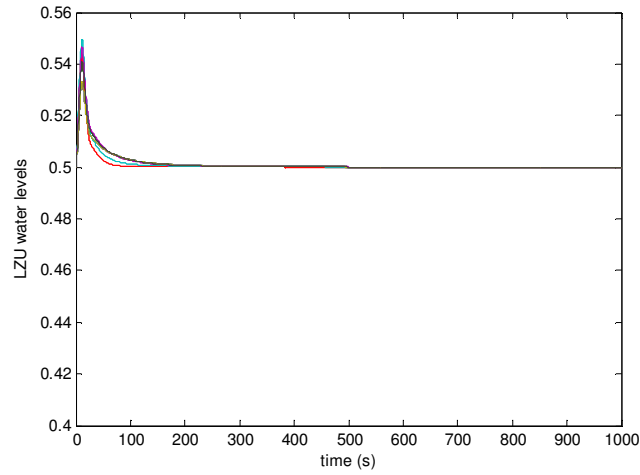


**Fig. 4.6 Simulation result of reactor power spatial control (1.0 FPU – 0.9 FPU, at a rate of 1%FP/second)**

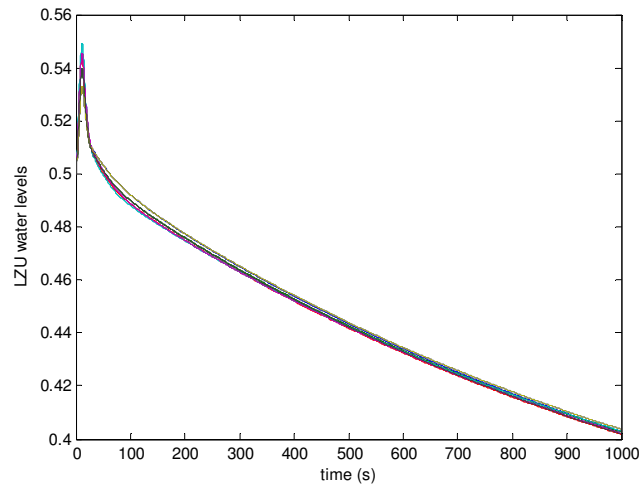
Another important parameter is the water levels in the liquid zone controllers, since the liquid zone controllers make significant contributions during load following transients. Fig. 4.7 and 4.8 represent the simulation of water level transients of LZUs. However, Fig. 4.7 does not include the model of the Xenon effect; while Fig. 4.8 does. It can be seen from Fig. 4.7 that without considering the Xenon effect, the water levels eventually reach an equilibrium state according to the power transient response. But from Fig. 4.8, water levels within LZU compartments keep on decreasing, which causes increasing positive



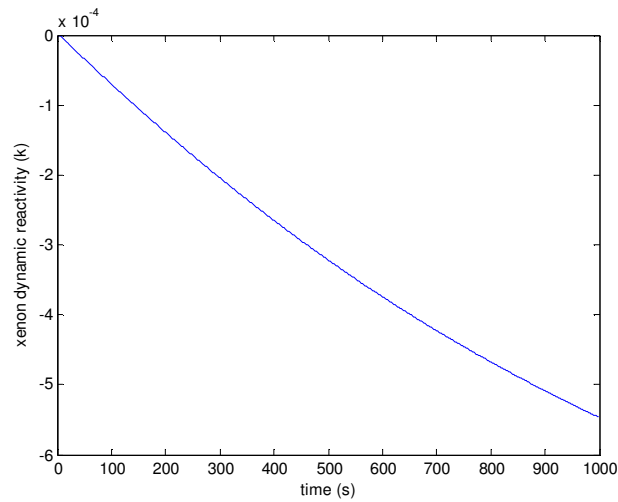
reactivity to compensate for the continuous accumulation of negative reactivity from Xenon. Simulation of the dynamic reactivity of corresponding Xenon accumulation is presented in Fig. 4.9. As the Xenon effect accumulates, negative reactivity decreases.



**Fig. 4.7 LZU water level transient simulation result (Xenon effect excluded)**

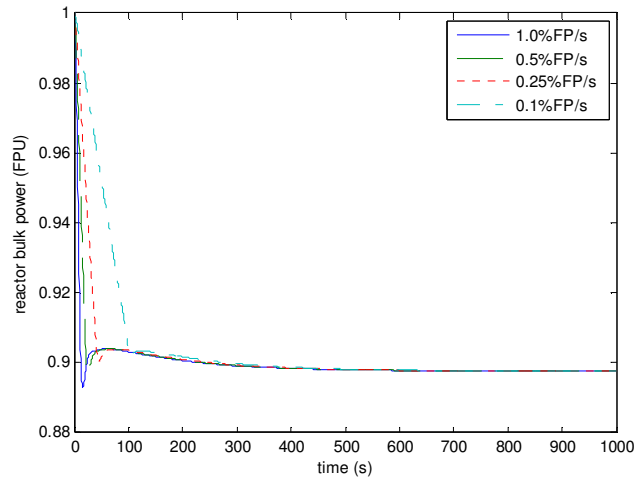


**Fig. 4.8 LZU water level transient simulation result (Xenon effect included)**



**Fig. 4.9 Simulation result of Xenon dynamic reactivity**

For comparison purposes, Fig. 4.10 illustrates the simulation of four power transients at different rates of power maneuvering. The range of power reduction is kept the same, i.e. 1.0 FPU to 0.9 FPU. However, the rates are respectively 1.0% FP/second, 0.5% FP/second, 0.25% FP/second, and 0.1% FP/second, which correspond to power-reducing times of 10 seconds, 20 seconds, 40 seconds and 100 seconds. Fig. 4.10 illustrates reactor bulk power following results. It can be observed that a smaller power reduction rate, there is a reduction in the overshoot power response.



**Fig. 4.10 Comparison of 4 power transients' simulations at different power changing rates**

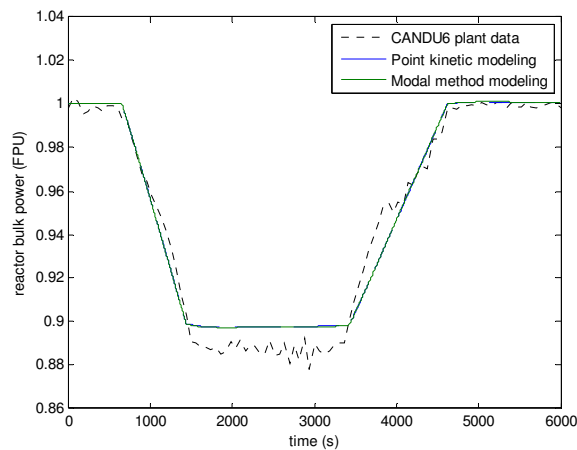
#### **4.4 Evaluation of 3-D reactor model under load following operation**

In order to assess the performance of the CANDU RRS MATLAB/SIMULINK simulation platform based on modal synthesis models, a load following transient is simulated and evaluated. The basic condition of the load following transient can be described as, the reactor power setpoint is reduced from 1.0 FPU to 0.9 FPU and subsequently returns to 1.0 FPU in 100 minutes (6000 seconds). Simulation results for this load following transient are presented in Fig. 4.11 to Fig. 4.15. However, in order to compare the modeling effects, Fig. 4.11 and 4.13 also include the simulation result obtained by using coupled point kinetic reactor models.

##### **4.4.1 Reactor power transients**

To control the reactor bulk power, the reactivity control mechanism is used to regulate the

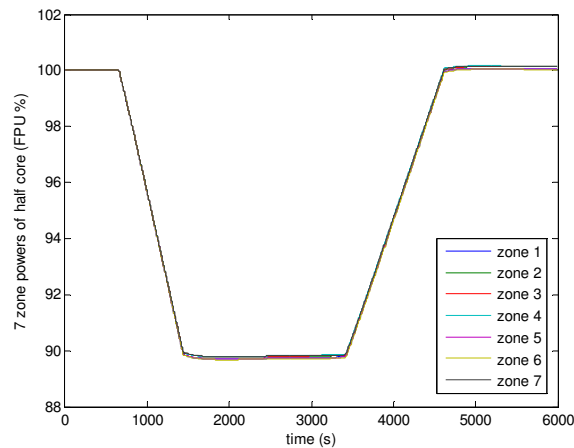
reactor power close to the desired set-point. The reactor bulk power responses under the above power demand for both the point kinetic and modal synthesis models are shown in Fig. 4.11 together with measured response from an existing CANDU-6 power plant under the identical power maneuver condition. It can be seen that the responses predicted from both models are consistent with the measured response. This demonstrates that the bulk power control function of the RRS with both the coupled point kinetic and the modal synthesis models is acceptable.



**Fig. 4.11 Changes in reactor bulk power in a load-following process**

For the reactor spatial control, the errors between the normalized powers in 14 zones and their averaged value are minimized such that the proper power distribution in the core can be maintained. The responses of the normalized power variation in 14 individual zones are simulated by using the modal synthesis model. Due to the axial symmetry of the core, simulation results of 7 zones within half core are illustrated in Fig. 4.12. The powers in

these zones are all very close to each other, which means that the spatial control functions in RRS have successfully limited any regional power tilt so that desired shapes of power distribution are maintained. The results are also presented in Table 4.2 and 4.3 for eight time instances. The normalized power and the relative changes in real power in each zone are listed. Table 4.2 shows that at each time instance, the normalized power in all the zones are very similar. Compared to the initial real power – the referenced target power, relative changes in the zonal actual powers for eight time instances are shown in Table 4.3. From both tables, it can be seen that the reactor zonal powers change in the same steps. Thus, by doing this in two steps, the shape of the zonal power distribution can be maintained.



**Fig. 4.12 Changes in zonal normalized powers during load-following process using modal synthesis method**

**Table 4.2 Normalized power distributions at eight time instances (in FPU)**

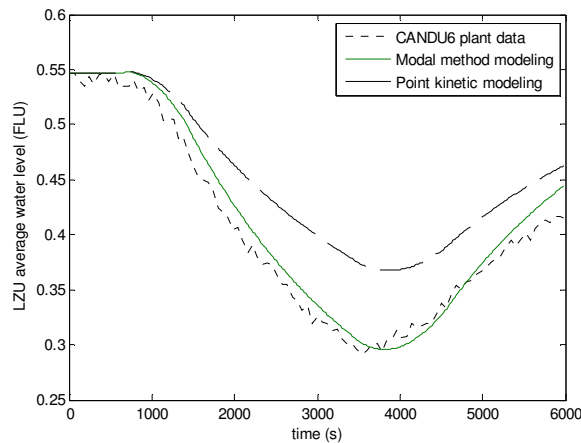
Time Zone	500 s	937 s	1300 s	2000 s	3000 s	3944 s	4271 s	5000 s
1	1	0.9649	0.9171	0.8970	0.8975	0.9416	0.9697	1.0007
2	1	0.9650	0.9177	0.8976	0.8979	0.9420	0.9701	1.0013
3	1	0.9650	0.9176	0.8976	0.8980	0.9421	0.9702	1.0013
4	1	0.9650	0.9175	0.8977	0.8983	0.9426	0.9707	1.0016
5	1	0.9649	0.9171	0.8970	0.8975	0.9416	0.9697	1.0007
6	1	0.9649	0.9170	0.8968	0.8971	0.9412	0.9693	1.0004
7	1	0.9650	0.9177	0.8978	0.8983	0.9424	0.9705	1.0015
Bulk	1	0.965	0.9174	0.8973	0.8978	0.9419	0.97	1.0011

**Table 4.3 Relative changes in actual power distributions at eight time instances (in MW)**

Time Zone	500 s	937 s	1300 s	2000 s	3000 s	3944 s	4271 s	5000 s
1	0	-9.3	-22	-27.4	-27.2	-15.5	-8	0.2
2	0	-9.3	-21.8	-27.1	-27	-15.3	-7.9	0.3
3	0	-12.2	-28.6	-35.5	-35.4	-20.1	-10.4	0.4
4	0	-10.8	-25.3	-31.3	-31.1	-17.6	-9	0.5
5	0	-12.2	-28.9	-35.9	-35.7	-20.3	-10.5	0.3
6	0	-9.3	-22.1	-27.4	-27.4	-15.6	-8.2	0.1
7	0	-9.3	-21.8	-27.1	-27	-15.3	-7.8	0.4
Bulk	0	-72.1	-170.2	-211.7	-210.6	-119.7	-61.8	2.3

#### 4.4.2 Water level transient in liquid zone units

As one of the important variables for reactivity adjustment, the controller signal - LZU water level is closely linked to the reactor model and reflects its physical properties during transients. The average water level responses in liquid zone controllers during a load-following transient can be shown in Fig. 4.13 together with the measured level responses. It can be seen that the average water level modeled by the modal synthesis model is more consistent with the measured data than that predicted by the point kinetic model. Using the measured data as a reference, the averaged water level errors are presented in Table 4.4. It can be seen that for both the accumulated and the maximum errors, the modal synthesis model is superior to the point kinetic model.



**Fig. 4.13 Comparison of LZU average water levels for load-following process**

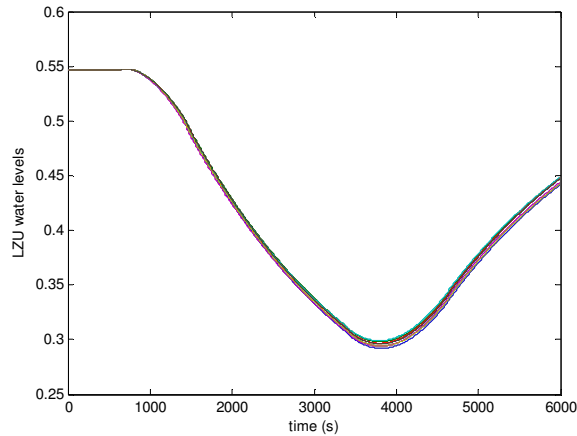
**Table 4.4 Response errors of the average levels for both reactor models**

Error Types	Point kinetic model	Modal synthesis model
Averaged accumulated error	0.047 FLU	0.009 FLU
Maximum error	0.076 FLU	0.004 FLU

From the above simulation results, it can be concluded that, although both reactor models can be used to describe the reactor dynamics, as far as the water levels in the LZC are concerned, the modal synthesis model produces simulation results closer to the real plant measurement.

Fig. 4.14 represents the simulation results of water level dynamics within 14 liquid zone controllers during a load following transient. In Fig. 4.14, 14 individual water level variations obtained from modal synthesis model simulation are plotted. Similar to simulations of 14 zone power transients in Fig. 4.12, these 14 curves also focus on the average water level simulated in Fig. 4.13. From Fig. 4.12 and Fig. 4.14, it can be concluded that the variations between the zone powers, as well as zone water levels, are restricted to a narrow area. Both the zone powers and the zone water levels are maintained close to the average level. In this way, the spatial control function of the RRS is realized in a certain extent.



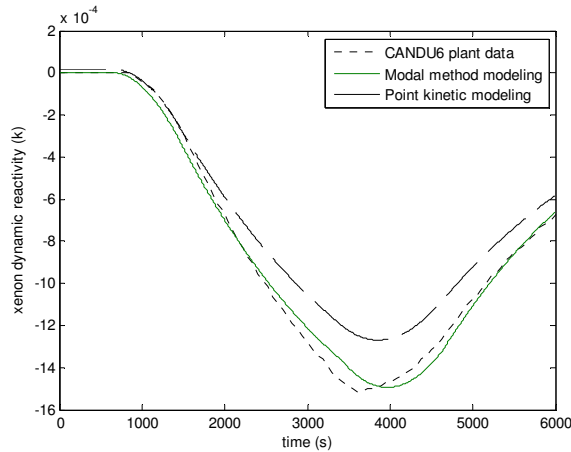


**Fig. 4.14 Simulation results of 14 LZU water level variations for load following transient**

#### 4.4.3 Xenon dynamics

Xenon buildup is one of the important components in the reactivity feedback system. Reactivity change due to Xenon buildup is defined as Xenon dynamic reactivity. Fig. 4.15 illustrates the dynamics of the Xenon reactivity during the load-following operation based on both the reactor models and the measured plant data. It can be observed that the behavior of Xenon dynamic reactivity of the modal synthesis model is more consistent with the measurement than that of the point kinetic model. This demonstrates that the modal synthesis model is a more accurate model. Furthermore, from Fig. 4.13 and Fig. 4.15, it can be seen that, as the Xenon negative reactivity accumulates, the water levels in the liquid zone controllers are continuously decreasing to compensate the Xenon negative reactivity and to stabilize the reactor power. In the modal synthesis model, the magnitude of the Xenon negative reactivity accumulation is larger than that of the point kinetic

model in Fig. 4.15. That is why the water level fluctuations are more significant as shown in Fig. 4.13. However, the important point is that the modal synthesis model lead to results that are closer to the real plant measurement.



**Fig. 4.15 Comparison of Xenon dynamic reactivity for load following operation**

#### **4.4.4 Neutron flux dynamics within regional overpower protection detectors**

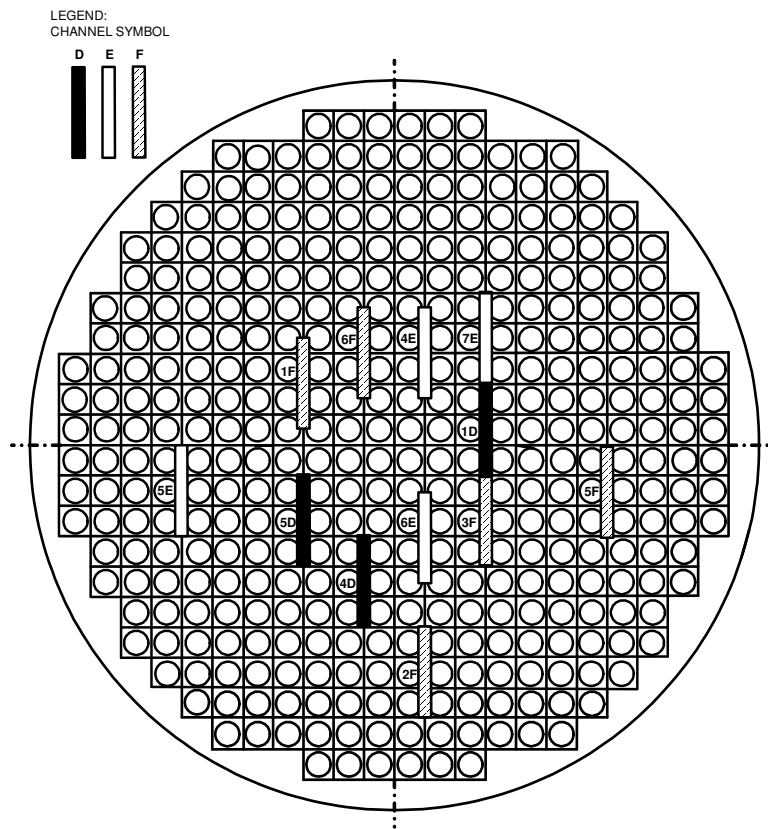
The Regional Overpower Protection (ROP) system is designed to protect the reactor against overpowers in the fuel caused by either a local peaking or a general power increase in the reactor load level. Within the core, there are two ROP systems: one for each of the two shutdown systems – SDS1 and SDS2. Each ROP system consists of several fast-responding self-powered flux detectors. They are distributed throughout the core within SDS1 and SDS2 assemblies. Each ROP detector has been designed with a pre-set trip setpoint (TSP). The standard TSP for CANDU reactors is around 1.23 [65]. The detectors for each shutdown system are divided into three logic channels with reactor

trip occurring on 2 out of 3 channels trip. That means when the normalized neutron fluxes of detectors within any 2 of 3 channels are over the TSP, the reactor trip signal is activated and the shutdown system is commanded.

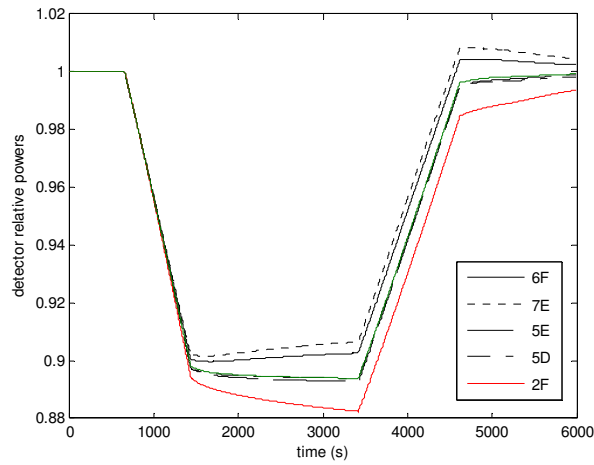
Selection of the detector layout and specification of the TSPs are both involved in the ROP system design and safety analysis, which are beyond the scope of this study. However, 3-D dynamic characteristics of the RRS simulation platform allows that it could provide a relatively accurate estimation of the neutron flux variation within the ROP detectors during a transient. This can provide a useful reference to the optimized design of the ROP system. The RRS simulation platform with the modal synthesis model plays a far more crucial in this process than the point kinetic model, since the latter only represents the uniformed zone power transient.

Fig. 4.16 shows a typical ROP detector distribution for SDS1 within the center cross section of the core. Fig. 4.17 illustrates the dynamic process of the neutron flux variation within several selected detectors during the load-following operation. The trajectories in Fig. 4.17 demonstrate that none of the normalized neutron fluxes of the selected detectors are over the TSP, and thus the trip signal is not activated. Furthermore, simulation results show that the followed trajectories of some ROP detectors' neutron flux are consistent with the setpoint, while others are not. Further studies show that bounded by the horizontal center plane, the trajectories of the above detectors overshoot upwards; comparably the below detectors overshoot downwards. In addition, the overshoot of the

trajectory is elevated by increasing the distance from the horizontal rather than the vertical central plane. The current control system design determines that the RRS cannot regulate the local power distribution to the referenced setpoint accurately, although it delivers control to the reactor bulk power and 14 zone powers. Hence, advanced control strategies will be investigated to improve the performance of the current control functions. How to develop the advanced control strategies will be discussed in Chapter V.

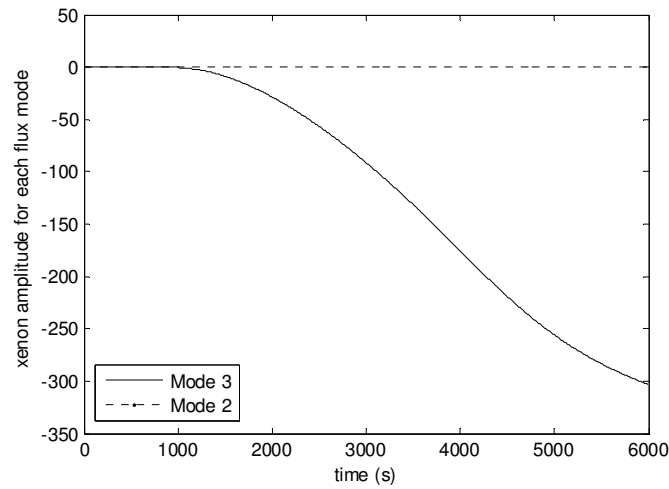


**Fig. 4.16 ROP detector location for SDS1 within the center cross section of the core**

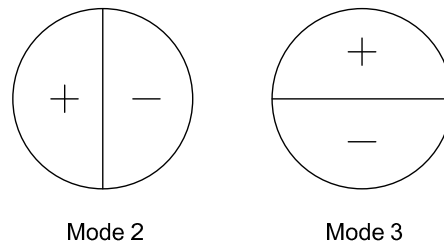


**Fig. 4.17 Simulation results of the neutron flux varying within selected ROP detectors for load following process**

In order to further illustrate the scenario represented in Fig. 4.17 about the different overshoot with the relationship of the horizontal versus the vertical central plane, Fig. 4.18 provides the simulation results of the Xenon amplitude dynamics for flux modes 2 and 3. Schematic representation of flux modes 2 and 3 are displayed in Fig. 4.19. In conjunction with the modal expansion Eqn. (3-8), Fig. 4.18 illustrates that, to the uniformed spatial distribution of Xenon reactivity, mode 3 contributes more than mode 2 does. This directly results in the more difficult power regulation in the vertical direction than that in the horizontal direction of the reactor core. And the overshoots of the ROP detectors' load-following trajectories appear with the boundary of the horizontal central plane and develop in the opposite directions. Certainly, improving this situation depends on the enhanced design of the current control system.



**Fig. 4.18 Simulation results of Xenon amplitudes for flux modes 2 and 3**

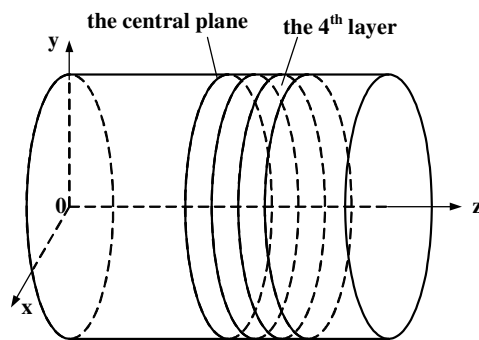


**Fig. 4.19 Schematic representation of flux modes 2 and 3 for the CANDU reactor**

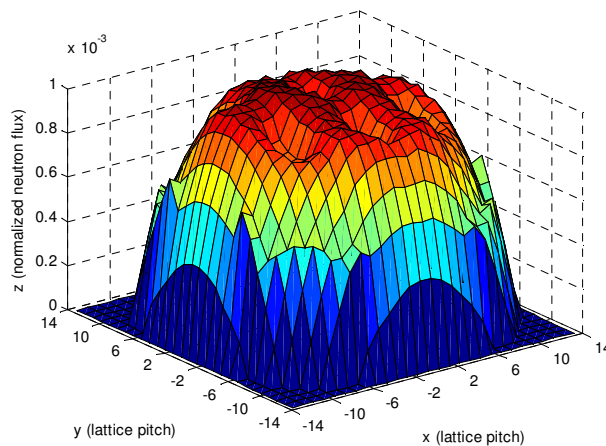
#### 4.4.5 Core neutron flux distribution during transients

Under the RRS control, the shape of the reactor neutron flux distribution has to be close to its nominal design shape to ensure the reactor's operational safety and optimal performance. For illustrative purposes, the CANDU core is sliced into 12 layers of the same thickness, as shown in Fig. 4.20, where the fourth layer from the right is chosen for subsequent illustrations. The central plane is also highlighted since it divides the reactor core into two symmetric halves. The neutron flux distributions modeled by the 3-D modal

synthesis model at the fourth layer are shown in Fig. 4.21 under 1.0 FPU reactor power. As can be seen in Fig. 4.21, the modal synthesis method can provide much detail in terms of peaks and valleys in the core power distribution. In particular, it can be observed that due to the neutron absorption of the liquid zone controllers, there are seven notches distributed in the related zones, indicating reduced neutron flux.



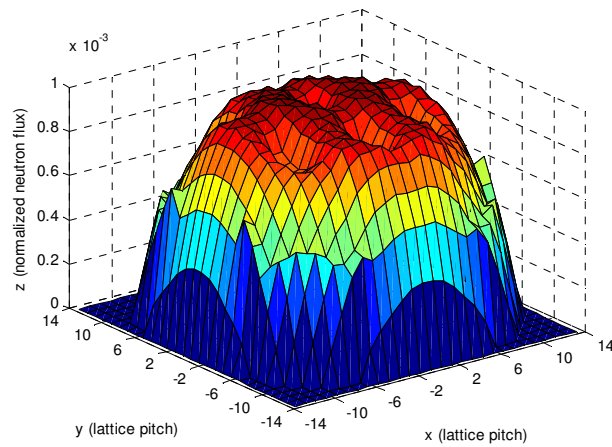
**Fig. 4.20 The relative position of the fourth layer within the CANDU reactor core**



**Fig. 4.21 Neutron flux distribution at the fourth layer along the z-direction (reactor power is 1.0 FPU)**

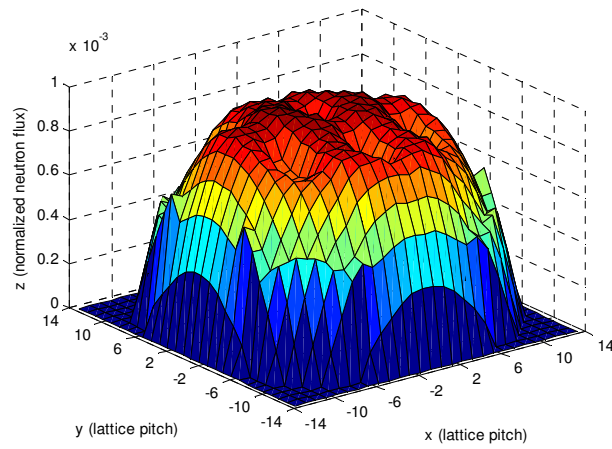
The variations of the neutron flux distribution on the fourth layer during the load

following transients are shown in Fig. 4.22 and Fig. 4.23 when the reactor bulk power is regulated to 0.95 FPU and 0.9 FPU respectively. It can be seen that, as the reactor power decreases, the magnitude of the local neutron flux also reduces. However, the shape of the flux distribution remains still similar to the initial shape, which demonstrates that the RRS' main function is maintaining the neutron flux distribution shape.



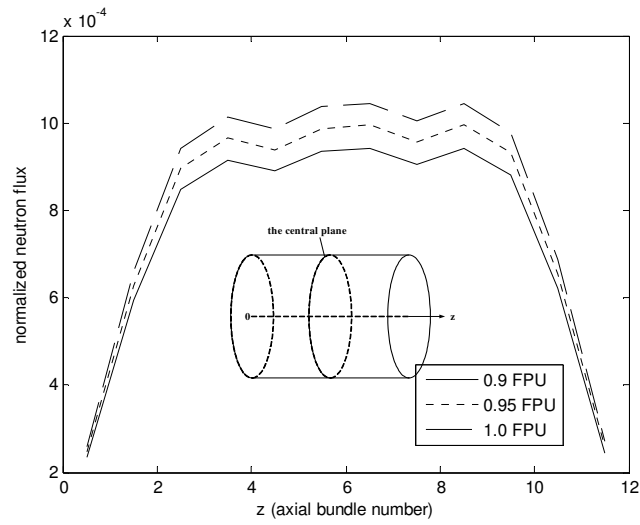
**Fig. 4.22 Neutron flux distribution at the fourth layer along the z-direction (reactor power is 0.95 FPU)**



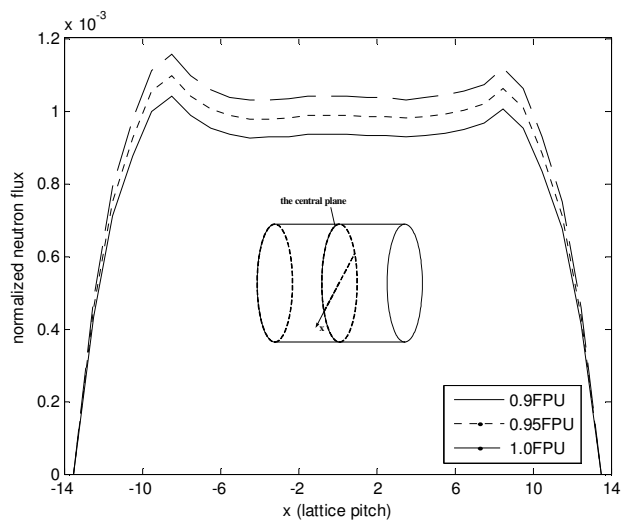


**Fig. 4.23 Neutron flux distribution at the fourth layer along the z-direction (reactor power is 0.9 FPU)**

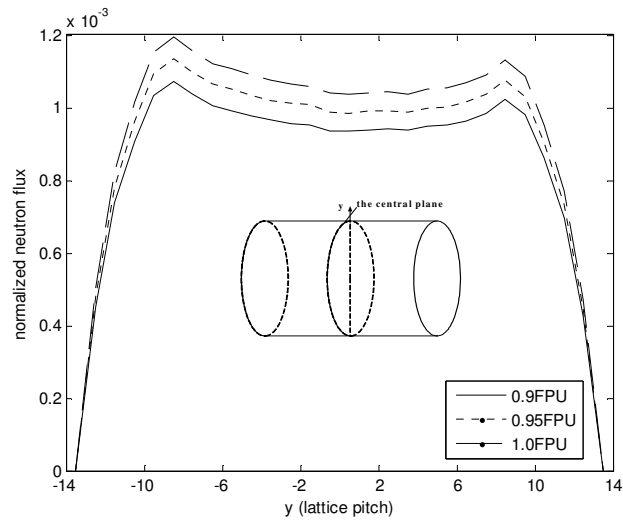
Further demonstrations of the flux distribution dynamics regarding these power levels are depicted in Fig. 4.24 (a), (b), and (c). In this figure group, corresponding to three reactor powers, simulation curves for flux distributions in x-, y- and z- directions are compared. It can be seen that, with the increase in the reactor power, the scope of the neutron flux distribution is enlarged, while the shape of the flux distribution is still maintained. This further illustrates the RRS's main function of maintaining the neutron flux distribution close to its nominal design shape.



**Fig. 4.24(a) Neutron flux distribution along the z-axis at different power levels**



**Fig 4.24(b) Neutron flux distribution along the x-axis within the central plane at different power levels**



**Fig 4.24(c) Neutron flux distribution along the y-axis within the central plane at different power levels**

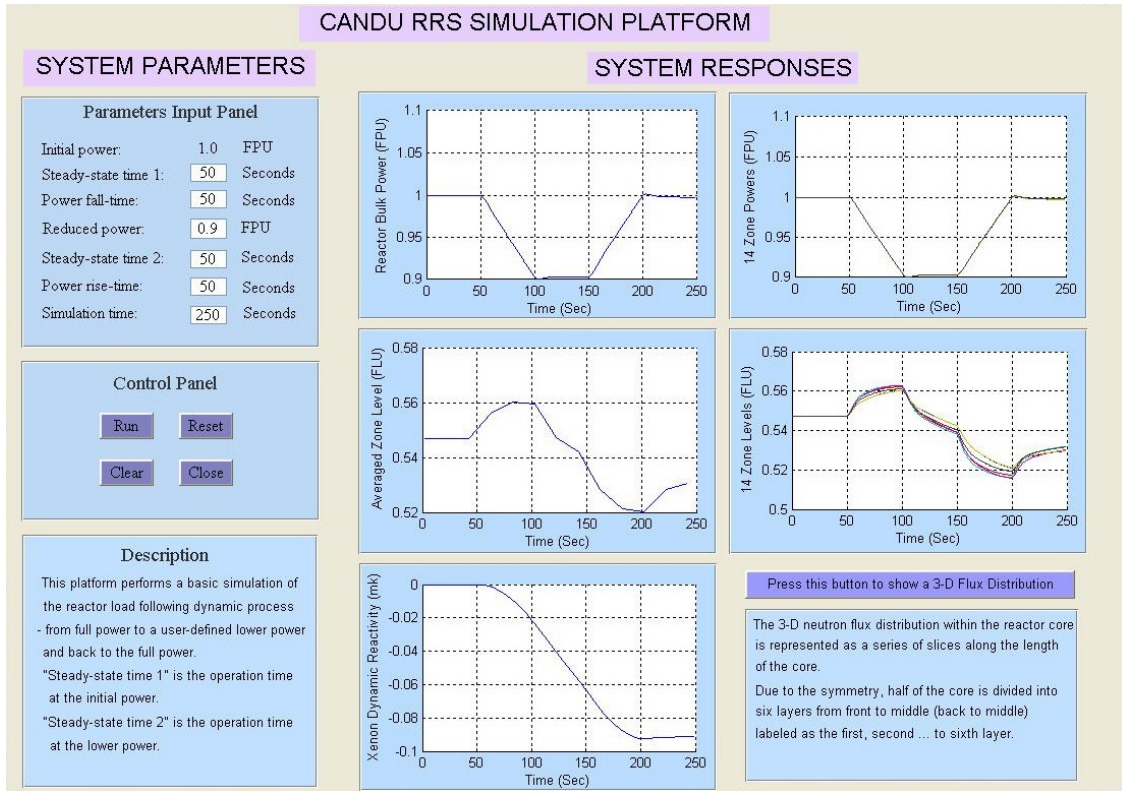
#### **4.5 CANDU RRS Graphical User Interface (GUI)**

A Graphical User Interface (GUI) allows users to perform tasks interactively. MATLAB GUI represents a convenient software environment for users to perform tasks such as creating and customizing plots, fitting curves and surfaces, and analyzing and filtering signals [66]. Users can also create custom GUIs for others to use – either by running them within MATLAB or as standalone applications that could be run independently in the MATLAB environment.

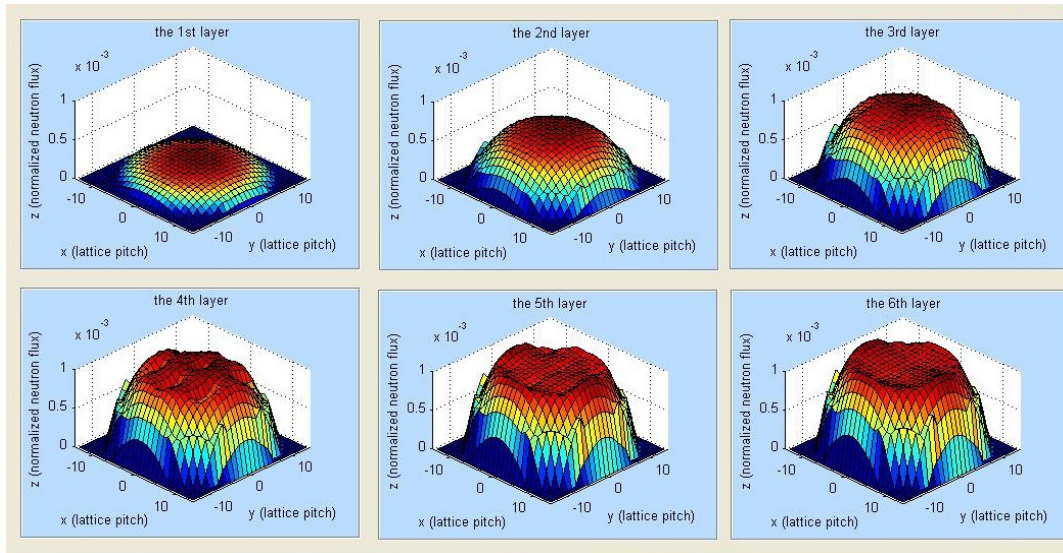
With the properties of MATLAB GUI, a user-friendly software package for CANDU RRS simulations can be created. The objective is to provide a convenient software environment for industrial users to perform related investigation, tests and even research

on the RRS and its internal routines and principles. The operation of this RRS application package does not have to depend on the MATLAB software environment. However, the MATLAB internal compiler has to be installed. Nevertheless, this still brings a flexible facility to the simulations of CANDU RRS, i.e., promptly obtaining simulation results such as all types of dynamic property responses of the reactor, even without the installation of MATLAB software.

Fig. 4.25 (a) and (b) represent the basic user interface and output display of the CANDU RRS GUI platform, including the 3-D flux distribution representation of the reactor core. From Fig. 4.25(a) it can be seen that the basic system parameters can be inputted to the “Parameter Input Panel”. After running, the reactor dynamic responses including reactor bulk power and zonal power responses, 14 zonal water levels and their averaged value, and Xenon buildup reactivity, could be depicted through the “System Responses” panel. Also, by pressing the blue strip button, the 3-D flux distribution within the core is represented, as shown in Fig. 4.25 (b). Furthermore, the user can modify the parameter values by “Parameters Input Panel” such that the corresponding system responses, in case of different transient conditions, can be generated. Detailed information about this software package is provided in Appendix D.



**Fig. 4.25(a) MATLAB GUI for CANDU RRS simulation platform**



**Fig. 4.25(b) 3-D flux distribution module of the CANDU RRS GUI**

## 4.6 Summary

The evaluation of the performance of the 3-D modal synthesis based reactor kinetic model in a closed-loop environment is carried out in a MATLAB/SIMULINK based RRS simulation platform. A notable advantage of the 3-D model is the level of details that it can reveal as compared to the coupled point kinetic model. Using the developed RRS simulation platform, the reactor internal behaviors can be revealed during load-following tests. The test results are also benchmarked against measurements from an existing power plant. It can be concluded that the 3-D reactor model produces more realistic view of the core neutron flux distribution, which is closer to the real plant measurements than that from a coupled point kinetic model. It is also shown that, through a vectorization process, the computational load of the 3-D model is comparable with that of the 14-zone coupled point kinetic model. Furthermore, the developed GUI software package for RRS' implementation represents a user friendly and independent application environment for education training and industrial utilizations.

## **V Power distribution control of CANDU reactors based on modal representation of reactor kinetics**

In this chapter, a state-feedback control strategy for CANDU reactor 3-D power distribution control is investigated. The reactor's neutronic kinetic model is represented by a 3-D modal model, and the control objectives are proposed. Linearization of the reactor model is then performed and evaluated. In the RRS simulations, the linearized reactor model demonstrates the same efficient performance as the nonlinear model. Based on the linear reactor model, a state-feedback control strategy regarding the proposed objectives is designed, and then implemented, with both the linearized and nonlinearized models towards a typical load following transient. Simulation results are analyzed, which validates the efficiency of the designed control law. Furthermore, ROP detectors are selected to investigate the local in-core power responses. A comparison of the achieved responses to those obtained from the RRS' simulations proves that the designed control strategy achieves superior performance on the 3-D power distribution regulating than the RRS does, and is therefore more successful in meeting the requirements of proposed CANDU reactor 3-D power distribution control objectives.

### **5.1 Brief introduction of the power distribution control problem**

Control of power distribution in the reactor core is a very important aspect of reactor operation, as the power distribution has direct implications of safety and fuel burn-up rate.

In CANDU reactors, long-term reactivity control is achieved through online refueling. The reactor regulating system (RRS) is employed to perform short-term power regulation to meet the reactor safety and power output requirements [67]. Control of the bulk and the differential power in the core is achieved through reactivity control devices, such as liquid zone controllers, adjustor rods and control absorbers [68]. Among these reactivity control devices, liquid zone controllers are primarily used to perform reactor power regulation. In CANDU reactors, the core has been divided into 14 zones, whereas a liquid controller is used in each zone. This chapter mainly concentrates on a new design of reactor power distribution control by taking advantages of modal representation of the reactor neutronic kinetics.

One of the main functions of RRS is to ensure that the reactor produces the maximal amount of power output without exceeding the physical limits of the fuel bundles and channel integrity. This is achieved through maintaining the reactor power level and the rate of change in power at specified values (bulk power control), and also keeping the core power distribution close to its design shape (spatial power control).

For the bulk power control, the desired power output is compared against the actual power output to produce a power error signal. This error signal is then used to regulate the levels in the liquid zone controllers to ensure that the actual power generated is close to the demand. From the core power distribution point of view, there is normally a desired power distribution shape for safe and efficient operation. For this reason, the reactor



power is often defined in terms of normalized power, rather than absolute power. The normalized power is essentially the ratio of the real power over the reference power. Because the reference power for each zone can be different, for the same normalized power, the real power in any particular zone can be different. In spatial power control, the desired average normalized power is calculated for each zone. The actual normalized zonal power is compared with the desired average normalized power to generate an error signal. There are 14 error signals in total, which are used by the respective liquid zone controllers to adjust zonal power so that the core power distribution is as close to the designed shape.

Although the existing RRS can carry out spatial power control using the above technique, it is still not able to achieve the power distribution shape ideally close to the nominal design. In this project, the developed 3-D modal-based neutronic kinetic model is used to develop new control strategies for more accurate 3-D power regulation for CANDU reactor core. In this modal synthesis method, the developed control strategy focuses on the dominant mode, which is the fundamental flux distribution adopted by the nominal design. As a result, the core power distribution during transients is closer to the nominal design shape than what a traditional RRS can achieve. A benefit of the improved core power distribution is also enhanced safety, because uncertainties and uneven power distribution have been reduced.

Over the years, significant amount of efforts have been made on the development of reactor kinetic models and subsequent control system designs. A coarse-mesh nodal reactor model is developed and used for spatial xenon-induced control [69]. The reactor model is comparable to the 14-coupled point kinetic model developed in [14]. However, these nodal models have their inherent limitations in spatial power distribution control as illustrated in Chapter I. For CANDU reactor control, a multivariable feedback control method is proposed based modal-based reactor model [9]. However, the research is limited to certain theoretical derivation, and the reactivity control devices are approximated by four spatial spots, which is significantly different to the current CANDU design. A 3-D power distribution control of a heating reactor is carried out in [70]. This work relies on a much simplified 3-D reactor neutronic kinetic model. The control objective is to ensure that the power distribution does not change significantly during a load-following process. As compared to the above works, the reactor model used in the current work reflects a real CANDU reactor core, and the resulting control system is much simpler to implement in practice.

## **5.2 Control oriented kinetics models for CANDU reactors**

### **5.2.1 Linearization of the reactor model**

A 3-D dynamic model for CANDU neutronic kinetics is described in Section 3.2 of Chapter III. This reactor model starts with the modal synthesis method and expands reactor dynamic variables such as neutron flux, delayed precursors' concentration, Iodine

and Xenon concentrations to the weighted sum of pre-designed neutron flux modes, such that the space-time dependant reactor dynamic system transforms to an only time-dependant one. The selected neutron flux modes have a (bi-) orthogonal property, which leads to the transformation of diffusion equations to the form of ordinary differential equations (ODE), and this makes the investigation of control strategies especially convenient. In Chapter IV, performance of this 3-D reactor model was evaluated through the closed-loop RRS' implementation and was demonstrated to be effectively used in the research and design of control problems. In Section 4.2.1, the reactor model has been written in a simple form with the criteria state-space format, as represented by Eqn. (4-1) to (4-4).

It is important to point out that the set of Eqns. (4-1) to (4-4) represents a nonlinear dynamic system in the state-space form. It is generally difficult to carry out control system design and analysis directly based on these equations. Linearization procedure has to be carried out first to convert nonlinear systems into linear ones around specific operating points. To linearize these equations, the modal kinetic Eqns. (3-5) to (3-8) are perturbed around the operating point as follows

$$N = N_0 + \Delta N \quad (5-1)$$

$$P = P_0 + \Delta P \quad (5-2)$$

$$I = I_0 + \Delta I \quad (5-3)$$

$$\mathbf{X} = \mathbf{X}_0 + \Delta\mathbf{X} \quad (5-4)$$

where the variables, N, P, I and X in the nonlinear equations are perturbed by  $\Delta N$ ,  $\Delta P$ ,  $\Delta I$  and  $\Delta X$  around the operating points,  $N_0$ ,  $P_0$ ,  $I_0$  and  $X_0$  for linearization. In the current, 100% full power operation at the fundamental mode condition is chosen as the operating point, as indicated in Eqn. (3-35)

$$\mathbf{N}_0 = [1, 0, \dots, 0]^T \quad (3-35)$$

It is to be noted that in the subsequent studies, the reactor power is allowed to change from 1.0 FPU to 0.9 FPU. In this research, the power maneuvering process is referred to the load-following case discussed in Chapter IV. Although reactor power varies in range from 1.0 FPU to 0.9 FPU, dynamic parameter changes in this range do not affect the linearization of the reactor model.

Then, substituting Eqns. (5-1) to (5-4) for Eqns. (4-1) to (4-4), removing the steady-state equations and omitting the higher-order infinitesimals, the set of Eqns. (4-1) to (4-4) becomes

$$\begin{aligned}
\frac{d}{dt} \begin{bmatrix} \Delta N \\ \Delta P \\ \Delta I \\ \Delta X \end{bmatrix}_{81 \times 1} &= \begin{bmatrix} \mathfrak{R}_{sck} + \frac{\mathfrak{R}_{L0}}{\Lambda} & blkdiag([\lambda_1 \cdots \lambda_6]) & 0 & -\sigma_X \varphi_f A_p \\ \frac{1}{\Lambda} blkdiag([\beta_1 \cdots \beta_6]^T) & -blkdiag(diag(\lambda_i)) & 0 & 0 \\ \frac{\gamma_I}{v\Lambda} I_{9 \times 9} & 0 & -\lambda_I I_{9 \times 9} & 0 \\ \frac{\gamma_X}{v\Lambda} I_{9 \times 9} - \sigma_X \varphi_f A blkdiag(X_0) & 0 & \lambda_I I_{9 \times 9} & -\lambda_X I_{9 \times 9} - \sigma_X \varphi_f A_p \end{bmatrix}_{81 \times 81} \begin{bmatrix} \Delta N \\ \Delta P \\ \Delta I \\ \Delta X \end{bmatrix}_{81 \times 1} \\
+ \begin{bmatrix} B_{9 \times 14} \\ 0 \end{bmatrix}_{81 \times 14} \Delta u_{14 \times 1} &
\end{aligned} \tag{5-5}$$

where  $\mathfrak{R}_{L0}$  is the modal coupled reactivity matrix  $\mathfrak{R}_L$  evaluated at the operating point.

$A_p$  is a submatrix of  $A$ , containing the first nine columns of  $A$ .

$\Delta u$  is a vector containing the control signals to vary the water levels in 14 liquid zone controllers. It can be represented as:

$$\Delta u = [\Delta u_1, \Delta u_2, \dots, \Delta u_{14}]^T \tag{5-6}$$

$B_{9 \times 14}$  is a constant matrix defined as

$$B_{9 \times 14} = \frac{3.33}{\Lambda} [\Delta \Theta_{1,1} \quad \cdots \quad \Delta \Theta_{14,1}]_{9 \times 14} \tag{5-7}$$

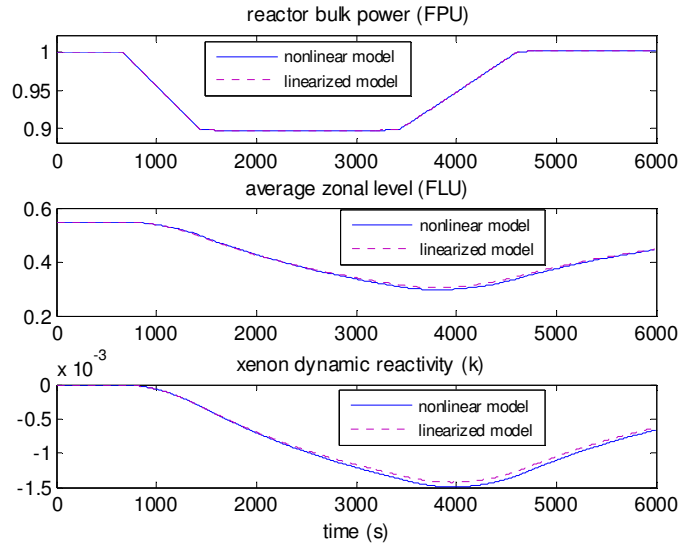
where  $\Delta \Theta_{n,1}$  is the first column of  $\Delta \Theta_n$ , which is the incremental modal reactivity of the  $n^{th}$  zone,  $n = 1$  to 14, when the water level in the zone increases from 0.25 full level unit (FLU) to 0.55 FLU. The detailed derivation of Eqn. (5-7) is described in Appendix E.

The detailed derivation procedure of linearization is also represented in Appendix E.

### 5.2.2 Validation of the linearized model

One efficient way to validate the linearized model is to make use of the developed CANDU RRS simulation platform, through which simulation results based on the original nonlinear models and the linearized model can be compared. A load-following scenario from Chapter IV has been utilized.

The reactor power is reduced from 1.0 FPU to 0.9 FPU at a rate of  $1.28 \times 10^{-4}$  FPU/s and returns to 1.0 FPU at a rate of  $8.33 \times 10^{-5}$  FPU/s. The entire process takes 6,000 seconds. The simulation results are shown in Fig. 5.1, where the bulk power, averaged zonal level and Xenon dynamic reactivity transients are compared. The simulation results have proved that the linear model can provide a reasonable approximation to the nonlinear model under this specific power maneuvering operation. From the results, it can be concluded that the linearized reactor model is sufficiently accurate to be used for investigations into new control strategies for the reactor regulation system.



**Fig. 5.1 Simulation results of reactor dynamics with two reactor models using RRS’ simulation**

### 5.3 Control of power distribution in the reactor

The control objective can be summarized as follows: regulating the perturbed time-amplitudes of neutron flux -  $\Delta N$  to a deducible trajectory, such that the normalized 3-D mesh powers can be regulated according to the pre-designed time-varying power load set-point. Consequently, the 3-D power distribution shape of the core is accurately maintained. Simultaneously, the system is robust enough to suppress potential disturbance and the controller movement is minimized during the transient.

According to the modal expansion Eqn. (3-5) about the neutron flux, if both sides of the equation are divided by the neutron flux at the initial full power operation, which is also the fundamental flux mode  $\psi_1(r)$ , the space-time 3-D core power distribution expressed

by the normalized power concept is represented by

$$P_{3D}(r,t) := \frac{\phi(r,t)}{\psi_1(r)} = n_1(t) + n_2(t) \frac{\psi_2(r)}{\psi_1(r)} + \dots + n_9(t) \frac{\psi_9(r)}{\psi_1(r)} \quad (5-8)$$

For a given flux amplitudes  $[n_1 \dots n_9]^T$  calculated by the reactor model, the normalized power of any mesh point in the core can be estimated by using Eqn. (5-8). This equation can also be used to evaluate the reactor bulk power as a function of time by integrating both sides over the reactor core volume. Hence, by using Eqn. (5-8), the reactor bulk power, 14 zonal powers and the power distribution at any mesh point can be predicted.

As mentioned in Section 5.1, the main goals of the reactor control during a power transient are to regulate the reactor bulk power according to power set-point, in the meantime, to maintain the shape of core power distribution as close to the nominal design as possible, to avoid overriding fuel bundle and exceeding the channel power limits. The current CANDU RRS is unable to precisely control the power distribution in the core. Using the new designed control method, more accurate core power distribution can be achieved such that the resulting power distribution is more closely resemble the nominal design shape. The efficient method to realize this objective is to regulate the dynamic of 3-D normalized power distribution exactly to the power set-point trajectory during the transient.

From Eqn. (5-8), it can be observed that, in order to minimize the time amplitudes of the



high order flux modes, i.e., if  $[n_2 \cdots n_9]^T = 0$ , the 3-D power distribution  $P_{3D}(r, t)$  is no longer a function of the spatial position  $r$ , which means that the power at every mesh structure, as well as the reactor bulk power, can be represented in terms of  $n_1(t)$  only. Consequently, control of the reactor bulk and spatial power during transients can be achieved by using a robust tracking and disturbance rejection technique, that is to minimize  $[n_2, \cdots, n_9]^T$  to  $[0, \cdots, 0]^T$  and regulate  $n_1$  to  $P_r(t)$ , where  $P_r(t)$  is the designed power set-point. Simultaneously, the influence of the disturbances can be suppressed. Furthermore, using the incremental concept as used in most areas of this chapter,

$$\begin{aligned}\Delta N &= [n_1, n_2, \cdots, n_9]^T - [1, 0, \cdots, 0]^T \\ &= [n_1 - 1, n_2, \cdots, n_9]^T\end{aligned}\quad (5-9)$$

the control objective is transformed to regulate the  $\Delta N$  to  $r_y$ , where  $r_y$  is defined as

$$r_y = [P_r(t) - 1, 0, \cdots, 0]^T \quad (5-10)$$

With the definition of

$$A_x = \begin{bmatrix} \Re_{sck} + \frac{\Re_{L0}}{\Lambda} & \text{blkdiag}((\lambda_1 \cdots \lambda_6)) & 0 & -\sigma_x \varphi_f A_p \\ \frac{1}{\Lambda} \text{blkdiag}((\beta_1 \cdots \beta_6)^T) & -\text{blkdiag}(\text{diag}(\lambda_i)) & 0 & 0 \\ \frac{\gamma_f}{v\Lambda} I_{9 \times 9} & 0 & -\lambda_f I_{9 \times 9} & 0 \\ \frac{\gamma_x}{v\Lambda} I_{9 \times 9} - \sigma_x \varphi_f A \text{blkdiag}(X_0) & 0 & \lambda_f I_{9 \times 9} & -\lambda_x I_{9 \times 9} - \sigma_x \varphi_f A_p \end{bmatrix}_{81 \times 81} \quad (5-11)$$

$$B_x = \begin{bmatrix} B \\ 0 \end{bmatrix}_{81 \times 1} \quad (5-12)$$

Eqn. (5-5) can be simplified to

$$\frac{dx}{dt} = A_x x + B_x \Delta u \quad (5-13)$$

Then, define the output  $y$  as follows

$$y = C_x x \quad (5-14)$$

in which

$$C_x = \begin{bmatrix} I_{9 \times 9} & \\ & O_{72 \times 72} \end{bmatrix}_{81 \times 81} \quad (5-15)$$

and  $O_{72 \times 72}$  is the zero matrix with the dimension of  $72 \times 72$ , such that  $y = \Delta N$ .

Eqns. (5-13) and (5-14) represent a standard space-time dynamic model of CANDU 3-D reactor kinetics. With this model the control problem can be synthesized by minimizing an optimum performance index - the quadratic cost function, as

$$J = \int_0^{t_f} \{x^T Q_x x + (y - r_y)^T Q_y (y - r_y) + \Delta u^T R \Delta u\} dt \quad (5-16)$$

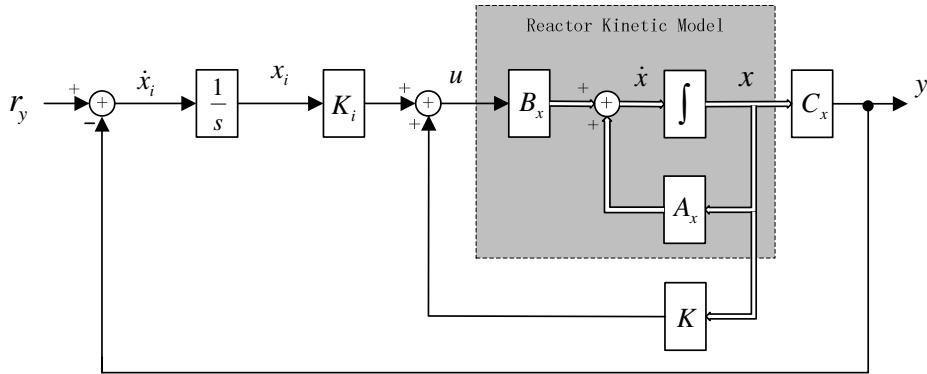
where  $Q_x$  and  $Q_y$  are non-negative definite matrices; and  $R$  is a positive definite matrix. In Eqn. (5-16), the item of  $x^T Q_x x$  minimizes the system state deviations. The second item,  $(y - r_y)^T Q_y (y - r_y)$ , regulates the  $y$ , which is  $\Delta N$ , to the desired

trajectory  $r_y$ , as specified by Eqn. (5-10). Subsequently, using Eqn. (5-1), i.e.  $N = N_0 + \Delta N$ , the real state  $N$  is regulated to  $r_y + N_0$ , i.e.  $[P_r(t), 0, \dots, 0]^T$ , as indicated by Eqn. (5-10).

Consequently, according to Eqn. (5-8), the 3-D power distribution dynamics within the core,  $P_{3D}(r,t)$ , can be regulated to  $P_r(t)$ .  $P_r(t)$  is the referenced power load set-point changing with time. That means, in this way, each mesh power within the core, rather than 14 zonal powers, changes according to the trajectory of  $P_r(t)$ . Hence, the power distribution shape can be maintained to the nominal designed shape accurately.

#### **5.4 Feedback control system design for the 3-D power distribution control**

A Linear-Quadratic-Integral (LQI) control [71] is used to synthesize the control system. Fig. 5.2 depicts a block diagram representation of state-feedback control of the reactor system.



**Fig. 5.2 A block diagram of the state-feedback design for CANDU reactor power distribution control**

Using a state augmentation technique with the definition of the following error signal

$$\frac{dx_i}{dt} := e = r_y - y = r_y - C_x x \quad (5-17)$$

An augmented dynamic system can be represented as

$$\frac{d}{dt} \begin{bmatrix} x \\ x_i \end{bmatrix}_{90 \times 1} = \begin{bmatrix} A_x & 0 \\ -C_x & 0 \end{bmatrix}_{90 \times 90} \begin{bmatrix} x \\ x_i \end{bmatrix} + \begin{bmatrix} B_x \\ 0 \end{bmatrix}_{90 \times 14} \Delta u_{14 \times 1} + \begin{bmatrix} 0 \\ r_y \end{bmatrix}_{90 \times 1} \quad (5-18)$$

Correspondingly, the output  $y$  becomes

$$y = [C_x \quad 0] \begin{bmatrix} x \\ x_i \end{bmatrix} \quad (5-19)$$

Using the LQR design technique method, the state-feedback control law can be represented as follow:

$$\Delta u = -[K \quad K_i] \begin{bmatrix} x \\ x_i \end{bmatrix} \quad (5-20)$$

This control law ensures that the output  $y$  tracks the reference command  $r_y$  by proper regulations of water levels in the liquid zone controllers. The newly designed control law will lead to 3-D power distribution within the core, as well as the reactor bulk power, having a similar dynamic process as the power setpoint does.

## **5.5 Performance evaluation of the power distribution control**

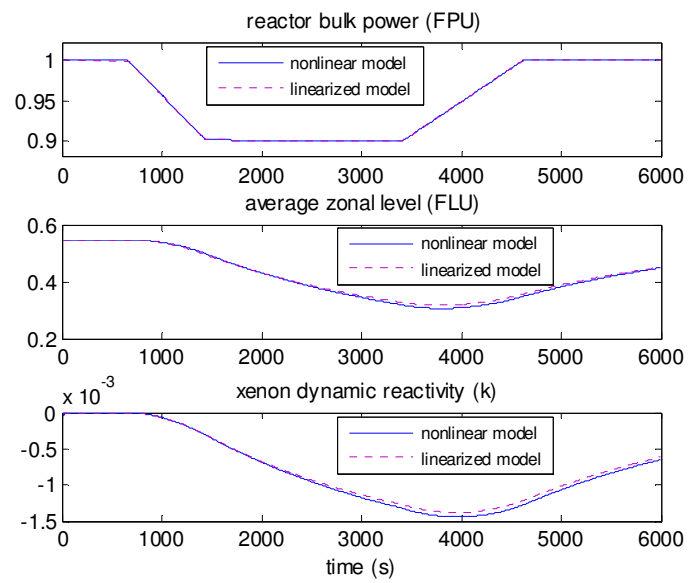
### **5.5.1 Simulations of Power Regulation based on Linear and Nonlinear Reactor Models**

MATLAB/SIMULINK software environment brings great convenience to the numerical simulation and control system design. Particularly, it has provided internal functions to solve common problems or equations. With the 'lqr' function [64] applied to the augmentation system represented by Eqn. (5-18), the feedback gain  $[K \quad K_i]$  is calculated, such that with the feedback control law provided by Eqn. (5-20) the augmentation system can be stabilized. Also, when the gains are separately manipulated to the control system shown in Fig. 5.2, the closed-loop is performed such that the output  $y$  is regulated to the reference signal  $r_y$ , and simultaneously the system state is stabilized and the controller has minimum movement. In this way, the 3-D reactor power control objectives are realized. Appendix F represents the SIMULINK module for the

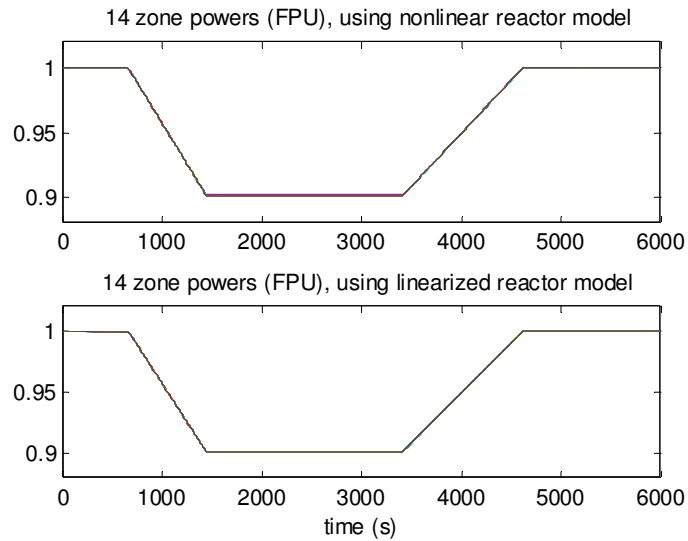
implementation of CANDU reactor power distribution control.

In order to demonstrate the implemented efficiency of the designed 3-D power control strategy, it is also performed regarding the original nonlinear reactor dynamic model. Fig. 5.3 provides simulation results about some dynamic responses, including reactor bulk power, averaged zonal level and Xenon dynamic reactivity, applying the 3-D control law to both reactor models. This dynamic information illustrates the power regulating function of the RRS, which also indicates the reactor's dynamic property. As a comparison, simulation results of both linear and nonlinear reactor models are displayed. Fig. 5.3 illustrates that the newly designed 3-D power control strategy achieves the consistent consequents regarding the bulk power control objective based on simulations to both linearized and nonlinear reactor models. The liquid zone controller signal and Xenon dynamic information also reveals that, implementing the new control strategy on the original reactor model achieves the same efficiency as the linearized model. Furthermore, Fig. 5.4 shows a comparison of 14 zone power simulation results when the designed control strategy is implemented based on two reactor models. The comparison shows that applications of the designed control strategy to both reactor models achieve the same objectives about RRS's spatial control function – maintaining the flux distribution through balancing 14 zone powers. All these demonstrations indicate that the designed 3-D power control strategy could perform the main power regulating functions of the RRS when it is implemented on not only the linearized reactor model, but also the

original nonlinear model. However, according to the designed 3-D power control objective, demonstrations of the new controller's advantages depend on the illustration of 3-D dynamic information. The detailed information about the reactor 3-D dynamic properties is revealed in the following sections.



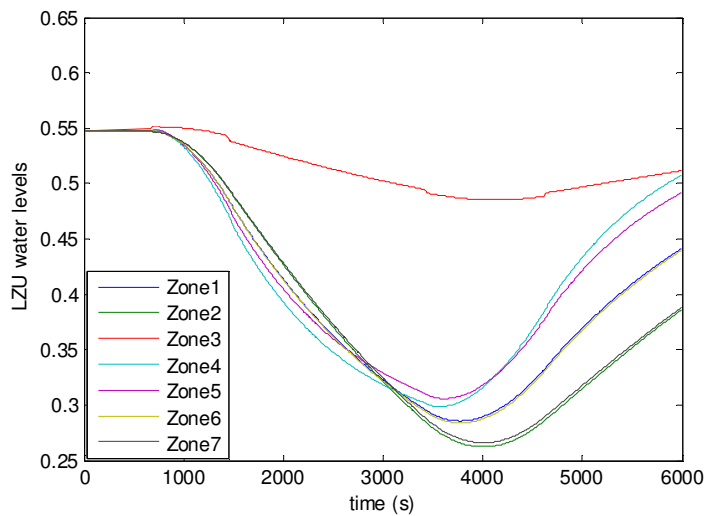
**Fig. 5.3 The closed-loop dynamic system responses of the designed control strategy under two reactor models**



**Fig. 5.4 Variations of 14 zonal powers under linearized and nonlinear reactor models**

Furthermore, Fig. 5.5 shows the transient simulation results of 14 zone water level response. As compared to Fig. 4.14 under the RRS control, this figure has an apparently different response about the zone water levels. From the perspective of control methods, the RRS converges all the zone levels to a common trajectory by minimizing their deviations from their average level, which results in Fig. 4.14. However, the new control method minimizes 14 water levels' deviations from their initial steady-state level (in this case, 0.547 FLU), which saves the operating energy of the controllers. RRS' protection on water level control is to prevent the liquid zone controllers from draining way. In Fig. 4.14, the lowest water level is around 0.3 FLU. In Fig. 5.5, the lowest water level is about 0.26, which is still far away from draining away in this case. Furthermore, the water level response is also related to the internal reactor kinetics, which will be further discussed in Section 5.5.3.





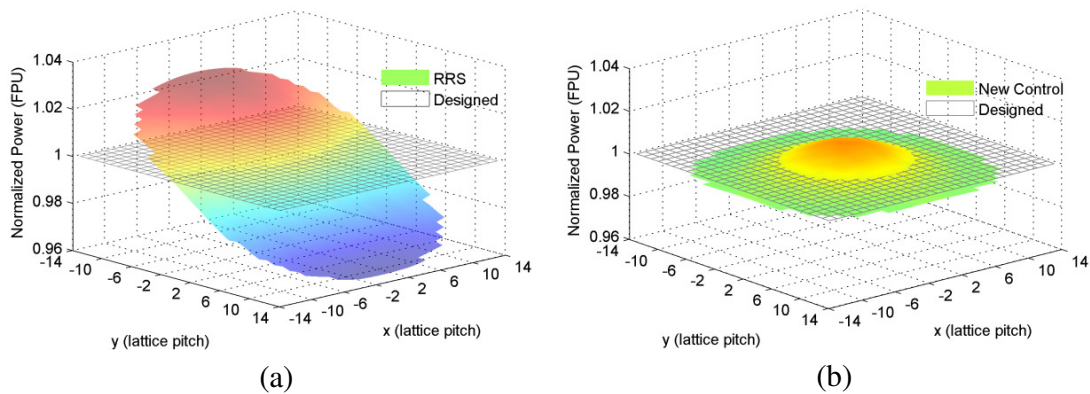
**Fig. 5.5 Simulation results of 14 zone water levels using the newly designed control strategy**

### 5.5.2 3-D power distribution of the closed-loop reactor system

Further demonstrations are manipulated regarding the power distribution shape changing within the core in a 3-D manner. A particular time spot,  $t=4620$  s, is selected, which represents the highest power level during the load-following process. Half of the reactor core is divided into 6 layers, due to its symmetric characteristic revealed in Chapter III. As a typical layer with 7 liquid zone controllers distributed, the fourth layer from the end plane is selected to show the 3-D power distributions in a mesh structure with the dimension of (28, 28).

Fig. 5.6 shows some of the 3-D normalized power distributions within the selected core layer under the different conditions. Fig. 5.6(a) represents the normalized power

distribution under the RRS' control. However, as a comparison, the nominal distribution shape is represented as a slab and the nominal power is equal to 1.0 everywhere within it. Then it can be seen that the normalized power distribution under RRS' control has a remarkable tilt along the y direction, although the relative error is stabilized within the range of 4%. This illustrates that in the time spot,  $t=4620s$ , the power distribution shape is still significantly different from the initial steady-state nominal designed shape. Furthermore, Fig. 5.6(b) provides a comparison of the power distributions under the new control and of the nominal design. It can be seen that, with the implementation of new control design, the power distribution tilt is greatly suppressed. This visually demonstrates that the newly designed control strategy provides a better performance with regards to maintaining the power distribution shape during the load-following transient than the RRS does.



**Fig. 5.6 Normalized power distributions of the fourth layer of the core at 4,620 s under two different control schemes (a) RRS control, and (b) new control scheme.**

Detailed information about the local power change under both control patterns is

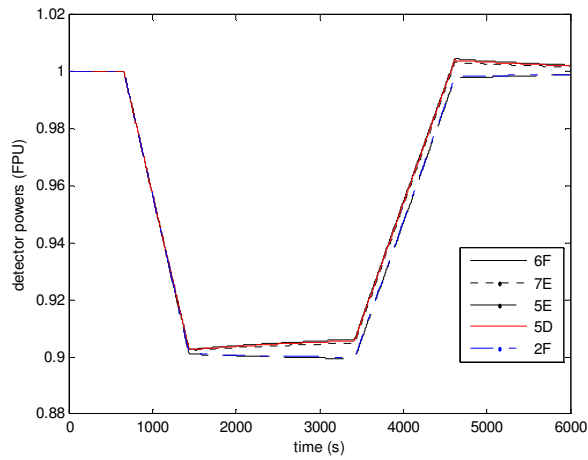
illustrated by Table 5.1. The mesh dimension can refer to Fig. 4.16. In this table some mesh powers are selected from layer 4 and compared with different control methods; this clearly shows that the power level decreases in y direction under RRS' control, and also deviates from the nominal power level. However, after the improved new control, all the mesh powers are changed to be very close to the nominal power level, which ensures that the power distribution shape is significantly similar to the nominal designed shape. Furthermore, more attention is paid to the high power level areas under RRS' control. With the new control strategy, the high power level in those areas has been suppressed, which typically contributes to the reactor's safe performance. This will be further illustrated in the next section.

**Table 5.1 Selected mesh power changes under different control methods**

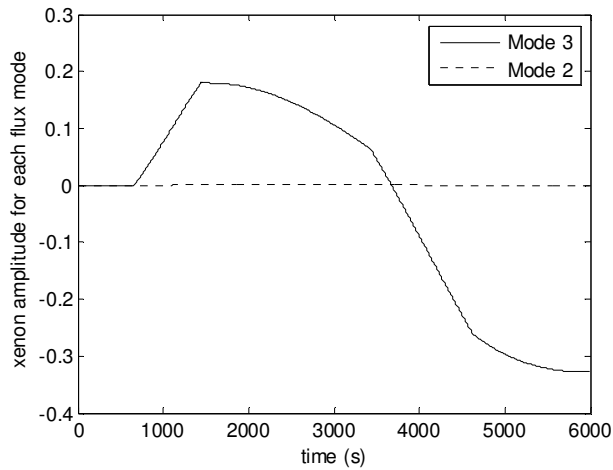
Mesh Dimensions	RRS Control	New Control
(2,14)	1.0262	0.9938
(7, 7)	1.0158	0.9943
(7, 14)	1.0245	0.9972
(7, 21)	1.0176	0.9943
(14, 7)	0.9975	0.9979
(14, 14)	1.0075	1.0008
(14, 21)	0.9993	0.9994
(21, 7)	0.9735	0.9956
(21, 14)	0.9729	1.0002
(21, 21)	0.9731	0.9960
(27, 14)	0.9613	0.9948

### 5.5.3 Power transients of ROP detectors under the new control strategies

In order to illustrate the changed reactor internal dynamics when the RRS control system is replaced by the designed 3-D control strategy, the same ROP detectors are selected as the simulation targets that are shown in Section 4.5.4. For a comparison, Fig. 5.7 provides simulation results of the power dynamics within ROP detectors when the new control law is implemented. Contrasted to Fig. 4.17, for both the upper and lower detectors, the responses of detectors' power transients are closer to the setpoint trajectory. This indicates that, the newly designed power distribution control strategy brings more efficiency to the power distribution regulating than the RRS control system. Consequently, the 3-D power distribution shape of the core is better maintained. Further illustration is provided by Fig. 5.8, which represents the corresponding Xenon amplitudes' dynamic response. It can be seen that, flux mode 3 still contributes more than mode 2 during the load-following transient. However, when compared to Fig. 4.18, the magnitude of Xenon amplitude with mode 3 is far smaller than that in Fig. 4.18. This reveals that the 3-D control strategy obtains a better function for suppressing the irregular spatial Xenon distribution, such that it could perform a more accurate regulating to the local power distribution than the RRS.



**Fig. 5.7 Simulation results of the power dynamics within selected ROP detectors implemented by 3-D control strategy**



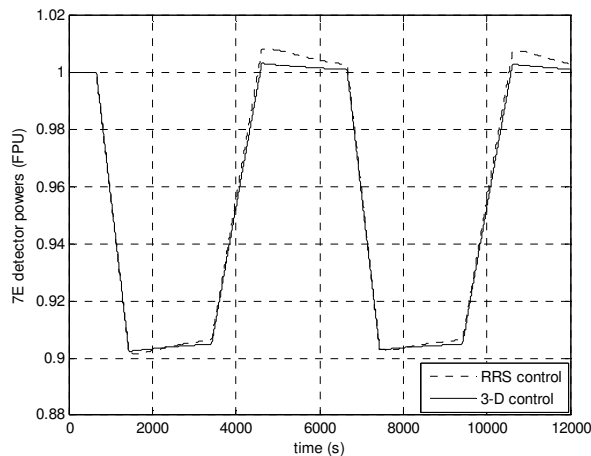
**Fig. 5.8 Simulation results of Xenon amplitudes for flux modes 2 and 3 implemented by 3-D control strategy**

By comparing Fig. 5.8 with Fig. 4.18, and comparing Fig. 5.5 with Fig. 4.14, because

mode 3 doesn't contribute much for Xenon dynamics in both cases, the water level still has the similar response within bilaterally symmetric zones such as zone 1 and 6, or zone 2 and 7, since the power level is similar within the symmetric zones; however, mode 2 contributes more for Xenon dynamics in both cases. In Fig. 4.17, reactor power in the upper areas is higher than the under areas. From the steady-state analysis way, in order to reduce the reactor power, the water level in the liquid zone controller such as zone 3 will be increased, as illustrated in Fig. 5.5. Following this, Xenon reactivity is build up in the upper areas, such that it makes up the negative amplitudes in Fig. 4.18 and leads to Fig. 5.8. This qualitatively analyzes that in Fig. 5.5 the water level in zone 3 is relatively higher than other zones, as well as the average level shown in Fig. 5.3, although the entire process belongs to the dynamic process, which is more complicated than the steady-state.

In order to further illustrate the benefit brought about by the new control strategy as compared to the RRS control, more simulation results are generated in Fig. 5.9. As shown in Fig. 5.7, the ROP detector – 7E has the highest power transient during the load following process when the RRS is implemented. Then this detector is selected as the simulation target, and two load following cycles are simulated. From Fig. 5.9 it can be seen that, using the new control strategy, the detector's power transient response is regulated closer to the setpoint trajectory than the RRS control. An important phenomenon to be noted is that, both highest power points have been significantly suppressed. This implies that the safety margin regarding postulated accidents is

increased within this load following process, if the safety margin is defined as the distance from the highest power point to TSP. Thus, it can be concluded that, if the newly designed power distribution control strategy replaces the RRS control logics, reactor operation becomes much safer than it used to be; or, by remaining the original safety margin, reactor operation could be adjusted to the higher power level, such that more economic benefits could be obtained.



**Fig. 5.9 Simulation results of 7E ROP detector power transients implemented by RRS and the new control strategy**

## 5.6 Summary

A CANDU reactor oriented 3-D neutronic kinetic model for control system design is represented. The linearized version is validated against the existing RRS through the load-following simulations. Using this model, a control objective for improving reactor 3-D power distribution control is proposed. Subsequently, a feedback control strategy

using the LQI method is designed to achieve the objective. The control system is then evaluated on both the linearized and original nonlinear reactor models. Typical ROP detectors are selected for investigating the local power dynamics. Case studies illustrate that the newly designed control strategy based on the linearized reactor model can produce a performance similar to the original nonlinear reactor model. By analyzing the ROP detectors' power transients, it is shown that the new control law can not only improve economical operation, but also improve safety as the uncertainties and the uneven power distribution are reduced.



## **VI Conclusions and suggestions for future works**

### **6.1 Conclusions**

A modal model for three-dimensional space-time neutronic behaviors of the CANDU reactor has been developed. Subsequently, a non-dimensional representative of the reactor kinetic model in MATLAB/SIMULINK software environment is proposed. A steady-state calculation method is described to determine the initial conditions for the simulation. Furthermore, implementation of the reactor modal model is carried out within a MATLAB/SIMULINK simulation platform for CANDU-RRS system. Load following studies are performed.

The evaluation of the performance of the 3-D modal synthesis model in a closed-loop environment is carried out. A notable advantage of the modal synthesis model is the level of details that it can be revealed as compared to coupled point kinetic models. Using the developed simulation platform, the reactor core power distribution can be monitored during load-following tests. The test results have also been benchmarked against measurements from an existing CANDU plant. It can be concluded that the 3-D modal synthesis model produces more accurate representation of the core neutron flux distribution, which is closer to the real plant measurements than that from a coupled point kinetic model. It is also shown that, through a vectorization process, the computational load of the 3-D model is comparable with that of 14-zone coupled point kinetic model

used in previous studies.

Based on the developed 3-D reactor kinetic model, a new control strategy for the 3-D reactor power distribution control is proposed. In order to investigate this control problem, the linearization of the reactor model is performed. The linearized model has been validated by the RRS simulation platform under load following simulation studies. A state-feedback control strategy based on linear quadratic integral (LQI) method is designed. The load following transient behavior is then simulated by implementing the new control strategy to both the linearized and original reactor models. Typical ROP detectors are selected for investigating the local power dynamics.

The conclusion is that the newly designed 3-D control strategy can also be used to control the original nonlinearized reactor model, and achieves satisfaction control on the 3-D reactor power distribution. By analyzing the ROP detectors' responses, it is concluded that the application of 3-D control strategy is able to improve the reactor performance, or potentially improves economy as compared with the current RRS.

## **6.2 Recommendation for future works**

a) From the perspective of control problem investigations, the order of 3-D reactor dynamic model is  $81 \times 81$ . This is still too large. If we can simplified this reactor model by replacing 6-group neutron delayed precursors with only one group delayed neutron precursors, the order of the reactor model can be reduced to  $27 \times 27$ . This will

significantly mitigate the computing burden during the implementation phase. However, the simplified reactor model has to be evaluated through the RRS' closed-loop implementations, as well as the linearization process.

b) If a) can be successfully realized, a new performance index optimizing the dynamic 3-D reactor power distribution can be proposed. This index is different from that in our research, although the final control objective is the same, i.e. maintaining the 3-D power distribution shape as close as the nominal shape. In fact, our index in this thesis is represented only by constraining the time-amplitudes of the neutron flux. However, the new index is represented by constraining the real 3-D mesh-power and the reactor bulk power to the dynamic power set-point (using the unit of FPU). The new index can be defined to minimize

$$J = \frac{1}{2} \int_0^T [(P^r - P_b)^2 + \int_V (P^r - P_i(V))^2 dV + u^T R u] dt \quad (6-1)$$

in which,  $T$  is the transient time;  $P^r$  is the dynamic level of power set-point;  $P_b$  is reactor bulk power;  $V$  is the reactor volume;  $P_i(V)$  is the 3-D pin-power;  $u$  represents the control signal – liquid zone water levels. This can be a real 3-D power optimum control.

## References

- [1] G. Bereznai, *Nuclear Power Plant Systems and Operation-CANDU Overview*, AECL & Chulalongkorn University, Bangkok, Thailand.
- [2] K. Weston, *Energy Conversion*, E-book of the University of Tulsa, the United States, 1992.
- [3] *Nuclear Power in an Age of Uncertainty*, Congress of the United States, Office of Technology Assessment, OTA-E-216, Feb. 1984.
- [4] B. Hanna, "CATHENA: A Thermal-hydraulic Code for CANDU Analysis," *Nuclear Engineering and Design*, vol. 180, no. 2, pp. 113-131, 1998
- [5] B. Rouben, "Overview of Current RFSP-code Capabilities for CANDU Core Analysis," *Transactions of the American Nuclear Society*, vol. 72, pp. 339-340, 1995.
- [6] M. Tayal, E. Mischkot, and H. Sills, "ELOCA-A: A Code for Radial and Axial Behavior of CANDU Fuel Elements at High Temperatures," *Nuclear Technology*, vol. 76, no. 2, pp. 209-220, 1987.
- [7] B. Frogner and H. Rao, "Control of Nuclear Power Plants," *IEEE Transactions on Automatic Control*, vol. AC-23, no. 3, pp. 405-417, 1978.
- [8] D. Cherchas and R. Lake, "An Optimal Control Algorithm for Nuclear Reactor Load

Cycling,” *Automatica*, vol. 13, pp. 279-285, 1977.

[9] D. Cherchas and C. Mewdell, “A Control Algorithm for Reactor Spatial Control During Nuclear Station Load Cycling,” *Journal of Dynamic Systems, Measurement, and control*, vol. 100, pp. 219-226, 1978.

[10] D. Cherchas and S. Ng, “Optimum Control of Neutron Flux during Nuclear Station Load Following,” *Automatica*, vol. 14, pp. 533-546, 1978.

[11] G. Yorke and D. Cherchas, “An Algorithm for Non-Linear Space-Time Nuclear Reactor Control,” *Automatica*, vol. 17, pp. 471-482, 1981.

[12] M. Berka and D. Cherchas, “A Discrete-time Algorithm for Nuclear Reactor Spatial Control,” *Automatica*, vol. 21, pp. 465-471, 1985.

[13] A. Tiwari, “Modeling and Control of a Large Pressurized Heavy Water Reactor,” Ph. D. dissertation, Indian Institute of Technology, Bombay, 1999.

[14] H. Javidnia, J. Jiang, and M. Borairi, “Modeling and Simulation of a CANDU Reactor for Control System Design and Analysis,” *Nuclear Technology*, vol. 165, no. 2, pp. 174-189, 2009.

[15] J. Luxat and G. Frescura, “Space-Time Neutronic Analysis of Postulated Loss-of-Coolant Accidents in CANDU Reactors,” *Nuclear Technology*, vol. 46, pp.

507-516, 1979.

[16] J. Koclas, *Reactor Control and Simulation*, Chulalongkorn University, Thailand, 1996; available on the Internet at <http://canteach.candu.org/library020044301.pdf>.

[17] T. Sutton and B. Aviles, "Diffusion Theory Methods for Spatial Kinetics Calculations," *Progress in Nuclear Energy*, vol. 30, pp. 119-182, 1996.

[18] W. Stacey, *Nuclear Reactor Physics*, John Wiley & Sons Inc., USA, 2001

[19] M. Khajavi, M. Menhaj, and A. Suratgar, "A Neural Network Controller for Load Following Operation of Nuclear Reactors," *Annals of Nuclear Energy*, vol. 29, pp. 751-760, 2002.

[20] F. McDonnell, A. Baudouin, P. Garvey, and J. Luxat, "CANDU Reactor Kinetics Benchmark Activity," *Nuclear Science and Engineering*, vol. 64, pp. 95-105, 1977.

[21] B. Monaghan, F. McDonnell and H. Hinds, "Hybrid Simulation of Reactor Kinetics in CANDU Reactors Using a Modal Approach," *Simulation*, vol. 35, pp. 21-33, Jul. 1980.

[22] J. Koclas, *Neutronic Analysis of Reactors*, Canteach Training Program, Thailand: Chulalongkorn University Technical Documents.

[23] W. Harmon Ray, "Multivariable process control - a survey," *Computers & Chemical Engineering*, vol. 7, no. 4, pp. 367-394, 1983.

- [24] T. Huang, and K. Han, "Design of Nuclear Reactor Control Systems by the Horowitz Method," *IEEE Transactions on Nuclear Science*, vol. NS-26, no. 1, pp. 959-970, 1979.
- [25] Z. Dong, "Nonlinear State-Feedback Dissipation Power Level Control for Nuclear Reactors," *IEEE Transactions on Nuclear Science*, vol. 58, no. 1, pp. 241-257, 2011.
- [26] H. Li, X. Huang, and L. Zhang, "Operation and Control Simulation of a Modular High Temperature Gas Cooled Reactor," *IEEE Transactions on Nuclear Science*, vol. 55, no. 4, pp. 2357-2365, 2008.
- [27] M. Park, and N. Cho, "Time-Optimal Control of Nuclear Reactor Power with Adaptive Proportional-Integral-Feedforward Gains," *IEEE Transactions on Nuclear Science*, vol. 40, no. 3, pp. 266-270, 1993.
- [28] M. Saif, "Suboptimal Projective Control of a Pressurized Water Reactor," *IEEE Transactions on Nuclear Science*, vol. 36, no. 6, pp. 2459-2465, 1989.
- [29] H. Ukai, and T. Iwazumi, "A New Approach to Control of Xenon Spatial Oscillation during Load Follow Operation via Robust Servo Systems", *IEEE Transactions on Nuclear Science*, vol. 41, no. 6, pp. 2675-2685, 1994.
- [30] H. Arab-Alibeik, and S. Setayeshi, "Adaptive Control of a PWR Core Power Using Neural Networks," *Annals of Nuclear Energy*, vol. 32, iss. 6, pp. 588-605, 2005.

[31] A. Parlos, A. Henry, F. Schweppe, L. Gould, and D. Lanning, "Nonlinear Multivariable Control of Nuclear Power Plants Based on the Unknown-but-Bounded Disturbance Model," *IEEE Transactions on Nuclear Science*, vol. 33, no. 2, pp. 130-137, 1988.

[32] K. Ott and R. Neuhold, *Introductory Nuclear Reactor Dynamics*, American Nuclear Society, La Grange Park, Ill., USA, 1985.

[33] Z. Cai and J. Pu, *Nuclear Power Reactor Neutron Dynamics*, National Defense Industry Press, Beijing, China, 2005.

[34] T. Sutton and B. Aviles, "Diffusion Theory Methods for Spatial Kinetics Calculations," *Progress in Nuclear Energy*, vol. 30, no. 2, pp. 119-182, 1996.

[35] MathWorks homepage: <http://www.mathworks.com/>

[36] *MATLAB SIMULINK - Simulation and Model Based Design*; available on the Internet at [http://www.tufts.edu/~rwhite07/PRESENTATIONS\\_REPORTS/simulink.pdf](http://www.tufts.edu/~rwhite07/PRESENTATIONS_REPORTS/simulink.pdf)

[37] Donald Ross Ferguson, *Solution of the Space-dependent Reactor Kinetics Equations in Three Dimensions*, 1971.

[38] R. Pevey, "Benchmarking Report for WIGGLE: A One-Dimensional Transient Diffusion Theory Code," Technical Report, Westinghouse Savannah River Company,



Aiken, SC, USA, 1990.

[39] T. Heames, "TWIGL: 2-D 2-Group Space-Time Diffusion Feedback," Technical Report, Argonne National Lab, IL, USA, 1979.

[40] D. Ferguson and K. Hansen, "Solution of the Space-Dependent Reactor Kinetics Equations in the Three Dimension," *Nuclear Science and Engineering*, vol. 51, pp. 189-205, 1973.

[41] K. Derstine, "DIF3D: A Code to Solve One-, Two-, and Three-Dimensional Finite-Difference Diffusion Theory Problems," Technical Report, Argonne National Lab, IL, USA, 1984.

[42] B. Rouben, "Overview of Current RFSP-Code Capabilities for CANDU Core Analysis," *Transactions of the American Nuclear Society*, vol. 72, pp. 339-340, 1995.

[43] A. Hoeld and O. Lupas, "Real-time Simulation of the Transient Behavior of Local and Global Pressurized Water Reactor Core and Plant Parameters," *Nuclear Science and Engineering*, vol. 85, no. 4, pp. 396-417, 1983.

[44] W. Shen, "On the Better Performance of the Coarse-Mesh Finite-Difference Method for CANDU-Type Reactors," *Annals of Nuclear Energy*, vol. 46, pp. 169-178, 2012.

[45] S. Kaplan, *Space-Time Kinetics*, Naval Reactor Physics Handbook, U.S.

Government Printing Office, Washington D. C., 1962.

[46] E. Wachspress, R. Burgess, and S. Baron, "Multichannel Flux Synthesis", *Nuclear Science and Engineering*, vol. 12, pp. 381-389, 1962.

[47] N. Gupta, "Nodal Methods for Three-Dimensional Simulators", *Progress in Nuclear Energy*, vol. 7, no. 3, pp. 127-149, 1981.

[48] M. Gregory, B. Aviles, and S. Yakura, "A Three-Dimensional Neutronics Model for Reactor Training Simulators", *Nuclear Science and Engineering*, vol. 92, no. 3, pp. 372-381, 1986.

[49] M. Yeung, and G. Jiang, "Development of an Efficient Three-Dimensional Reactor Core Model for Simulator Applications," *Nuclear Technology*, vol. 97, no. 3, pp. 352-361, 1992.

[50] B. Arsenault, "Spatial kinetics (\*CERBERUS module)," Workshop Notes, Atomic Energy of Canada Limited, Mississauga, ON, Canada, 2008; available on the Internet at: <http://canteach.candu.org/library/20054306.pdf>

[51] M. Khajavi, M. Menhaj, and A. Suratgar, "A Neural Network Controller for Load Following Operation of Nuclear Reactors," *Annals of Nuclear Energy*, vol. 29, pp. 751-760, 2002.

[52] S. Shimjith, A. Tiwari, M. Naskar, and B. Bandyopadhyay, "Space Time Kinetics Modeling of Advanced Heavy Water Reactor for Control Studies," *Annals of Nuclear Energy*, vol. 37, iss. 3, pp. 310-324, 2010.

[53] B. Monaghan, F. McDonnell, and H. Hinds, "Hybrid Simulation of Reactor kinetics in CANDU Reactors Using a Modal Approach", *Simulation*, vol. 35, no. 1, pp. 21-33, 1980.

[54] B. Arsenault, "Flux and Power Mapping in RFSP," Workshop Notes. Atomic Energy of Canada Limited, Mississauga, Ontario, Canada, 2008; available on the Internet at: <http://canteach.candu.org/library/20054309.pdf>

[55] *CANDU6 Technical Summary*, Atomic Energy of Canada Limited, 2005.

[56] *CANDU fundamentals*, Atomic Energy of Canada Limited; available on the Internet at: <http://canteach.candu.org/library/20040711.pdf>.

[57] *CANDU 6 Generating Station Physics Design Manual*, Atomic Energy of Canada Limited, 1999.

[58] B. Rouben, "Introduction to Reactor Physics," Atomic Energy of Canada Limited, 2008; available on the Internet at: <http://canteach.candu.org/library/20040501.pdf>

[59] M. Gold, and A. Wight, "SMOKIN – A Family of Codes for Reactor Space-Time

Neutronics Calculations Based on Modal Kinetics – Theory Manual,” Report No. 90133, Nuclear Safety Department, Ontario Hydro, 1990.

[60] W. Stacey, *Space-Time Nuclear Reactor Kinetics*, Academic Press, New York and London, 1969.

[61] G. Kugler, “An Iterative Procedure for Calculating the Higher Harmonics of the Diffusion Equation - the MONIC Code”, Technical Report, Atomic Energy of Canada Limited, 1976.

[62] H. Jokstad, M. Louka, and M. Tsuiki, “Core Data Viewer”, Institute for Energy Technology, Halden, Norway; available on the Internet at: <http://www2.hrp.no/coredataviewer/papers/ife-core-data-viewer.pdf>

[63] H. Jokstad, M. Louka, and M. Tsuiki, “Norway's Institute for Energy Technology has Developed a 3D Core Monitoring Application”, *Nuclear Engineering International*, vol. 53, no. 652, pp. 21-23, 2008.

[64] B. Vick, "MATLAB Commands and Functions," Virginia Technical University; on Internet: <http://www.hkn.umn.edu/resources/files/matlab/MatlabCommands.pdf>

[65] C. J. Jeong and H. Choi, “Regional Overpower Protection System Analysis for the Direct Use of Spent Pressurized Water Reactor Fuel in CANDU Reactors (DUPIC)”, *IEEE Transactions on Nuclear Science*, vol. 52, no. 1, pp. 450-456, Feb. 2005.

[66] MATLAB GUI – Creating Graphical User Interface in MATLAB, The MathWorks Inc.; available on the Internet at: <http://www.mathworks.com/discovery/matlab-gui.html>

[67] E. Varin, J. Koclas, and R. Roy, “Modeling of the CANDU-6 Reactor Regulating System”, *Transactions of the American Nuclear Society*, vol. 73, pp. 428-430, Dec. 1995.

[68] IAEA, *Modern Instrumentation and Control for Nuclear Power Plants: A Guidebook*, Technical Reports Series No. 387, 1999.

[69] A. P. Tiwari, B. Bandyopadhyay, and G. Govindarajan, "Spatial Control of a Large Pressurized Heavy Water Reactor," *IEEE Transactions on Nuclear Science*, vol. 43, no. 4, pp. 2440-2453, 1996.

[70] W. Liu, and Z. Luo, “The Three-dimensional Power Distribution Control in Load Following of the Heating Reactor,” *Annals of Nuclear Energy*, vol. 28, iss. 8, pp. 741-754, 2001.

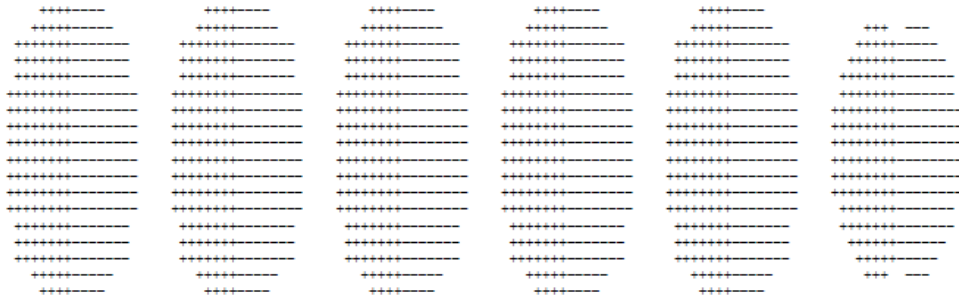
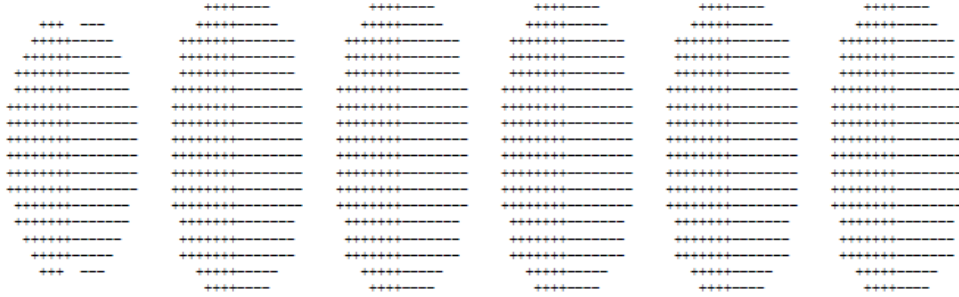
[71] B. Anderson, and J. Moore, *Optimal Control – Linear Quadratic Methods*, Prentice Hall, Englewood Cliffs, New Jersey, 1990.

## Appendix A

The following picture-groups illustrate the different neutron flux distributions corresponding to 13 flux modes represented by Table 3.2. For each flux mode, 12 two dimensional flux distribution figures are arrayed regarding 12 layers divided in the axial direction of the CANDU reactor core. “+” sign indicates the positive values; and “-” sign indicates the negative values.

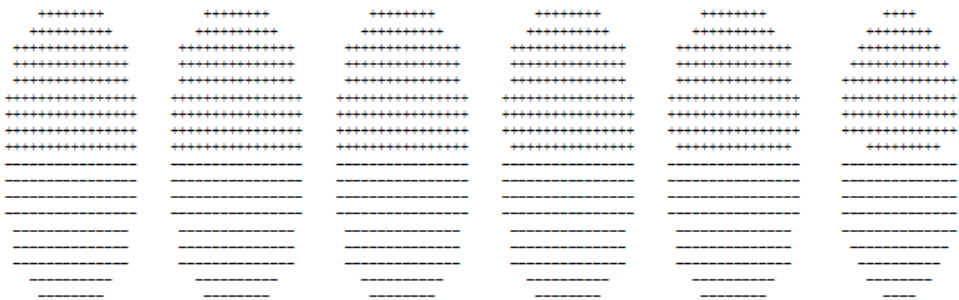
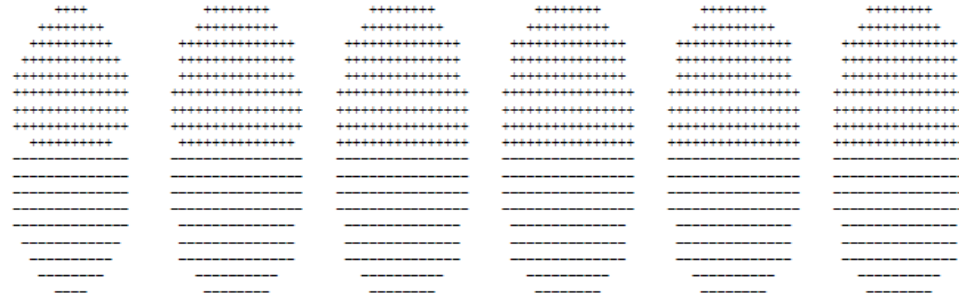


FIRST AZ. 1



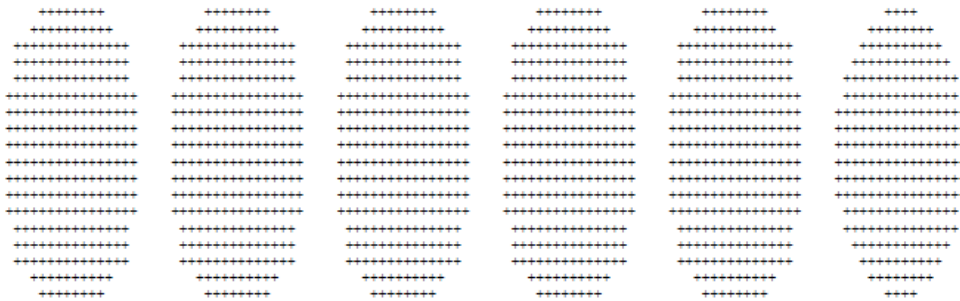
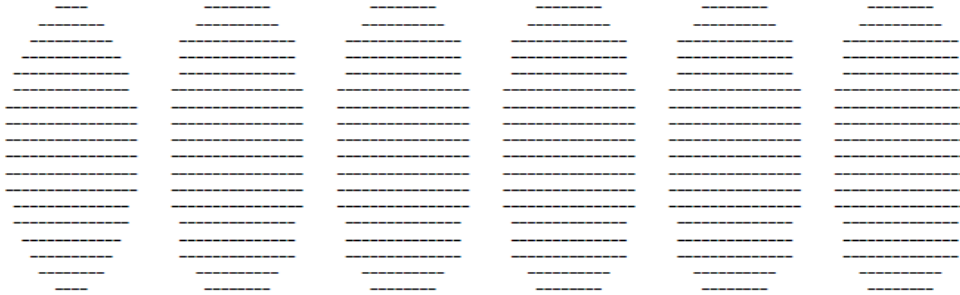
DIMENSION 10976

FIRST AZ. 2



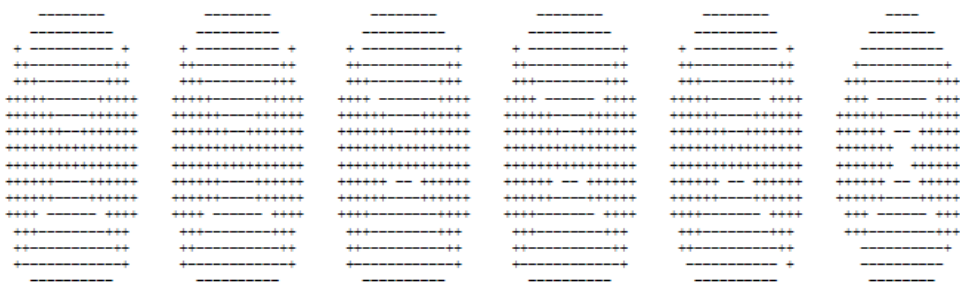
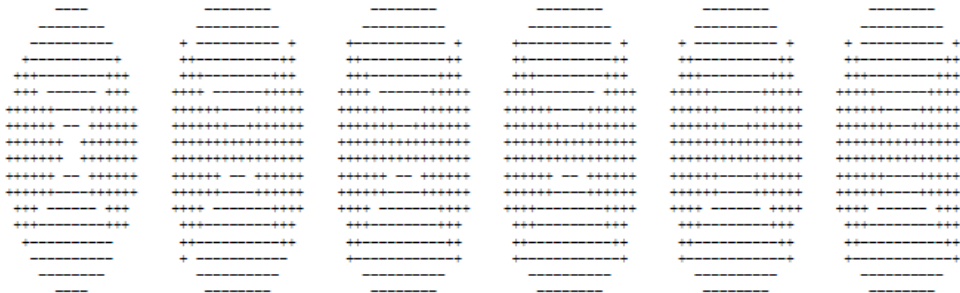
DIMENSION 10976

FIRST AX. 1



DIMENSION 10976

2ND AZ. 1



DIMENSION 10976





1STAX/AZ. 2



DIMENSION 10976

FIRST RD. 1



DIMENSION 10976

3RD AZ. 2



DIMENSION 10976

1AX/2AZ. 2



DIMENSION 10976

3RD AZ. 1



DIMENSION 10976

1AX/2AZ. 1



DIMENSION 10976

## Appendix B

The following process represents a detailed derivation procedure of the reactor dynamic Eqns. (3-13) to (3-16).

Substituting the modal expansion Eqns. (3-5) to (3-8) into the reactor diffusion Eqns. (3-1) to (3-4), multiplying them throughout by the spatial mode function  $\psi_k(r)$  ( $k \in [1, M]$ ) and integrating over the reactor volume, the following equations can be obtained:

$$\begin{aligned} \frac{1}{v} \int_V \sum_{i=1}^M \psi_k(r) \psi_i(r) dV \frac{d}{dt} n_i(t) &= \int_V \sum_{i=1}^M \psi_k(r) (\nabla D \nabla - \Sigma_a) \psi_i(r) dV \cdot n_i(t) + \int_V \sum_{i=1}^M \psi_k(r) (1 - \beta) v \Sigma_f \psi_i(r) dV \cdot n_i(t) \\ &+ \frac{1}{v} \sum_j \lambda_j \int_V \sum_{i=1}^M C_{ij}(t) \psi_k(r) \psi_i(r) dV_f - \frac{1}{v} \sigma_{ax} \sum_{m=1}^M (X_m(t) - X_m^s) \sum_{i=1}^M n_i(t) \int_V \psi_m(r) \psi_i(r) \psi_k(r) dV_f \end{aligned} \quad (\text{B-1})$$

$$\frac{1}{v} \int_V \sum_{i=1}^M \psi_k(r) \psi_i(r) dV_f \frac{d}{dt} C_{ij}(t) = -\frac{1}{v} \lambda_j \sum_{i=1}^M C_{ij}(t) \int_V \psi_k(r) \psi_i(r) dV_f + \beta_j v \Sigma_f \int_V \sum_{i=1}^M n_i(t) \psi_k(r) \psi_i(r) dV_f \quad (\text{B-2})$$

$$\frac{1}{v} \int_V \sum_{i=1}^M \psi_k(r) \psi_i(r) dV_f \frac{d}{dt} I_i(t) = -\frac{1}{v} \lambda_i \int_V \sum_{i=1}^M I_i(t) \psi_k(r) \psi_i(r) dV_f + \gamma_i \Sigma_f \int_V \sum_{i=1}^M n_i(t) \psi_k(r) \psi_i(r) dV_f \quad (\text{B-3})$$

$$\begin{aligned} \frac{1}{v} \int_V \sum_{i=1}^M \psi_k(r) \psi_i(r) dV_f \frac{d}{dt} X_i(t) &= -\frac{1}{v} \lambda_x \int_V \sum_{i=1}^M X_i(t) \psi_k(r) \psi_i(r) dV_f + \gamma_x \Sigma_f \int_V \sum_{i=1}^M n_i(t) \psi_k(r) \psi_i(r) dV_f \\ &+ \frac{1}{v} \lambda_i \int_V \sum_{i=1}^M I_i(t) \psi_k(r) \psi_i(r) dV_f - \frac{1}{v} \sigma_{ax} \sum_{m=1}^M X_m(t) \sum_{i=1}^M n_i(t) \int_V \psi_m(r) \psi_i(r) \psi_k(r) dV_f \end{aligned} \quad (\text{B-4})$$

Applying the bi-orthogonality properties and approximated bi-orthogonality over the whole reactor of the flux modes, as illustrated by

$$\begin{aligned}\langle \psi_k | C | \psi_m \rangle &= 0, k \neq m \\ \langle \psi_k | C | \psi_m \rangle &\neq 0, k = m\end{aligned}\quad (3-11)$$

And

$$\langle \psi_k | \psi_m \rangle_{\text{reactor}} \ll \langle \psi_m | \psi_m \rangle_{\text{reactor}}, k \neq m \quad (3-12)$$

Eqns. (B-1) to (B-4) become

$$\begin{aligned}\frac{1}{v} \langle \psi_k(r) \psi_k(r) \rangle_{V_f} \frac{d}{dt} n_k(t) &= \sum_{i=1}^M \langle \psi_k(r) (\nabla D \nabla - \Sigma_a + (1 - \beta) v \Sigma_f) \psi_i(r) \rangle_{V_f} \cdot n_i(t) \\ &+ \frac{1}{v} \sum_j \lambda_j C_{kj}(t) \langle \psi_k(r) \psi_k(r) \rangle_{V_f} - \frac{1}{v} \sigma_{ax} \sum_{m=1}^M (X_m(t) - X_m^s) \sum_{i=1}^M n_i(t) \langle \psi_m(r) \psi_i(r) \psi_k(r) \rangle_{V_f}\end{aligned}\quad (B-5)$$

$$\frac{1}{v} \langle \psi_k(r) \psi_k(r) \rangle_{V_f} \frac{d}{dt} C_{kj}(t) = -\frac{1}{v} \lambda_j C_{kj}(t) \langle \psi_k(r) \psi_k(r) \rangle_{V_f} + \beta_j \sum_{i=1}^M \langle \psi_k(r) v \Sigma_f \psi_i(r) \rangle_{V_f} n_i(t) \quad (B-6)$$

$$\frac{1}{v} \langle \psi_k(r) \psi_k(r) \rangle_{V_f} \frac{d}{dt} I_k(t) = -\frac{1}{v} \lambda_I I_k(t) \langle \psi_k(r) \psi_k(r) \rangle_{V_f} + \frac{1}{v} \gamma_I \sum_{i=1}^M \langle \psi_k(r) v \Sigma_f \psi_i(r) \rangle_{V_f} n_i(t) \quad (B-7)$$

$$\begin{aligned}\frac{1}{v} \langle \psi_k(r) \psi_k(r) \rangle_{V_f} \frac{d}{dt} X_k(t) &= -\frac{1}{v} \lambda_X X_k(t) \langle \psi_k(r) \psi_k(r) \rangle_{V_f} + \frac{1}{v} \gamma_X \sum_{i=1}^M n_i(t) \langle \psi_k(r) v \Sigma_f \psi_i(r) \rangle \\ &+ \frac{1}{v} \lambda_I I_k(t) \langle \psi_k(r) \psi_k(r) \rangle_{V_f} - \frac{1}{v} \sigma_{ax} \sum_{m=1}^M X_m(t) \sum_{i=1}^M n_i(t) \langle \psi_m(r) \psi_i(r) \psi_k(r) \rangle_{V_f}\end{aligned}\quad (B-8)$$

If both sides of Eqn. (B-5) are divided by  $\frac{1}{v}\langle\psi_k(r)\psi_k(r)\rangle_V$  and both sides of Eqns. (B-6)

to (B-8) are divided by  $\frac{1}{v}\langle\psi_k(r)\psi_k(r)\rangle_{V_f}$ , Eqns. (B-9) to (B-12) can be obtained as

follows,

$$\frac{d}{dt}n_k(t) = \frac{\sum_{i=1}^M \langle\psi_k(r)(\nabla D \nabla - \Sigma_a + (1-\beta)v\Sigma_f)\psi_i(r)\rangle_V}{\frac{1}{v}\langle\psi_k(r)\psi_k(r)\rangle_V} \cdot n_i(t) \quad (\text{B-9})$$

$$+ \sum_j \lambda_j C_{kj}(t) - \sigma_{ax} \sum_{m=1}^M (X_m(t) - X_m^s) \sum_{i=1}^M n_i(t) \frac{\langle\psi_m(r)\psi_i(r)\psi_k(r)\rangle_{V_f}}{\langle\psi_k(r)\psi_k(r)\rangle_V}$$

$$\frac{d}{dt}C_{kj}(t) = -\lambda_j C_{kj}(t) + \beta_j \frac{\sum_{i=1}^M \langle\psi_k(r)v\Sigma_f\psi_i(r)\rangle_{V_f} n_i(t)}{\frac{1}{v}\langle\psi_k(r)\psi_k(r)\rangle_{V_f}} \quad (\text{B-10})$$

$$\frac{d}{dt}I_k(t) = -\lambda_I I_k(t) + \frac{1}{v} \gamma_I \frac{\sum_{i=1}^M \langle\psi_k(r)v\Sigma_f\psi_i(r)\rangle_{V_f} n_i(t)}{\frac{1}{v}\langle\psi_k(r)\psi_k(r)\rangle_{V_f}} \quad (\text{B-11})$$

$$\frac{d}{dt}X_k(t) = -\lambda_X X_k(t) + \frac{1}{v} \gamma_X \frac{\sum_{i=1}^M \langle\psi_k(r)v\Sigma_f\psi_i(r)\rangle_{V_f} n_i(t)}{\frac{1}{v}\langle\psi_k(r)\psi_k(r)\rangle_{V_f}} \quad (\text{B-12})$$

$$+ \lambda_I I_k(t) - \sigma_{ax} \sum_{m=1}^M X_m(t) \sum_{i=1}^M n_i(t) \frac{\langle\psi_m(r)\psi_i(r)\psi_k(r)\rangle_{V_f}}{\langle\psi_k(r)\psi_k(r)\rangle_{V_f}}$$

Recall the simplified operators on behalf of neutron loss and production,

$$R(r,t) = \nabla D \nabla - \Sigma_a(r,t) \quad (\text{3-19})$$

$$F(r,t) = v\Sigma_f(r,t) \quad (\text{3-20})$$

Then define the initial and incremental values of both operators, such that

$$R(r, t) = R_0 + \Delta R \quad (\text{B-13})$$

$$F(r, t) = F_0 + \Delta F \quad (\text{B-14})$$

Both sides of Eqns. (B-9) to (B-12) are divided by  $F_0$ , such that the dynamic equations become

$$\begin{aligned} \frac{d}{dt} n_k(t) = & \frac{\sum_{i=1}^M \langle \psi_k(r) (R_0 + (1-\beta)F_0) \psi_i(r) \rangle_V}{\frac{1}{v} \langle \psi_k(r) \psi_k(r) \rangle_V} \cdot n_i(t) + \frac{\sum_{i=1}^M \langle \psi_k(r) ((\Delta R + (1-\beta)\Delta F) \delta(r)) \psi_i(r) \rangle_V}{\frac{1}{v} \langle \psi_k(r) \psi_k(r) \rangle_V} \cdot n_i(t) \\ & + \sum_j \lambda_j C_{kj}(t) - \sigma_{ax} \sum_{m=1}^M (X_m(t) - X_m^s) \sum_{i=1}^M n_i(t) \frac{\langle \psi_m(r) \psi_i(r) \psi_k(r) \rangle_{V_f}}{\langle \psi_k(r) \psi_k(r) \rangle_V} \end{aligned} \quad (\text{B-15})$$

$$\frac{d}{dt} C_{kj}(t) = -\lambda_j C_{kj}(t) + \beta_j \frac{\sum_{i=1}^M \langle \psi_k(r) (F_0 + \Delta F \delta(r)) \psi_i(r) \rangle_{V_f} n_i(t)}{\frac{1}{v} \langle \psi_k(r) \psi_k(r) \rangle_{V_f}} \quad (\text{B-16})$$

$$\frac{d}{dt} I_k(t) = -\lambda_I I_k(t) + \frac{1}{v} \gamma_I \frac{\sum_{i=1}^M \langle \psi_k(r) (F_0 + \Delta F \delta(r)) \psi_i(r) \rangle_{V_f} n_i(t)}{\frac{1}{v} \langle \psi_k(r) \psi_k(r) \rangle_{V_f}} \quad (\text{B-17})$$

$$\begin{aligned} \frac{d}{dt} X_k(t) = & -\lambda_X X_k(t) + \frac{1}{v} \gamma_X \frac{\sum_{i=1}^M \langle \psi_k(r) (F_0 + \Delta F \delta(r)) \psi_i(r) \rangle_{V_f} n_i(t)}{\frac{1}{v} \langle \psi_k(r) \psi_k(r) \rangle_{V_f}} \\ & + \lambda_I I_k(t) - \sigma_{ax} \sum_{m=1}^M X_m(t) \sum_{i=1}^M n_i(t) \frac{\langle \psi_m(r) \psi_i(r) \psi_k(r) \rangle_{V_f}}{\langle \psi_k(r) \psi_k(r) \rangle_{V_f}} \end{aligned} \quad (\text{B-18})$$



Applying the steady-state equation, i.e.

$$(R_0 + \frac{1}{k_k} F_0) \psi_k = 0 \quad (3-9)$$

and defining the prompt neutron generation time for  $k^{\text{th}}$  mode, i.e.

$$l_k^* = \frac{\langle \psi_k | \frac{1}{v} | \psi_k \rangle}{\langle \psi_k | F_0 | \psi_k \rangle} \quad (3-18)$$

the dynamic equations can be deduced to

$$\begin{aligned} \frac{d}{dt} n_k(t) = & \frac{(1 - \frac{1}{k_k} - \beta)}{l_k^*} \cdot n_k(t) + \frac{1}{l_k^*} \frac{\sum_{i=1}^M \langle \psi_k(r) ((\Delta R + (1 - \beta) \Delta F) \delta(r)) \psi_i(r) \rangle_V}{\langle \psi_k(r) F_0 \psi_k(r) \rangle_V} \cdot n_i(t) \\ & + \sum_j^J \lambda_j C_{kj}(t) - \sigma_{ax} \sum_{m=1}^M (X_m(t) - X_m^s) \sum_{i=1}^M n_i(t) \frac{\langle \psi_m(r) \psi_i(r) \psi_k(r) \rangle_{V_f}}{\langle \psi_k(r) \psi_k(r) \rangle_V} \end{aligned} \quad (B-19)$$

$$\frac{d}{dt} C_{kj}(t) = -\lambda_j C_{kj}(t) + \frac{\beta_j}{l_k^*} n_k(t) + \beta_j \frac{\sum_{i=1}^M \langle \psi_k(r) (\Delta F \delta(r)) \psi_i(r) \rangle_{V_f} n_i(t)}{\frac{1}{v} \langle \psi_k(r) \psi_k(r) \rangle_{V_f}} \quad (B-20)$$

$$\frac{d}{dt} I_k(t) = -\lambda_l I_k(t) + \frac{\gamma_l}{v l_k^*} n_k(t) + \frac{1}{v} \gamma_l \frac{\sum_{i=1}^M \langle \psi_k(r) (\Delta F \delta(r)) \psi_i(r) \rangle_{V_f} n_i(t)}{\frac{1}{v} \langle \psi_k(r) \psi_k(r) \rangle_{V_f}} \quad (B-21)$$

$$\begin{aligned}
\frac{d}{dt} X_k(t) = & -\lambda_X X_k(t) + \frac{\gamma_X}{\nu l_k^*} n_k(t) + \frac{1}{\nu} \gamma_X \frac{\sum_{i=1}^M \langle \psi_k(r) (\Delta F \delta(r)) \psi_i(r) \rangle_{V_f} n_i(t)}{\frac{1}{\nu} \langle \psi_k(r) \psi_k(r) \rangle_{V_f}} \\
& + \lambda_I I_k(t) - \sigma_{ax} \sum_{m=1}^M X_m(t) \sum_{i=1}^M n_i(t) \frac{\langle \psi_m(r) \psi_i(r) \psi_k(r) \rangle_{V_f}}{\langle \psi_k(r) \psi_k(r) \rangle_{V_f}}
\end{aligned} \tag{B-22}$$

Eqns. (B-19) to (B-22) can be further simplified to the criteria state-space equations, i.e.

Eqns. (3-13) to (3-16).

$$\frac{dn_k(t)}{dt} = \frac{\rho_{sck} - \beta}{l_k^*} n_k(t) + \frac{1}{l_k^*} \sum_{i=1}^M (\rho_{ki} + \rho_{ki}^X) n_i(t) + \sum_j \lambda_j C_{kj}(t) \tag{3-13}$$

$$\frac{dC_{kj}(t)}{dt} = \frac{\beta_j}{l_k^*} n_k(t) - \lambda_j C_{kj}(t) \tag{3-14}$$

$$\frac{dI_k(t)}{dt} = \frac{\gamma_I}{\nu l_k^*} n_k(t) - \lambda_I I_k(t) \tag{3-15}$$

$$\frac{dX_k(t)}{dt} = \frac{\gamma_X}{\nu l_k^*} n_k(t) + \lambda_I I_k(t) - \lambda_X X_k(t) - \sigma_X \phi_f \sum_{i=1}^M \sum_{m=1}^M A_{kim} X_m(t) n_i(t) \tag{3-16}$$

A few new parameters are defined as follows.

The subcritical reactivity of mode  $k$  is defined as

$$\rho_{sck} = 1 - \frac{1}{k_k} \tag{3-17}$$

The modal cross-coupling reactivity between  $k^{\text{th}}$  and  $m^{\text{th}}$  modes due to the perturbation  $[\Delta R(r) + \Delta F(r)]\delta(r)$  within a certain area  $\delta(r)$  can be defined as

$$\rho_{ki} = \frac{\langle \psi_k | [\Delta R(r) + \Delta F(r)] \delta(r) | \psi_i \rangle}{\langle \psi_k | F_0 | \psi_k \rangle} \quad (3-21)$$

$\phi_f$  is defined as the flux-squared weighted fundamental mode for the fuel flux, i.e.

$$\phi_f = \frac{\langle \psi_1 | \psi_1 | \psi_1 \rangle_f}{\langle \psi_1 | \psi_1 \rangle_f} \quad (3-22)$$

$A_{kim}$  is the coupling volume integration of all the modes, defined as

$$A_{kim} = \frac{\langle \psi_k | \psi_i | \psi_m \rangle_f}{\langle \psi_k | F_0 | \psi_k \rangle_f \phi_f} \quad (3-23)$$

$\rho_{ki}^X$  is the modal reactivity reflecting Xenon reactivity build-up, defined as

$$\rho_{ki}^X = -\sigma_X \phi_f l_k^* \sum_{m=1}^M A_{kim} (X_m(t) - X_m^s) \quad (3-24)$$

Analog to Eqn. (3-8),  $X_m^s$  in Eqn. (3-24) can be defined by

$$X^s(r) = \frac{1}{\nu} \sum_{i=1}^M \psi_i(r) X_i^s \quad (3-25)$$

## Appendix C-1

The following derivation represents the vectorization procedure for modal kinetic Eqns. (3-13) to (3-16) in Section 3.5.

Since there are 9 flux modes chosen to be used in this research, then define  $k=1,2,\dots,9$ .

Define:

$$W_k = \frac{\rho_{sck} - \beta}{\Lambda} \quad (\text{C-1})$$

Applying Eqn. (C-1) to Eqn. (3-13), Eqn. (3-13) can be deduced to the following matrix form, i.e. Eqn. (C-2).

$$\begin{aligned}
\frac{d}{dt} \begin{bmatrix} n_1 \\ \vdots \\ n_9 \end{bmatrix} &= \begin{bmatrix} W_1 & & \\ & \ddots & \\ & & W_9 \end{bmatrix} \begin{bmatrix} n_1 \\ \vdots \\ n_9 \end{bmatrix} + \frac{1}{\Lambda} \begin{bmatrix} \rho_{11} & \cdots & \rho_{19} \\ \vdots & \ddots & \vdots \\ \rho_{91} & \cdots & \rho_{99} \end{bmatrix} \begin{bmatrix} n_1 \\ \vdots \\ n_9 \end{bmatrix} + \frac{1}{\Lambda} \begin{bmatrix} \rho_{11}^x & \cdots & \rho_{19}^x \\ \vdots & \ddots & \vdots \\ \rho_{91}^x & \cdots & \rho_{99}^x \end{bmatrix} \begin{bmatrix} n_1 \\ \vdots \\ n_9 \end{bmatrix} + \begin{bmatrix} [\lambda_1 \cdots \lambda_6] \begin{bmatrix} C_{11} \\ \vdots \\ C_{16} \end{bmatrix} \\ \vdots \\ [\lambda_1 \cdots \lambda_6] \begin{bmatrix} C_{91} \\ \vdots \\ C_{96} \end{bmatrix} \end{bmatrix}_{9 \times 1} \\
&= \begin{bmatrix} W_1 & & \\ & \ddots & \\ & & W_9 \end{bmatrix} \begin{bmatrix} n_1 \\ \vdots \\ n_9 \end{bmatrix} + \frac{1}{\Lambda} \begin{bmatrix} \rho_{11} & \cdots & \rho_{19} \\ \vdots & \ddots & \vdots \\ \rho_{91} & \cdots & \rho_{99} \end{bmatrix} \begin{bmatrix} n_1 \\ \vdots \\ n_9 \end{bmatrix} + \frac{1}{\Lambda} \begin{bmatrix} \rho_{11}^x & \cdots & \rho_{19}^x \\ \vdots & \ddots & \vdots \\ \rho_{91}^x & \cdots & \rho_{99}^x \end{bmatrix} \begin{bmatrix} n_1 \\ \vdots \\ n_9 \end{bmatrix} \\
&+ \begin{bmatrix} [\lambda_1 \cdots \lambda_6] & & \\ & \ddots & \\ & & [\lambda_1 \cdots \lambda_6] \end{bmatrix}_{9 \times 54} \begin{bmatrix} C_{11} \\ \vdots \\ C_{16} \\ \vdots \\ C_{91} \\ \vdots \\ C_{96} \end{bmatrix}_{54 \times 1}
\end{aligned} \tag{C-2}$$

Then Eqn. (C-2) can be written to a simpler form, i.e. Eqn. (3-31).

Define

$$\Delta X_m = X_m(t) - X_m^s \tag{C-3}$$

Eqn. (3-24) can be transformed to

$$\rho_{ki}^x = (-\sigma_x \varphi_f \Lambda) [A_{ki1} \quad \cdots \quad A_{ki9}] \begin{bmatrix} \Delta X_1 \\ \vdots \\ \Delta X_9 \end{bmatrix} \tag{C-4}$$

Eqn. (C-4) can be used to further simplify the Xenon item in the right side of Eqn.

(C-2), such that the vectorization of Eqn. (3-31) can be directly implemented in SIMULINK. The detailed procedure can be referred to the vectorization of Eqn. (3-34).

As for Eqn. (3-14), it can be vectorized by the following procedure, i.e. Eqn. (C-5).

$$\begin{aligned}
 \frac{d}{dt} \begin{bmatrix} C_{11} \\ \vdots \\ C_{16} \\ \vdots \\ C_{91} \\ \vdots \\ C_{96} \end{bmatrix}_{54 \times 1} &= - \begin{bmatrix} \lambda_1 & & & \\ & \ddots & & \\ & & \lambda_6 & \\ & & & \ddots \\ \lambda_1 & & & \\ & \ddots & & \\ & & \lambda_6 & \end{bmatrix} \begin{bmatrix} C_{11} \\ \vdots \\ C_{16} \\ \vdots \\ C_{91} \\ \vdots \\ C_{96} \end{bmatrix}_{54 \times 1} + \frac{1}{\Lambda} \begin{bmatrix} \beta_1 \\ \vdots \\ \beta_6 \\ \vdots \\ \beta_1 \\ \vdots \\ \beta_6 \end{bmatrix}_{54 \times 1} \\
 &= - \begin{bmatrix} \lambda_1 & & & \\ & \ddots & & \\ & & \lambda_6 & \\ & & & \ddots \\ & & & & \lambda_1 & & \\ & & & & & \ddots & \\ & & & & & & \lambda_6 \end{bmatrix}_{54 \times 54} \begin{bmatrix} C_{11} \\ \vdots \\ C_{16} \\ \vdots \\ C_{91} \\ \vdots \\ C_{96} \end{bmatrix}_{54 \times 1} + \frac{1}{\Lambda} \begin{bmatrix} \beta_1 \\ \vdots \\ \beta_6 \\ \vdots \\ \beta_1 \\ \vdots \\ \beta_6 \end{bmatrix}_{54 \times 9} \begin{bmatrix} n_1 \\ \vdots \\ n_9 \end{bmatrix} \quad (C-5)
 \end{aligned}$$

Eqn. (C-5) can be written to a simpler form, i.e. Eqn. (3-32).

Eqn. (3-15) is easily vectorized to the following form, i.e. Eqn. (C-6).

$$\frac{d}{dt} \begin{bmatrix} I_1 \\ \vdots \\ I_9 \end{bmatrix} = -\lambda_I \begin{bmatrix} I_1 \\ \vdots \\ I_9 \end{bmatrix} + \frac{\gamma_I}{v\Lambda} \begin{bmatrix} n_1 \\ \vdots \\ n_9 \end{bmatrix} \quad (3-33)$$

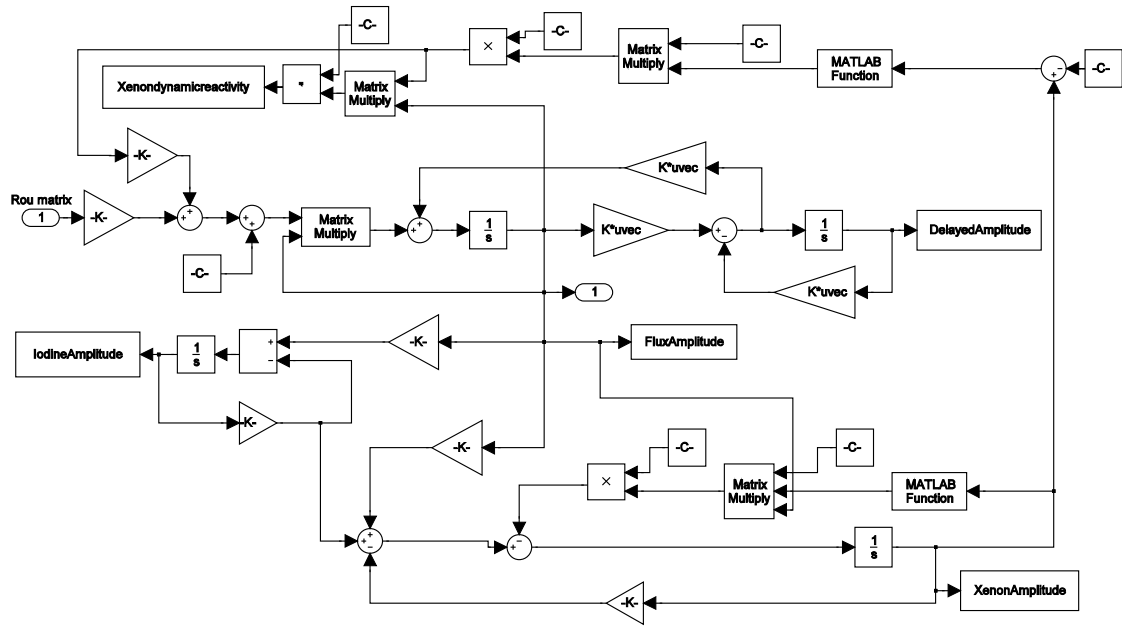
Furthermore, since Eqn. (3-16) is involved in the Xenon feedback item, the vectorization becomes more complex. The detailed vectorization process is illustrated by the following equation, i.e. Eqn. (C-6).

$$\begin{aligned}
\frac{d}{dt} \begin{bmatrix} X_1 \\ \vdots \\ X_9 \end{bmatrix} &= -\lambda_x \begin{bmatrix} X_1 \\ \vdots \\ X_9 \end{bmatrix} + \lambda_I \begin{bmatrix} I_1 \\ \vdots \\ I_9 \end{bmatrix} + \frac{\gamma_x}{v\Lambda} \begin{bmatrix} n_1 \\ \vdots \\ n_9 \end{bmatrix} - \sigma_x \phi_f \begin{bmatrix} \begin{bmatrix} A_{111} \cdots A_{119} \\ \vdots \\ A_{191} \cdots A_{199} \end{bmatrix} \begin{bmatrix} X_1 \\ \vdots \\ X_9 \end{bmatrix} \\ \vdots \\ \begin{bmatrix} A_{911} \cdots A_{919} \\ \vdots \\ A_{991} \cdots A_{999} \end{bmatrix} \begin{bmatrix} X_1 \\ \vdots \\ X_9 \end{bmatrix} \end{bmatrix} \begin{bmatrix} n_1 \\ \vdots \\ n_9 \end{bmatrix} \quad (\text{C-6}) \\
&= -\lambda_x \begin{bmatrix} X_1 \\ \vdots \\ X_9 \end{bmatrix} + \lambda_I \begin{bmatrix} I_1 \\ \vdots \\ I_9 \end{bmatrix} + \frac{\gamma_x}{v\Lambda} \begin{bmatrix} n_1 \\ \vdots \\ n_9 \end{bmatrix} - \sigma_x \phi_f \begin{bmatrix} \begin{bmatrix} A_{111} \cdots A_{119} \\ \vdots \\ A_{191} \cdots A_{199} \end{bmatrix} \begin{bmatrix} X_1 \\ \vdots \\ X_9 \end{bmatrix} \\ \vdots \\ \begin{bmatrix} A_{911} \cdots A_{919} \\ \vdots \\ A_{991} \cdots A_{999} \end{bmatrix} \begin{bmatrix} X_1 \\ \vdots \\ X_9 \end{bmatrix} \end{bmatrix} \begin{bmatrix} n_1 \\ \vdots \\ n_9 \end{bmatrix} \\
&= -\lambda_x \begin{bmatrix} X_1 \\ \vdots \\ X_9 \end{bmatrix} + \lambda_I \begin{bmatrix} I_1 \\ \vdots \\ I_9 \end{bmatrix} + \frac{\gamma_x}{v\Lambda} \begin{bmatrix} n_1 \\ \vdots \\ n_9 \end{bmatrix} - \sigma_x \phi_f \begin{bmatrix} \begin{bmatrix} A_{111} \cdots A_{119} & \cdots & A_{191} \cdots A_{199} \\ \vdots & \ddots & \vdots \\ A_{911} \cdots A_{919} & \cdots & A_{991} \cdots A_{999} \end{bmatrix} \begin{bmatrix} X_1 \\ \vdots \\ X_9 \end{bmatrix} \\ \vdots \\ \begin{bmatrix} X_1 \\ \vdots \\ X_9 \end{bmatrix} \end{bmatrix} \begin{bmatrix} n_1 \\ \vdots \\ n_9 \end{bmatrix}
\end{aligned}$$

Consequently, Eqn. (C-6) can also be written in a state-space form, as indicated by Eqn. (3-34).

In this way, the reactor dynamic model has been represented in the state-space form, i.e. the set of Eqns. (3-31) to (3-34). This state-space form is not only convenient for implementation in MATLAB/SIMULINK, but also is suitable for investigating the reactor control problem, which will be discussed in Chapter V.

## Appendix C-2



**Fig. C-2 SIMULINK module of reactor kinetic modal modeling**

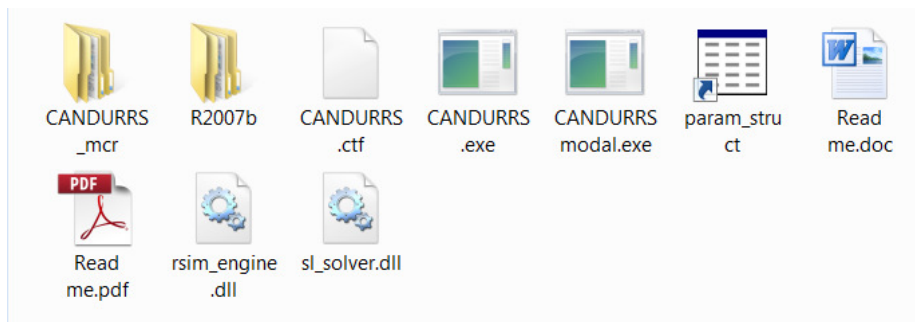


## Appendix D

This MATLAB/GUI simulation platform represents a basic tool to simulate the CANDU reactor dynamics (including a 3-D flux distribution) controlled by the Reactor Regulating System (RRS) during a load following process.

### *Installation of this software package:*

This software package contains all the files as shown in Fig. D-1.



**Fig. D-1 Files of CANDU RRS GUI software package**

If the MATLAB R2007b is already installed on the computer (and the default path is: C:\Program Files\MATLAB\), execute CANDURRS.exe to perform the simulations. If the installing path is not the default path, please copy the folder – R2007b in this package to C:\Program Files\MATLAB\. Then, run the simulation.

If the MATLAB R2007b has not been installed on the computer, follow the following steps to install the MATLAB compiler. The simulations can then be run. Please note that different versions of MATLAB may not be compatible.

1. Double click "MCRInstaller.exe" to install the MATLAB compiler. The default path should be: C:\Program Files\MATLAB.
2. Right click "My Computer" - choose "Advanced" - choose "Environment Variables" - choose "System variables" - choose "Path" and double click it to edit the values - Add the following paths to the variable value by ";"

C:\Program Files\MATLAB\MATLAB Component Runtime\v77\runtime\win32

C:\Program Files\MATLAB\MATLAB Component Runtime\v77\bin\win32

3. Copy the folder – R2007b in this package to C:\Program Files\MATLAB\.
4. (Optional) if the simulations cannot be executed, please copy the files - rsim\_engine.dll and sl\_solver.dll to C:\Program Files\MATLAB\MATLAB Component Runtime\v77\bin\win32.
5. Execute the file - CANDURRS.exe to run the simulations.

***How to use this simulation package:***

“Steady-state time 1” is the time duration for which the reactor is at the initial power.

“Power down time” is the time instance at which the power is reduced to a lower level.

“Reduced Power” is the new power level after reduction.

“Steady-state time 2” is the time interval of the reactor operation at the reduced power level.

“Power rise time” is the time taken for the reactor to increase the power from the lower level to the initial level.

“Simulation time” is the total time period for simulation.

Press “Run” button to initiate the simulations.

Press “Reset” button to reset the parameters.

Press “Clear” button to remove the existing figures.

Press “Close” button to exit the simulation program.

***Open source code:***

The source code of this software package is shown in Appendix G. It contains two files:

CANDURRS.m, and ThreeD.m.

## Appendix E

This appendix represents the linearization process of the nonlinear reactor model,

$$\frac{d}{dt} \mathbf{N} = (\mathfrak{R}_{scx} + \frac{\mathfrak{R}_L + \mathfrak{R}_X}{\Lambda}) \mathbf{N} + \text{blkdiag}([\lambda_1 \cdots \lambda_6]) \cdot \mathbf{P} \quad (4-1)$$

$$\frac{d}{dt} \mathbf{P} = \frac{1}{\Lambda} \text{blkdiag}([\beta_1 \cdots \beta_6]^T) \cdot \mathbf{N} - \text{blkdiag}(\text{diag}(\lambda_i)) \cdot \mathbf{P} \quad (4-2)$$

$$\frac{d}{dt} \mathbf{I} = \frac{\gamma_I}{v\Lambda} \mathbf{N} - \lambda_I \mathbf{I} \quad (4-3)$$

$$\frac{d}{dt} \mathbf{X} = \frac{\gamma_X}{v\Lambda} \mathbf{N} + \lambda_I \mathbf{I} - \lambda_X \mathbf{X} - \sigma_X \phi_f \mathbf{A} \cdot \text{blkdiag}(\mathbf{X}) \cdot \mathbf{N} \quad (4-4)$$

where

$$\mathbf{N} = (n_1 \cdots n_9)^T; \quad \mathbf{P} = ((C_{11} \cdots C_{16}) \cdots (C_{91} \cdots C_{96}))^T; \quad \mathbf{I} = (I_1 \cdots I_9)^T; \quad \text{and} \quad \mathbf{X} = (X_1 \cdots X_9)^T. \quad (4-5)$$

Define,  $\mathfrak{R}_{L0}$  as the initial modal reactivity in terms of the initial water levels in the liquid zone controllers, and  $\Delta\mathfrak{R}_L$  as the incremental modal reactivity induced by the water level changes.

The corresponding steady-state equations can be written as

$$0 = (\mathfrak{R}_{sck} + \frac{\mathfrak{R}_{L0}}{\Lambda})N_0 + blkdiag([\lambda_1 \cdots \lambda_6]) \cdot P_0 \quad (\text{E-1})$$

$$0 = \frac{1}{\Lambda} blkdiag([\beta_1 \cdots \beta_6]^T) \cdot N_0 - blkdiag(diag(\lambda_i)) \cdot P_0 \quad (\text{E-2})$$

$$0 = \frac{\gamma_I}{v\Lambda} N_0 - \lambda_I I_0 \quad (\text{E-3})$$

$$0 = \frac{\gamma_X}{v\Lambda} N_0 + \lambda_I I_0 - \lambda_X X_0 - \sigma_X \phi_f A \cdot blkdiag(X_0) \cdot N_0 \quad (\text{E-4})$$

The perturbation equations of the state variables are represented by Section 5.2.1, as follows

$$N = N_0 + \Delta N \quad (5-1)$$

$$P = P_0 + \Delta P \quad (5-2)$$

$$I = I_0 + \Delta I \quad (5-3)$$

$$X = X_0 + \Delta X \quad (5-4)$$

Applying the perturbation equations to the nonlinear reactor model, i.e. Eqns. (4-1) to (4-4), the new state-space reactor model can be expressed as

$$\frac{d}{dt} \Delta N = (\mathfrak{R}_{sck} + \frac{(\mathfrak{R}_{L0} + \Delta \mathfrak{R}_L) + \mathfrak{R}_X}{\Lambda})(N_0 + \Delta N) + blkdiag([\lambda_1 \cdots \lambda_6]) \cdot (P_0 + \Delta P) \quad (\text{E-5})$$

$$\frac{d}{dt} \Delta \mathbf{P} = \frac{1}{\Lambda} \text{blkdiag}([\beta_1 \cdots \beta_6]^T) \cdot (\mathbf{N}_0 + \Delta \mathbf{N}) - \text{blkdiag}(\text{diag}(\lambda_i)) \cdot (\mathbf{P}_0 + \Delta \mathbf{P}) \quad (\text{E-6})$$

$$\frac{d}{dt} \Delta \mathbf{I} = \frac{\gamma_I}{v\Lambda} (\mathbf{N}_0 + \Delta \mathbf{N}) - \lambda_I (\mathbf{I}_0 + \Delta \mathbf{I}) \quad (\text{E-7})$$

$$\frac{d}{dt} \Delta \mathbf{X} = \frac{\gamma_X}{v\Lambda} (\mathbf{N}_0 + \Delta \mathbf{N}) + \lambda_I (\mathbf{I}_0 + \Delta \mathbf{I}) - \lambda_X (\mathbf{X}_0 + \Delta \mathbf{X}) - \sigma_X \phi_f \mathbf{A} \cdot \text{blkdiag}(\mathbf{X}_0 + \Delta \mathbf{X}) \cdot (\mathbf{N}_0 + \Delta \mathbf{N}) \quad (\text{E-8})$$

Applying the steady state equations, i.e. Eqns. (E-1) to (E-4) to the new reactor model and removing the high-order infinitesimals, the reactor model can be written as

$$\frac{d}{dt} \Delta \mathbf{N} = (\mathfrak{R}_{SCK} + \frac{\mathfrak{R}_{L0}}{\Lambda}) \Delta \mathbf{N} + \text{blkdiag}([\lambda_1 \cdots \lambda_6]) \cdot \Delta \mathbf{P} + \frac{\mathfrak{R}_X}{\Lambda} \mathbf{N}_0 + \frac{\Delta \mathfrak{R}_L}{\Lambda} \mathbf{N}_0 \quad (\text{E-9})$$

$$\frac{d}{dt} \Delta \mathbf{P} = \frac{1}{\Lambda} \text{blkdiag}([\beta_1 \cdots \beta_6]^T) \cdot \Delta \mathbf{N} - \text{blkdiag}(\text{diag}(\lambda_i)) \cdot \Delta \mathbf{P} \quad (\text{E-10})$$

$$\frac{d}{dt} \Delta \mathbf{I} = \frac{\gamma_I}{v\Lambda} \Delta \mathbf{N} - \lambda_I \Delta \mathbf{I} \quad (\text{E-11})$$

$$\frac{d}{dt} \Delta \mathbf{X} = \frac{\gamma_X}{v\Lambda} \Delta \mathbf{N} + \lambda_I \Delta \mathbf{I} - \lambda_X \Delta \mathbf{X} - \sigma_X \phi_f \mathbf{A} \cdot \text{blkdiag}(\mathbf{X}_0) \cdot \Delta \mathbf{N} - \sigma_X \phi_f \mathbf{A} \cdot \text{blkdiag}(\Delta \mathbf{X}) \cdot \mathbf{N}_0 \quad (\text{E-12})$$

Then, write  $\frac{\mathfrak{R}_X}{\Lambda} \mathbf{N}_0$  in Eqn. (E-9) to a standard form.

Since

$$\mathbf{N}_0 = [1, 0, \dots, 0]^T \quad (3-35)$$

and,

$$\rho_{ki}^x = (-\sigma_x \varphi_f \Lambda) [A_{ki1} \quad \cdots \quad A_{ki9}] \begin{bmatrix} \Delta X_1 \\ \vdots \\ \Delta X_9 \end{bmatrix} \quad (\text{C-4})$$

It is obtained that

$$\begin{aligned} & \frac{\mathfrak{R}_x}{\Lambda} N_0 \\ &= \frac{1}{\Lambda} \begin{bmatrix} \rho_{11}^x & \cdots & \rho_{19}^x \\ \vdots & \ddots & \vdots \\ \rho_{91}^x & \cdots & \rho_{99}^x \end{bmatrix} [1, 0, \dots, 0]^T \\ &= \frac{1}{\Lambda} \begin{bmatrix} \rho_{11}^x \\ \vdots \\ \rho_{91}^x \end{bmatrix} \\ &= (-\sigma_x \varphi_f) A_p \Delta X \end{aligned} \quad (\text{E-13})$$

in which,

$$A_p = \begin{bmatrix} A_{111} & \cdots & A_{119} \\ \vdots & \ddots & \vdots \\ A_{911} & \cdots & A_{919} \end{bmatrix} \quad (\text{E-14})$$

The controller signal item, i.e.  $\frac{\Delta \mathfrak{R}_L}{\Lambda} N_0$  in Eqn. (E-9) is to be written to the standard form containing 14 liquid zone water levels.

$$\frac{\Delta \mathfrak{R}_L}{\Lambda} N_0 = \frac{1}{\Lambda} (\Delta \mathfrak{R}_{L1} + \cdots + \Delta \mathfrak{R}_{L14}) N_0 \quad (\text{E-15})$$

where,  $\Delta\mathfrak{R}_{L1}$  to  $\Delta\mathfrak{R}_{L14}$  respectively represent the modal reactivity change induced by the water level change in each liquid zone controller.

Introducing new variables:

Let  $\Theta_{55,1}$  and  $\Theta_{25,1}$  respectively be the modal reactivity for water levels in zone 1 - 0.55 FLU and 0.25 FLU. Similarly,  $\Theta_{55,14}$  and  $\Theta_{25,14}$  represent respectively the modal reactivity for the water levels in zone 14 - 0.55 FLU and 0.25 FLU. The two water levels are chosen since the water levels changes from 0.25 FLU to 0.55 FLU for the simulations in Chapter IV. The nonlinearity of the modal reactivity change within this area is not considered. The modal reactivity matrix has a dimension of  $9 \times 9$ .

With the water level  $(l_1 \cdots l_{14})^T$  linearly interpolated between 0.25 FLU and 0.55 FLU, the modal reactivity for each water level can be represented as

$$\mathfrak{R}_{L1} = 3.33(\Theta_{55,1} - \Theta_{25,1}) \cdot l_1 + (1.83\Theta_{25,1} - 0.83\Theta_{55,1}) \quad (\text{E-16})$$

Similarly, it can be shown that

$$\mathfrak{R}_{L14} = 3.33(\Theta_{55,14} - \Theta_{25,14}) \cdot l_1 + (1.83\Theta_{25,14} - 0.83\Theta_{55,14}) \quad (\text{E-17})$$

The modal reactivity changes due to the water level changes can be shown as

$$\Delta\mathfrak{R}_{L1} = 3.33(\Theta_{55,1} - \Theta_{25,1}) \cdot \Delta l_1 \quad (\text{E-18})$$



and

$$\Delta \mathfrak{R}_{L14} = 3.33(\Theta_{55,14} - \Theta_{25,14}) \cdot \Delta I_{14} \quad (\text{E-19})$$

Let  $\Delta \Theta_1$  to  $\Delta \Theta_{14}$  be the incremental modal reactivity of each zone when the water level increases from 0.25 FLU to 0.55 FLU, then,

$$\Delta \mathfrak{R}_{L1} = 3.33 \Delta \Theta_1 \cdot \Delta I_1 \quad (\text{E-20})$$

and

$$\Delta \mathfrak{R}_{L14} = 3.33 \Delta \Theta_{14} \cdot \Delta I_{14} \quad (\text{E-21})$$

Subsequently,

$$\begin{aligned} & \frac{\Delta \mathfrak{R}_L}{\Lambda} N_0 \\ &= \frac{1}{\Lambda} (\Delta \mathfrak{R}_{L1} + \dots + \Delta \mathfrak{R}_{L14}) N_0 \\ &= \frac{3.33}{\Lambda} (\Delta \Theta_1 \cdot \Delta I_1 + \dots + \Delta \Theta_{14} \cdot \Delta I_{14}) N_0 \\ &= \frac{3.33}{\Lambda} (\Delta \Theta_1 \cdot N_0 \cdot \Delta I_1 + \dots + \Delta \Theta_{14} \cdot N_0 \cdot \Delta I_{14}) \\ &= \frac{3.33}{\Lambda} (\Delta \Theta_{1,1} \cdot \Delta I_1 + \dots + \Delta \Theta_{14,1} \cdot \Delta I_{14}) \\ &= \frac{3.33}{\Lambda} \begin{bmatrix} \Delta \Theta_{1,1} & \dots & \Delta \Theta_{14,1} \end{bmatrix}_{9 \times 14} \begin{bmatrix} \Delta I_1 \\ \vdots \\ \Delta I_{14} \end{bmatrix}_{14 \times 1} \end{aligned} \quad (\text{E-22})$$

in which  $\Delta \Theta_{1,1}$  to  $\Delta \Theta_{14,1}$  is the first column of  $\Delta \Theta_1$  to  $\Delta \Theta_{14}$  respectively.

Let  $\Delta u$  is the control signal – incremental water levels within 14 liquid zone controllers.

It can be represented as

$$\Delta u = [\Delta l_1, \Delta l_2, \dots, \Delta l_{14}]^T \quad (5-7)$$

Then Eqn. (E-22) can be rewritten to a format which contains the control signal –incremental 14 water levels.

$$\frac{\Delta \mathfrak{R}_L}{\Lambda} N_0 = \frac{3.33}{\Lambda} [\Delta \Theta_{1,1} \dots \Delta \Theta_{14,1}]_{9 \times 14} \Delta u \quad (E-23)$$

The coupling item  $-\sigma_x \phi_f A \cdot blkdiag(\Delta X) \cdot N_0$  in Eqn. (E-12) can also be written to a format containing a constant multiplied by  $\Delta X$ .

$$-\sigma_x \phi_f A \cdot blkdiag(\Delta X) \cdot N_0 = -\sigma_x \phi_f A_p \cdot \Delta X \quad (E-24)$$

Thus, the set of Eqns. (E-9) to (E-12) can be written to

$$\frac{d}{dt} \Delta N = (\mathfrak{R}_{SCK} + \frac{\mathfrak{R}_{L0}}{\Lambda}) \Delta N + blkdiag([\lambda_1 \dots \lambda_6]) \cdot \Delta P - \sigma_x \phi_f A_p \cdot \Delta X + \frac{3.33}{\Lambda} [\Delta \Theta_{1,1} \dots \Delta \Theta_{14,1}] \cdot \Delta u \quad (E-25)$$

$$\frac{d}{dt} \Delta P = \frac{1}{\Lambda} blkdiag([\beta_1 \dots \beta_6]^T) \cdot \Delta N - blkdiag(diag(\lambda_i)) \cdot \Delta P \quad (E-26)$$

$$\frac{d}{dt} \Delta I = \frac{\gamma_l}{v\Lambda} \Delta N - \lambda_l \Delta I \quad (E-27)$$

$$\frac{d}{dt} \Delta X = \left( \frac{\gamma_X}{v\Lambda} - \sigma_X \phi_f A \cdot \text{blkdiag}(X_0) \right) \cdot \Delta N + \lambda_l \Delta I - (\lambda_X + \sigma_X \phi_f A_p) \cdot \Delta X \quad (\text{E-28})$$

The system can then be put into a standard state-space format,

$$\begin{aligned} \frac{d}{dt} \begin{bmatrix} \Delta N \\ \Delta P \\ \Delta I \\ \Delta X \end{bmatrix}_{81 \times 1} &= \begin{bmatrix} \mathfrak{R}_{\text{scK}} + \frac{\mathfrak{R}_{L0}}{\Lambda} & \text{blkdiag}([\lambda_1 \cdots \lambda_6]) & 0 & -\sigma_X \phi_f A_p \\ \frac{1}{\Lambda} \text{blkdiag}([\beta_1 \cdots \beta_6]^T) & -\text{blkdiag}(\text{diag}(\lambda_l)) & 0 & 0 \\ \frac{\gamma_l}{v\Lambda} I_{9 \times 9} & 0 & -\lambda_l I_{9 \times 9} & 0 \\ \frac{\gamma_X}{v\Lambda} I_{9 \times 9} - \sigma_X \phi_f A \cdot \text{blkdiag}(X_0) & 0 & \lambda_l I_{9 \times 9} & -\lambda_X I_{9 \times 9} - \sigma_X \phi_f A_p \end{bmatrix}_{81 \times 81} \begin{bmatrix} \Delta N \\ \Delta P \\ \Delta I \\ \Delta X \end{bmatrix}_{81 \times 1} \\ &+ \begin{bmatrix} B_{9 \times 14} \\ 0 \end{bmatrix}_{81 \times 14} \Delta u_{14 \times 1} \end{aligned} \quad (\text{5-5})$$

in which,

$$I_{9 \times 9} = \begin{bmatrix} 1 & & & \\ & \ddots & & \\ & & \ddots & \\ & & & 1 \end{bmatrix}_{9 \times 9} \quad (\text{5-6})$$

$B_{9 \times 14}$  is the matrix constant, defined by

$$B_{9 \times 14} = \frac{3.33}{\Lambda} [\Delta \Theta_{1,1} \cdots \Delta \Theta_{14,1}]_{9 \times 14} \quad (\text{5-8})$$



## Appendix G

### ***“CANDURRS.m”***

```
function varargout = CANDURRS(varargin)
%CANDURRS M-file for CANDURRS.fig
%
%   CANDURRS, by itself, creates a new CANDURRS or raises the existing
%   singleton*.
%
%   H = CANDURRS returns the handle to a new CANDURRS or the handle to
%   the existing singleton*.
%
%   CANDURRS('Property','Value',...) creates a new CANDURRS using the
%   given property value pairs. Unrecognized properties are passed via
%   varargin to CANDURRS_OpeningFcn. This calling syntax produces a
%   warning when there is an existing singleton*.
%
%   CANDURRS('CALLBACK') and CANDURRS('CALLBACK',hObject,...) call the
%   local function named CALLBACK in CANDURRS.M with the given input
%   arguments.
%
%   *See GUI Options on GUIDE's Tools menu. Choose "GUI allows only one
%   instance to run (singleton)".
%
% See also: GUIDE, GUIDATA, GUIHANDLES
%
% Edit the above text to modify the response to help CANDURRS
%
% Last Modified by GUIDE v2.5 07-Jun-2011 14:12:17
%
% Begin initialization code - DO NOT EDIT
gui_Singleton = 1;
gui_State = struct('gui_Name',       mfilename, ...
                  'gui_Singleton',  gui_Singleton, ...
                  'gui_OpeningFcn', @CANDURRS_OpeningFcn, ...
                  'gui_OutputFcn',  @CANDURRS_OutputFcn, ...
                  'gui_LayoutFcn',  [], ...
                  'gui_Callback',    []);
if nargin && ischar(varargin{1})
```

```

    gui_State.gui_Callback = str2func(varargin{1});
end

if nargin
    [varargout{1:nargout}] = gui_mainfcn(gui_State, varargin{:});
else
    gui_mainfcn(gui_State, varargin{:});
end
% End initialization code - DO NOT EDIT

% --- Executes just before CANDURRS is made visible.
function CANDURRS_OpeningFcn(hObject, eventdata, handles, varargin)
% This function has no output args, see OutputFcn.
handles.output = hObject;
% Update handles structure
guidata(hObject, handles);
% UIWAIT makes CANDURRS wait for user response (see UIRESUME)
% uiwait(handles.figure1);
% --- Outputs from this function are returned to the command line.
function varargout = CANDURRS_OutputFcn(hObject, eventdata, handles)
% varargout cell array for returning output args (see VARARGOUT);
varargout{1} = handles.output;
function Ttotal_editText_Callback(hObject, eventdata, handles)
% hObject    handle to Ttotal_editText (see GCBO)
input = str2num(get(hObject, 'String'));
%checks to see if input is empty. if so, default input1_editText to zero
if (isempty(input))
    set(hObject, 'String', '0')
end
guidata(hObject, handles);

```

```

% --- Executes during object creation, after setting all properties.
function Ttotal_editText_CreateFcn(hObject, eventdata, handles)
% hObject    handle to Ttotal_editText (see GCBO)
if ispc && isequal(get(hObject,'BackgroundColor'),
get(0,'defaultUicontrolBackgroundColor'))
    set(hObject,'BackgroundColor','white');
end

function Power2_editText_Callback(hObject, eventdata, handles)
% hObject    handle to Power2_editText (see GCBO)
input = str2num(get(hObject,'String'));
%checks to see if input is empty. if so, default input1_editText to zero
if (isempty(input))
    set(hObject,'String','0')
end
guidata(hObject, handles);
% --- Executes during object creation, after setting all properties.
function Power2_editText_CreateFcn(hObject, eventdata, handles)
% hObject    handle to Power2_editText (see GCBO)
if ispc && isequal(get(hObject,'BackgroundColor'),
get(0,'defaultUicontrolBackgroundColor'))
    set(hObject,'BackgroundColor','white');
end

function Tstep1_editText_Callback(hObject, eventdata, handles)
% hObject    handle to Tstep1_editText (see GCBO)
input = str2num(get(hObject,'String'));
%checks to see if input is empty. if so, default input1_editText to zero
if (isempty(input))
    set(hObject,'String','0')
end

```

```

guidata(hObject, handles);
% --- Executes during object creation, after setting all properties.
function Tstep1_editText_CreateFcn(hObject, eventdata, handles)
% hObject    handle to Tstep1_editText (see GCBO)
if ispc && isequal(get(hObject, 'BackgroundColor'),
get(0, 'defaultUiControlBackgroundColor'))
    set(hObject, 'BackgroundColor', 'white');
end

function Tstep2_editText_Callback(hObject, eventdata, handles)
% hObject    handle to Tstep2_editText (see GCBO)
input = str2num(get(hObject, 'String'));
%checks to see if input is empty. if so, default input1_editText to zero
if (isempty(input))
    set(hObject, 'String', '0')
end
guidata(hObject, handles);
% --- Executes during object creation, after setting all properties.
function Tstep2_editText_CreateFcn(hObject, eventdata, handles)
% hObject    handle to Tstep2_editText (see GCBO)
if ispc && isequal(get(hObject, 'BackgroundColor'),
get(0, 'defaultUiControlBackgroundColor'))
    set(hObject, 'BackgroundColor', 'white');
end

function Tpowerdown_editText_Callback(hObject, eventdata, handles)
% hObject    handle to Tpowerdown_editText (see GCBO)
input = str2num(get(hObject, 'String'));
%checks to see if input is empty. if so, default input1_editText to zero
if (isempty(input))
    set(hObject, 'String', '0')

```



```

end

guidata(hObject, handles);
% --- Executes during object creation, after setting all properties.
function Tpowerdown_editText_CreateFcn(hObject, eventdata, handles)
% hObject    handle to Tpowerdown_editText (see GCBO)
if ispc && isequal(get(hObject,'BackgroundColor'),
get(0,'defaultUiControlBackgroundColor'))
    set(hObject,'BackgroundColor','white');
end

function Tpowerrise_editText_Callback(hObject, eventdata, handles)
% hObject    handle to Tpowerrise_editText (see GCBO)
input = str2num(get(hObject,'String'));
%checks to see if input is empty. if so, default input1_editText to zero
if (isempty(input))
    set(hObject,'String','0')
end

guidata(hObject, handles);
% --- Executes during object creation, after setting all properties.
function Tpowerrise_editText_CreateFcn(hObject, eventdata, handles)
% hObject    handle to Tpowerrise_editText (see GCBO)
if ispc && isequal(get(hObject,'BackgroundColor'),
get(0,'defaultUiControlBackgroundColor'))
    set(hObject,'BackgroundColor','white');
end

% --- Executes on button press in Run_pushbutton.
function Run_pushbutton_Callback(hObject, eventdata, handles)
% hObject    handle to Run_pushbutton (see GCBO)
Ttotal_input=get(handles.Ttotal_editText,'String');
Ttotal=str2num(Ttotal_input);

```

```

%
Power2_input=get(handles.Power2_editText,'String');
Power2=str2num(Power2_input); %0.9
Powerdiff=1.0-Power2;
%
Tstep1_input=get(handles.Tstep1_editText,'String');
Tstep1=str2num(Tstep1_input); %660s
Tstep2_input=get(handles.Tstep2_editText,'String');
%
Tpowerdown_input=get(handles.Tpowerdown_editText,'String');
Tpowerdown=str2num(Tpowerdown_input);
Tpowerrise_input=get(handles.Tpowerrise_editText,'String');
Tpowerrise=str2num(Tpowerrise_input);
Prate=100*Powerdiff/Tpowerdown*0.0043429; % power down rate
Prate2=100*Powerdiff/Tpowerrise*0.0043429; % power rise rate
Tstep2=str2num(Tstep2_input)+Tstep1+Tpowerdown;
%
%use exe model. 20110629
asim=0:0.02:Ttotal;
bsim=[];
for i=1:(Ttotal/0.02+1)
    bsim=[bsim Ttotal];
end
Tend_mat=[asim;bsim];
save Tend.mat Tend_mat;

% Load model's parametere structure from MAT-file (must ship this MAT-file
% with model and GUI executables to customers for stand alone application)
load param_struct.mat
% Update parameters in model's parameter structure based on user input
rtP.parameters.values = [Power2 Powerdiff Prate Prate2 Tstep1 Tstep2];

```

```

save updated_param_struct.mat rtP;
% Execute simulation with new parameters
!CANDURRSmodal -p updated_param_struct.mat -o output.mat

load output.mat;

axes(handles.axes1)
plot(rt_tout, rt_BuckReactorPower);grid on;
xlabel('Time (Sec)');
ylabel('Reactor Bulk Power (FPU)');

axes(handles.axes2)
plot(rt_tout, rt_simout);grid on;
xlabel('Time (Sec)');
ylabel('14 Zone Powers (FPU)');

axes(handles.axes3)
plot(rt_tout, rt_ZCUlevel);grid on;
xlabel('Time (Sec)');
ylabel('14 Zone Levels (FLU)');

axes(handles.axes5)
plot(rt_AVRwaterlevel.time,rt_AVRwaterlevel.signals.values);grid on;
xlabel('Time (Sec)');
ylabel('Averaged Zone Level (FLU)');

axes(handles.axes4)
plot(rt_tout, rt_Xenodynamicreactivity.signals.values*1000);grid on;
xlabel('Time (Sec)');
ylabel('Xenon Dynamic Reactivity (mk)');
%%%%%%%%%%%%%%%%%%%%%%%%%%%%%%%%%%%%%%%%%%%%%%%%%%%%%%%%%%%%%%%%%%%%%%%%

```

```

% induce the modes data 20110720
x = [-13.5 -12.5 -11.5 -10.5 -9.5 -8.5 -7.5 -6.5 -5.5 -4.5 -3.5 -2.5 -1.5
-0.5 0.5 1.5 2.5 3.5 4.5 5.5 6.5 7.5 8.5 9.5 10.5 11.5 12.5 13.5];
y = x';
z = [0.5 1.5 2.5 3.5 4.5 5.5 6.5 7.5 8.5 9.5 10.5 11.5];
%fundamental mode
model(:, :, 1) = [];
% For space reasons, data of model1 to mode9 are omitted here. 201207%
.....
mode9(:, :, 12) = [];

modesigma =
model*rt_FluxAmplitude.signals.values(end,1)+mode2*rt_FluxAmplitude.sign
als.values(end,2)+mode3*rt_FluxAmplitude.signals.values(end,3)+mode4*rt_
FluxAmplitude.signals.values(end,4)+mode5*rt_FluxAmplitude.signals.value
s(end,5)+mode6*rt_FluxAmplitude.signals.values(end,6)+mode7*rt_FluxAmpli
tude.signals.values(end,7)+mode8*rt_FluxAmplitude.signals.values(end,8)+
mode9*rt_FluxAmplitude.signals.values(end,9);

save output.mat modesigma x y z;

% --- Executes on button press in Distribution_pushbutton.
function Distribution_pushbutton_Callback(hObject, eventdata, handles)
% hObject    handle to Distribution_pushbutton (see GCBO)
run('ThreeD');

% --- Executes on button press in Reset_pushbutton.
function Reset_pushbutton_Callback(hObject, eventdata, handles)
% hObject    handle to Reset_pushbutton (see GCBO)
set(handles.Ttotal_editText, 'String', '0');
set(handles.Tpowerdown_editText, 'String', '0');

```

```

set(handles.Tpowerrise_editText, 'String', '0');
set(handles.Power2_editText, 'String', '0');
set(handles.Tstep1_editText, 'String', '0');
set(handles.Tstep2_editText, 'String', '0');

% --- Executes on button press in Clear_pushbutton.
function Clear_pushbutton_Callback(hObject, eventdata, handles)
% hObject    handle to Clear_pushbutton (see GCBO)
cla(handles.axes1, 'reset');
cla(handles.axes2, 'reset');
cla(handles.axes3, 'reset');
cla(handles.axes4, 'reset');
cla(handles.axes5, 'reset');

guidata(hObject, handles);
clear;

% --- Executes on button press in Close_pushbutton.
function Close_pushbutton_Callback(hObject, eventdata, handles)
% hObject    handle to Close_pushbutton (see GCBO)
button=questdlg('Do you want to close the window?');
switch button
    case 'Yes'
        delete(handles.figure1);
        delete('output.mat');
        delete('Tend.mat');
        delete('updated_param_struct.mat');
        clear;
    case 'no'
        default;
    case 'cancel'

```

```
        default;
end
```

### ***“ThreeD.m”***

```
function varargout = ThreeD(varargin)
% THREED M-file for ThreeD.fig
%   THREED, by itself, creates a new THREED or raises the existing
%   singleton*.
%   H = THREED returns the handle to a new THREED or the handle to
%   the existing singleton*.
%   THREED('CALLBACK',hObject,eventData,handles,...) calls the local
%   function named CALLBACK in THREED.M with the given input arguments.
%   THREED('Property','Value',...) creates a new THREED or raises the
%   existing singleton*. Starting from the left, property value pairs are
%   applied to the GUI before ThreeD_OpeningFunction gets called. An
%   unrecognized property name or invalid value makes property application
%   stop. All inputs are passed to ThreeD_OpeningFcn via varargin.
%   *See GUI Options on GUIDE's Tools menu. Choose "GUI allows only one
%   instance to run (singleton)".
% See also: GUIDE, GUIDATA, GUIHANDLES
% Edit the above text to modify the response to help ThreeD
% Last Modified by GUIDE v2.5 24-May-2011 16:54:50
% Begin initialization code - DO NOT EDIT
gui_Singleton = 1;
gui_State = struct('gui_Name',       mfilename, ...
                  'gui_Singleton',  gui_Singleton, ...
                  'gui_OpeningFcn', @ThreeD_OpeningFcn, ...
                  'gui_OutputFcn',  @ThreeD_OutputFcn, ...
                  'gui_LayoutFcn',  [] , ...
                  'gui_Callback',   []);
```

```

if nargin && ischar(varargin{1})
    gui_State.gui_Callback = str2func(varargin{1});
end

if nargin
    [varargout{1:nargout}] = gui_mainfcn(gui_State, varargin{:});
else
    gui_mainfcn(gui_State, varargin{:});
end

% End initialization code - DO NOT EDIT

% --- Executes just before ThreeD is made visible.
function ThreeD_OpeningFcn(hObject, eventdata, handles, varargin)
% This function has no output args, see OutputFcn.
% hObject    handle to figure
% Choose default command line output for ThreeD
handles.output = hObject;
% Update handles structure
guidata(hObject, handles);
% UIWAIT makes ThreeD wait for user response (see UIRESUME)
% uiwait(handles.figure1);
% --- Outputs from this function are returned to the command line.
function varargout = ThreeD_OutputFcn(hObject, eventdata, handles)
% varargout  cell array for returning output args (see VARARGOUT);
varargout{1} = handles.output;

load('output.mat');
%
axes(handles.axes1)
surf(x,y,modesigma(:,:,1));grid on;

```

```

xlabel('x (lattice pitch)');
ylabel('y (lattice pitch)');
zlabel('z (normalized neutron flux)');
title('the 1st layer');
xlim([-14 14]);
ylim([-14 14]);
zlim([0 1e-3]);

%
axes(handles.axes12)
surf(x,y,modesigma(:,:,2));grid on;
xlabel('x (lattice pitch)');
ylabel('y (lattice pitch)');
zlabel('z (normalized neutron flux)');
title('the 2nd layer');
xlim([-14 14]);
ylim([-14 14]);
zlim([0 1e-3]);

%
axes(handles.axes13)
surf(x,y,modesigma(:,:,3));grid on;
xlabel('x (lattice pitch)');
ylabel('y (lattice pitch)');
zlabel('z (normalized neutron flux)');
title('the 3rd layer');
xlim([-14 14]);
ylim([-14 14]);
zlim([0 1e-3]);

%
axes(handles.axes14)
surf(x,y,modesigma(:,:,4));grid on;
xlabel('x (lattice pitch)');

```



```

ylabel('y (lattice pitch)');
xlabel('z (normalized neutron flux)');
title('the 4th layer');
xlim([-14 14]);
ylim([-14 14]);
zlim([0 1e-3]);
%
axes(handles.axes15)
surf(x,y,modesigma(:,:,5));grid on;
xlabel('x (lattice pitch)');
ylabel('y (lattice pitch)');
xlabel('z (normalized neutron flux)');
title('the 5th layer');
xlim([-14 14]);
ylim([-14 14]);
zlim([0 1e-3]);
%
axes(handles.axes16)
surf(x,y,modesigma(:,:,6));grid on;
xlabel('x (lattice pitch)');
ylabel('y (lattice pitch)');
xlabel('z (normalized neutron flux)');
title('the 6th layer');
xlim([-14 14]);
ylim([-14 14]);
zlim([0 1e-3]);

```

## Appendix H

### Copyright Permission

#### ELSEVIER LICENSE TERMS AND CONDITIONS

Oct 15, 2012

---

---

This is a License Agreement between Lingzhi Xia ("You") and Elsevier ("Elsevier") provided by Copyright Clearance Center ("CCC"). The license consists of your order details, the terms and conditions provided by Elsevier, and the payment terms and conditions.

**All payments must be made in full to CCC. For payment instructions, please see information listed at the bottom of this form.**

Supplier Elsevier Limited  
The Boulevard, Langford Lane  
Kidlington, Oxford, OX5 1GB, UK

Registered 1982084

Company  
Number

Customer name Lingzhi Xia

License number 3010271383451

License date Oct 15, 2012

Licensed content Elsevier  
publisher

Licensed content Nuclear Engineering and Design

publication

Licensed content Performance evaluation of a 3-D kinetic model for CANDU reactors in a  
title closed-loop environment

Licensed content Lingzhi Xia, Jin Jiang, Hooman Javidnia, John C. Luxat  
author

Licensed content February 2012  
date

Licensed content 243  
volume number

Licensed content  
issue number

Number of pages 11

Start Page 76

End Page 86

Type of Use reuse in a thesis/dissertation

Intended other  
publisher of new  
work

Portion full article

Format both print and electronic

Are you the Yes  
author of this  
Elsevier article?

Will you be No  
translating?

Order reference

number

Title of your thesis/dissertation      Development of 3-D Neutronic Kinetic Model and Control for CANDU Reactors

Expected completion date      Oct 2012

Estimated size (number of pages)      212

Elsevier VAT number      GB 494 6272 12

Permissions price      0.00 USD

VAT/Local Sales Tax      0.0 USD / 0.0 GBP

Total      0.00 USD

Terms and Conditions

# CURRICULUM VITAE

**Name:** Lingzhi Xia  
**Place of Birth:** Jingjiang, Jiangsu Province, China  
**Year of Birth:** 1981

## Education:

**2006 - 2012**      **Ph. D.**  
Department of Electrical and Computer Engineering  
The University of Western Ontario, London, Ontario, Canada

**2001 - 2004**      **M. Eng. Sc.**  
Department of Nuclear Engineering and Technology  
Xi'an Jiaotong University, Xi'an, Shaanxi, China

**1997 - 2001**      **B. Eng.**  
Department of Nuclear Engineering and Technology  
Xi'an Jiaotong University, Xi'an, Shaanxi, China

## Experience:

**07/2004 - 07/2006**      **Engineer**  
Department of Reactor Core Design  
Shanghai Nuclear Engineering Research and Design Institute  
Shanghai, China

## Honors and Rewards:

First prize in the 3rd Conference of Nuclear Academy of Shaanxi Province, 2003.12  
Excellent Student Scholarship, XJTU, 2002-2003 Academic year  
Excellent Student Scholarship, Graduate School of XJTU, 2001-2002 Academic year

## Publications:

L. Xia and J. Jiang, "CANDU Reactor Space-Time Kinetic Model for Load Following Studies", *Journal of Engineering for Gas Turbines and Power, ASME Transactions*, vol. 133, iss. 5, May 2011.

L. Xia, J. Jiang, H. Javidnia, and J. C. Luxat, "Performance Evaluation of a 3-D Kinetic Model for CANDU Reactors in a Closed-loop Environment", *Nuclear Engineering and Design*, vol. 243, iss. 0, pp. 76-86, Feb. 2012.

L. Xia, J. Jiang, and J. C. Luxat, "Design and Analysis of CANDU Reactor Control Systems based on a 3-D Reactor Kinetic Model", Submitted to *ANS Nuclear Technology*, Oct. 2012.